LATE QUATERNARY HYDROLOGICAL CHANGES IN NORTH AFRICA BASED ON GEOCHEMICAL AND MICROFOSSIL ANALYSES IN SEDIMENTS FROM THE EASTERN MEDITERRANEAN SEA

ハレッド, サイェド シヌーシ モハメド

https://doi.org/10.15017/1931716

出版情報：九州大学, 2017, 博士（理学）, 課程博士
バージョン：
権利関係：

LATE QUATERNARY HYDROLOGICAL CHANGES IN NORTH AFRICA BASED ON GEOCHEMICAL AND MICROFOSSIL ANALYSES IN SEDIMENTS FROM THE EASTERN MEDITERRANEAN SEA

by

Khaled Sayed Sinoussy Mohamed

B.A., Alexandria University

(2006)

M.Sc., Alexandria University

(2012)

SUBMITTED IN PARTIAL FULFILLMENT OF THE

REQUIREMENTS FOR THE DEGREE OF

DOCTOR OF PHILOSOPHY

At the

DEPARTMENT OF EARTH AND PLANETARY SCIENCES

GRADUATE SCHOOL OF SCIENCE

KYUSHU UNIVERSITY

FEBRUARY 2018

Signature of Author: _____

Department of Earth and Planetary Sciences Graduate School of Sciences,

Kyushu University, February 2018

Certified by: _____

Thesis supervisor

Abstract

Aim of this thesis is to understand the hydrological cycle system effect of the North African monsoon since the Last Glacial Maximum (LGM) on terrestrial ecosystems and effect of humid periods on marine ecosystems of the Eastern Mediterranean Sea (EMS). In particular, the focus is placed on the drastic regime shift from arid conditions of LGM to the humid and vegetated conditions of the mid-Holocene in North Africa. The timing of this regime shift is investigated in order to determine the hydrological cycle and expansion of C4 plants in North Africa showed a covariance with processional cycle or millennial scale. In order to achieve this objective, variations in compound-specific hydrogen and carbon isotopes of sedimentary n-alkanes of ODP site 967B are scrutinized. $\delta D_{n\text{-}alkanes}$, a proxy for precipitation, ranging from -199‰ to -127‰, co-varied with insolation change response to orbital forcing. Depleted $\delta D_{n\text{-}alkanes}$ were found from deglaciation to middle Holocene, suggesting increased precipitation during the African Humid Period (AHP) from 15 ka to 5 ka caused by northward migration of the Intertropical Convergence Zone (ITCZ). On the contrary, lower precipitation was inferred by enriched $\delta D_{n\text{-}alkanes}$ during LGM and late Holocene. $\delta^{13}C_{n\text{-}alkanes}$ at Site 967 did not show a trend in harmony with $\delta D_{n\text{-}alkanes}$ but exhibiting millennial-scale variations ranging from -25.9‰ to -33.2‰. These $\delta^{13}C_{n\text{-}alkanes}$ values are consistently C4 grass dominated environment in the watershed area of River Nile since LGM even during AHP. The greening of Sahara Desert was dominated by C4 plants during AHP coupled with formation of Sapropel layers in EMS fueled by African monsoon changes in North Africa. Discharge of freshwater into EMS via Nile River and Wadi connective system could alter marine ecosystems in EMS. Both planktic and benthic foraminiferal assemblages in sediment core from Nile deep-sea fan were examined together with *Globigerinoides ruber* (a planktic foraminiferal species living in surface water) $\delta^{13}C$ and $\delta^{18}O$ analysis. Isotopic excursions on both $\delta^{13}C$ and $\delta^{18}O$ of *Globigerinoides ruber* were observed during sapropel S3 and S4 layers. These isotopic excursions are interpreted as signature of enhanced freshwater discharge caused by increased precipitation and terrigenous input in watershed area of Nile River. Increased %*Globigerina bulloides*, a high productivity indicator, suggest nutrient rich condition during then. Benthic foraminiferal assemblages were employed to reconstruct oxygen (O_2) conditions in pore water. Notable species turnover to deep infauna species, dysoxic indicator, were observed in sapropel layers. Low species diversities of both planktic and benthic foraminifera are likely due to thermocline shallowing by enhanced freshwater discharge and dysoxic bottom water caused by high productivity during sapropel layer formations.

Acknowledgement

This thesis would not have been possible without the support, patience, and guidance of many, many people. Firstly, I would like to thank my supervisor Prof. Yusuke Okazaki for his continuous guidance and support. During my time at the Kyushu university, he always found time to answer my questions, often with a good sense of humor. Thank you for encouraging my research and for allowing me to grow as a research scientist. Your advice on research have been helped me come up with the thesis topic. For that I am very thankful. I would also like to thank my second supervisor Prof. Hiroshi Naraoka for his guidance, support and teaching me biomarkers and specific compound isotopes techniques. It was he who in the first instance allowed me the possibility of entering the field of specific compound isotopes and biomarkers. He let me to work liberally in his laboratory, for all of that I am very thankful. Also, thanks go to Prof. Osamu Seki who helped me in compound specific isotopes and welcomed me at his laboratory, Hokkaido University. Additional thanks go to the members (both past and present) of the Paleoclimate group for the many discussions events, group meetings, and other special events. Finally, I also want to thank my family and my friends for encouraging and supporting me for difficult times.

Table of contents

List of Figures

Figure 3. 5. Relative abundance of benthic foraminiferal species at core M70b-St#822. Sapropel layers (gray color) are indicated.

Figure 3. 6. Absolute abundance of benthic foraminiferal species at core M70b-St#822. Sapropel layers (gray color) are indicated.

Figure 3. 7. SEM photographs of selected foraminifera species (scale bar = 200 µm for Figs. 1-10; 13-14, and = 150 µm for Figs. 11-12, 15). 1-2 *Globigerinoides ruber* (D'Orbigny), 1839, 420 cm. 3-4 *Globigerinoides obliquus* Bolli 1957, 450 cm. 5-6 *Globigerina bulloides* D'Orbigny, 1826, 450 cm. 7-8 *Globigerina calida* Parker 1962, 440 cm. 9-10 *Globorotalia truncatulinoides* (d'Orbigny), 1839, 410 cm. 11-12 *Globigerinoides immaturus* Le Roy 1939, 420 cm. 13-14 *Turborotalia clarkei* Rogl and Bolli 1973, 410 cm. 15 *Orbulina universa* D'Orbigny, 1839, 430 cm.

Figure 3. 8. SEM photographs of selected foraminifera species (scale bar = 200 µm for Figs. 1-7, 9-14, and = 150 µm for Figs. 15-16, and = 100 µm for Fig. 8). 1-2 *Globigerinita glutinata* (Egger), 1895, 410 cm. 3-4 *Gyroidina soldanii* d'Orbigny, 1826, 410 cm. 5-6 *Gyroidina orbicularis* d'Orbigny, 1826, 410 cm. 7 *Bulimina costata* d'Orbigny, 1852, 340 cm. 8 *Uvigerina mediterranea* Hofker, 1932, 370 cm. 9 *Bolivina acuminata* (Natland), 1946, 380 cm. 10 *Bolivina advena* Cushman var. *striatella* Cushman, 1925, 380 cm. 11-12 *Cassidulina crassa* d'Orbigny, 1839, 380 cm. 13-14 *Cassidulina laevigata* d'Orbigny, 1826, 200 cm. 15-16 *Hoeglundina elegans* d'Orbigny, 1826, 380 cm.

List of Tables

Chapter 1. Introduction

1.1. The Eastern Mediterranean Sea

The Eastern Mediterranean-Levant region is located at the convergence of the Eurasian continent, the Saharan-Arabian desert and the Mediterranean Sea. The almost land locked Mediterranean Sea maintains its sole connection to the Atlantic Ocean via the Gibraltar Strait. As a result, sea surface conditions are diverse with west to east salinity and sea surface temperature (SST) increases and a corresponding productivity decrease (Antoine et al., 1995; Malanotte-Rizzoli et al., 1999; Pinardi and Mosetti, 2000). Precipitation over the Levantine Basin is mainly originated in the northeast Atlantic Ocean, passing over Europe and the Mediterranean Sea (Eshel, 2002; Rindsberger et al., 1983); sporadically, sub-tropic warm air over the southern Mediterranean resulted in precipitation over the Levantine basin (Dayan, 1986). Cold dry Arctic air that penetrates into the eastern Mediterranean region results in an increase in surface water density, leading to the formation of the Levantine Intermediate Water (LIW) off the island of Rhodes (Malanotte-Rizzoli et al., 1999; Pinardi and Mosetti, 2000). The African monsoonal system is associated with the low-latitude rainfall system (Rossignol-Strick, 1985) that directly influences the North Africa vegetation cover and indirectly influences the hydrography of the Levantine Basin. This system fluctuates in time, and is at its highest strength during periods of June maximum insulation in the Northern Hemisphere that coincide with elevated River Nile discharge (Haynes Jr, 1987; Rossignol-Strick, 1985; Rossignol-Strick et al., 1982). The River Nile was recognized as an important source of freshwater during Sapropel layer deposition in EMS (Kholeif, 2010; Scrivner et al., 2004) besides, rainfall on the entire Mediterranean Sea from Atlantic sources (Kallel et al., 1997; Bar-Matthews et al., 2000). Beside freshwater discharge from River Nile, several studies discussed rainfall effect over the entire Mediterranean Sea and the influx of Black Sea water during periods of sapropel formation (Almogi-Labin et al., 2009, refrence are theirin). The Nile deep-sea system is the largest sedimentary accumulation in EMS, and one of the largest modern deep-sea turbidite systems. It is more than 600 km wide and 300 km long, and consists of a mud-rich sediments delivered by Nile River (Reading and Richards, 1994). Since the late Miocene the accumulation of the Nile deep-sea sediments began to form above mobile Messinian evaporites (Gaullier et al., 2000; Loncke et al., 2006).

1.2. The Nile System

The Nile Delta is a delta located in the northern Egypt where the Nile River flowing into the EMS. The Nile Delta is formed where the supply of pluvial sediment has been abundant, and wave and current action have not been sufficient to disperse it. Of the numerous tributaries of the Nile that once existed, the Rosetta Branch to the west and the Damietta Branch to the east, are now present. The

Nile River crosses equatorial Africa (White Nile), tropical areas (Blue Nile and Atbara River) and areas with arid climates (Main Nile) to discharge into EMS through a large arcuate delta. Most of the discharge from the Nile River is originated from the Ethiopian Highlands and the Blue Nile system which influenced strongly by wet summer monsoon (seasonal flood) (Said, 1981; Williams et al., 2000). The steep Ethiopian Highlands generate abundant terrigenous particles and 70% of the present-day water discharge. Conversely, Sudd swamps (White Nile) act as a sediment filter. Fine-grained Nile sediment originate from alumina and iron-rich soil of Ethiopia, and have particular depositional features distinct from those of other soils of the Mediterranean region (Manohar, 1981). The main clay minerals are montmorillonite (smektite), illite, and kaolinite, which form most of the fluvial load and are spread on the outskirts of the Nile cone and in the south-eastern corner of the Levantine Basin. The coarse fraction, which is mostly composed of quartz, also originates in Ethiopia and in Sudan, mainly from eroded Nubian sandstones. These sands used to arrive mainly during the June to September Nile floods. Additional sands originate in the Eastern and Western Desert of Sudan and the numerous Egypt wadis but very irregularly. These sediments averaged about 80–160 million tons per year before completion of the Aswan High Dam in 1964 but were then reduced significantly. Reduction in sediment supply began with the building of the Delta Barrages, completed in 1881, and the Aswan Dam completed in 1902. The Aswan High Dam has a big impact on the reduction of sediment supply to the Nile Delta. These include severe erosion along the delta coastline and penetration of saline water from the sea into river mouths, lagoons, and groundwater. The Nile Deep Sea Fan is the largest deep-sea sedimentary basin of EMS, and it differs from most other large subsea fans as being developed in a relatively small, enclosed sea (Stanley and Maldonado, 1977). Deposited sediments in the Nile Deep Sea Fan are expected to be recorded not only EMS paleoceanographic changes but also North African climatic histories. Therefore, sedimentary data from the Nile Deep Sea Fan is important to understand a role of Nile River flow modulated by the African monsoon and corresponding changes in ocean circulation and stratification in EMS (Kholeif and Ibrahim, 2010).

1.3. Geology of the Nile

Average flow of the Nile River at its mouth is 2800 m^3 per second or 84×10^6 m^3 per year, which is very low compared to its length (6825 km) or area of its watershed (2.87 million km^2). This deficit is due mainly to the fact that much of the basin is subjected to an arid climate and therefore that the water undergoes high evaporation (Ducassou et al., 2006). The Main Nile, north of 18°N and whose total load is $230 \pm 20 \times 10^6$ tons per year (Garzanti et al., 2006), receives its water from three main sources: The White Nile, which flows through a part of equatorial Africa, the Blue Nile and the Atbara River, which lie at the Ethiopian highlands. The White Nile, which rises in Lake Victoria contributes

nearly one third of the total load, but only for a minor proportion of sediment as the White Nile has a very low liquid flow. Indeed, its course through the bush and the Sudan savannah is with little slope and many marshes. Sediments of the White Nile found in the deep basin and the delta are almost devoid of pyroxene (3%). On the other hand, abundant amphibole (97%) are derived from erosion of land metamorphic granites (Foucault and Stanley, 1989). The Blue Nile, which originates at Lake Tana in the Ethiopian highlands, contributes more than half the total load the main Nile (56%) (Foucault and Stanley, 1989) and its sediment load us $140 \pm 20 \times 10^6$ tons per year (Garzanti et al., 2006). This tributary brings pyroxenes, but also alkali feldspar and hornblende (Ca amphibole). Proportion of the hornblende is 79% against 21% for pyroxenes (Foucault and Stanley, 1989). Water discharge of the Blue Nile is 1620 m^3 per second on annual average and increases up to 5000 to 6000 m^3 per second during floods. The Atbara River contributes a small portion of the total load of the Nile River ($82 \pm 10 \times 10^6$ tons per year), carrying numerous fragments of volcanic rocks as well as olivine and augite from basaltic rocks (Garzanti et al., 2006). Pyroxenes (91%) are more abundant than amphibole (9%) (Foucault and Stanley, 1989). Differential flow for the three tributaries is based on the difference of surface of their respective drainage area and the variation of precipitation. Indeed, the Blue Nile and the Atbara River have a term shorter than the White Nile, but with a slope gradient greater, and draining rain water in the Ethiopian highlands that are subject to intense rainfall at the monsoons summer. Therefore, the Blue Nile and the Atbara River contribute a significant role in sediment load of the main Nile.

1.4. Evolution of the Nile

During the Neogene, the Nile River has undergone various trips through the arid expanses of the Sahara. Since the incision of the valley in the late Miocene, the river has experienced four major episodes: the Eonile, the Paleonile, the Prenile, and Neonile (Said, 1993, 1981). The Neonile was set up during the Holocene. With increased equatorial African lake levels, caused the addition of Lakes Victoria and Albert in the drainage basin of the Nile River. During 12 to 10 ka, widened Nile River caused a realignment of silt deposited by previous Neonile. Since 10 ka, rainfall on the Ethiopian highlands and the south of Egypt had significantly increased for 6 kyrs. Because of increased flow from the Ethiopian highland and equatorial African lakes, the present Nile River regime has been established.

1.5. Present African Climate

As a part of the Hadley cell circulation, trade winds from both hemispheres blow from the subtropics toward the tropics. Because warm dry air carried by the trade winds passes over the tropical

ocean, water vapor continuously evaporates from the sea surface. The region near the equator where the trade winds from both hemispheres meet is called the intertropical convergence zone (ITCZ) (Meehl and van Loon, 1979). Water vapor carried by the trade winds rises and contributes abundant rainfall along the ITCZ. Position of the ITCZ is near the equator in winter whereas migrates northward in summer. Warm and moist winds blow from the Indian Ocean in summer. The westward deflection of wind due to Coriolis effect provides part of the moisture-laden air currents over the Ethiopia. Upon reaching the Ethiopian highlands, they are forced to rise and condense to form precipitation. As a result, the Ethiopian highland, a Nile River source, receives long rainy season from July to September (Nicholson, 1996).

1.6. Monsoon and Astronomical Theory

Astronomical theory of paleoclimate explains the glacial-interglacial cycles during the Quaternary (e.g., Loutre and Berger, 2005). Climate is sensitive to both the total amount and the latitudinal and seasonal distribution of solar radiation onto the earth's surface. Three astronomical cycles are of relevance to these aspects: the eccentricity (cyclicity of 100 ka and 400 ka), the obliquity (cyclicity of 41 ka), and the precession (cyclicity of 19 and 23 ka), which are denoted as 'Milankovitch cycles'. Tuenter et al., (2003) suggests that both precession and obliquity mainly responsible for an intensity of the African summer monsoon and the signals are recorded in EMS sediments throughout the Pleistocene as a consequence of changes in Nile River discharge (Rossignol-Strick, 1985). Glacial-interglacial climatic oscillations had a large influence on the Mediterranean environments (Rose et al., 1999). Wet and dry periods are called 'pluvial' and 'arid' periods, respectively have been evidenced in Nile River (Said, 1993; Williams et al., 2000) and EMS (Weldeab et al., 2002) deposits. The Nile River floods in pluvial periods are responsible for supplying organic rich sediments (Kidd et al., 1978).

1.7. African Humid Period

North Africa was subjected to a wetter and warmer period between 15 ka and 5 ka known as African Humid Period (AHP, Barker et al., 2004; deMenocal et al., 2000; Junginger and Trauth, 2013). Numbers of marine core sediments (deMenocal et al., 2000; Ehrmann et al., 2017), lake core sediment (Berke et al., 2012; Tierney et al., 2008) and archaeological sites (Kuper and Kröpalin, 2006; Stanley et al., 2003) documented that AHP peaked between 9 ka and 6 ka when sapropel S1 deposited in EMS (Ritchie et al., 1985). Summer insolation paced by precessional cycle plays a principal role in greening and desertification of the Saharan Desert through precipitation in North Africa (deMenocal et al., 2000).

1.8. Sapropels

Sapropel is a dark-colored sediment with rich in organic matter. Numbers of sapropel layers are found in EMS sediments and have been the subject of numerous studies on the geographical distribution, age and formation (Casford et al., 2003; Cramp and O'Sullivan, 1999; Kallel et al., 2000a, b; Kroon et al., 1998). Saporpel layers in EMS may be laminated or bioturbated depending on their thickness and sedimentation rate: homogeneous (S1), color banded (S3, S5, S7 and S9) or composite (S4, S6 and S8). These black deposits may contain near the coast, macroscopic plant debris of continental origin. Sapropel layers contain planktic foraminifera, but are almost devoid of benthic foraminifera (Casford et al., 2003). The absence of benthos and excellent preservation of organic matter are strong evidences for anoxia bottom water. Sapropels formed both in interglacial periods and glacial periods, suggesting no direct relationship to glacial and interglacial cycle although most sapropels were formed during interglacial periods except for sapropel S6 during marine isotope stage (MIS) 6. Quantitative estimation for each sapropel duration is difficult because organic matter on sediment surface is oxidized when anoxia conditions cease. In addition, bacterial activity may degrade in situ organic matter in sapropel deposited 200 kyrs ago (Coolen et al., 2002). Two major hypotheses to form sapropels: (1) biological process by enhanced biological productivity linked to riverine nutrient supply (Calvert et al., 1992); and (2) physical process by water stagnation and oxygen deficiency in bottom water leading to organic matter preservation. Enhanced freshwater discharge leads to a reduction of surface water density, which hampers intermediate and deep water ventilation (Ducassou, 2006). Sapropels in EMS have been correlated across the basins and their timings are well dated based on radiocarbon dating for sapropel S1 (6.1-10.2 ka) (De Lange et al., 2008) and astronomical tuning dating for the rest of the sapropels (Cita et al., 1977; Emeis and Sakamoto, 1998). However, existence of sapropel 2 is not certain (Cita et al., 1977).

References

Almogi-Labin, A., Bar-Matthews, M., Shriki, D., Kolosovsky, E., Paterne, M., Schilman, B., Ayalon, A., Aizenshtat, Z., Matthews, A., 2009. Climatic variability during the last ~90 ka of the southern and northern Levantine Basin as evident from marine records and speleothems. Quat. Sci. Rev. 28, 2882–2896. doi:10.1016/j.quascirev.2009.07.017

Antoine, D., Morel, A., André, J.-M., 1995. Algal pigment distribution and primary production in the eastern Mediterranean as derived from coastal zone color scanner observations. J. Geophys. Res. doi:10.1029/95JC00466

Barker, P.A., Talbot, M.R., Street-Perrott, F.A., Marret, F., Scourse, J., Odada, E.O., 2004. Late Quaternary climatic variability in intertropical Africa, in: Past Climate Variability through Europe

and Africa. Springer Netherlands, Dordrecht, pp. 117–138. doi:10.1007/978-1-4020-2121-3_7

Casford, J.S.L., Rohling, E.J., Abu-Zied, R.H., Fontanier, C., Jorissen, F.J., Leng, M.J., Schmiedl, G., Thomson, J., 2003. A dynamic concept for eastern Mediterranean circulation and oxygenation during sapropel formation, in: Palaeogeography, Palaeoclimatology, Palaeoecology. pp. 103–119. doi:10.1016/S0031-0182(02)00601-6

Cita, M.B., Vergnaud-Grazzini, C., Robert, C., Chamley, H., Ciaranfi, N., D'Onofrio, S., 1977. Paleoclimatic record of a long deep sea core from the eastern Mediterranean. Quat. Res. 8, 205–235. doi:10.1016/0033-5894(77)90046-1

Coolen, M.J.L., Cypionka, H., Sass, A.M., Sass, H., Overmann, J., 2002. Ongoing modification of Mediterranean pleistocene sapropels mediated by prokaryotes. Science (80-.). 296, 2407–2410. doi:10.1126/science.1071893

Cramp, A., O'Sullivan, G., 1999. Neogene sapropels in the Mediterranean: A review. Mar. Geol. 153, 11–28. doi:10.1016/S0025-3227(98)00092-9

Dayan, U., 1986. Climatology of Back Trajectories from Israel Based on Synoptic Analysis. J. Clim. Appl. Meteorol. 25, 591–595. doi:10.1175/1520-0450(1986)025<0591:COBTFI>2.0.CO;2

De Lange, G.J., Thomson, J., Reitz, A., Slomp, C.P., Speranza Principato, M., Erba, E., Corselli, C., 2008. Synchronous basin-wide formation and redox-controlled preservation of a Mediterranean sapropel. Nat. Geosci. 1, 606–610. doi:10.1038/ngeo283

deMenocal, P., Ortiz, J., Guilderson, T., Adkins, J., Sarnthein, M., Baker, L., Yarusinsky, M., 2000a. Abrupt onset and termination of the African Humid Period:: rapid climate responses to gradual insolation forcing. Quat. Sci. Rev. 19, 347–361. doi:10.1016/S0277-3791(99)00081-5

deMenocal, P., Ortiz, J., Guilderson, T., Adkins, J., Sarnthein, M., Baker, L., Yarusinsky, M., 2000b. Abrupt onset and termination of the African Humid Period: Rapid climate responses to gradual insolation forcing, in: Quaternary Science Reviews. pp. 347–361. doi:10.1016/S0277-3791(99)00081-5

Ducassou, E., 2006. No Evolution du système turbiditique profond du Nil au cour du Quaternaire récentTitle. http://www.theses.fr. Bordeaux 1.

Emeis, K.-C., Sakamoto, T., 1998. The sapropel theme of leg 160, in: Proceedings of the Ocean Drilling Program. pp. 29–36. doi:10.2973/odp.proc.sr.160.058.1998

Eshel, G., 2002. Mediterranean climates. Isr. J. Earth Sci. 51, 157–168. doi:10.1560/DMG1-06P2-908U-WDYY

Foucault, A., Stanley, D.J., 1989. Late Quaternary palaeoclimatic oscillations in East Africa recorded by heavy minerals in the Nile delta. Nat. (London, United Kingdom). doi:10.1038/339044a0

Garzanti, E., Andò, S., Vezzoli, G., Ali Abdel Megid, A., El Kammar, A., 2006. Petrology of Nile River

sands (Ethiopia and Sudan): Sediment budgets and erosion patterns. Earth Planet. Sci. Lett. 252, 327–341. doi:10.1016/j.epsl.2006.10.001

Gaullier, V., Mart, Y., Bellaiche, G., Mascle, J., Vendeville, B.C., Zitter, T., 2000. Salt tectonics in and around the Nile deep-sea fan: insights from the PRISMED II cruise. Geol. Soc. London, Spec. Publ. 174, 111–129. doi:10.1144/GSL.SP.1999.174.01.07

Haynes Jr, C.V., 1987. Holocene migration rates of the Sudano-Sahelian wetting front, Arba'in Desert, eastern Sahara, in: Prehistory of Arid North Africa : Essays in Honor of Fred Wendorf. pp. 69–84.

Junginger, A., Trauth, M.H., 2013. Hydrological constraints of paleo-Lake Suguta in the Northern Kenya Rift during the African Humid Period (15-5kaBP). Glob. Planet. Change 111, 174–188. doi:10.1016/j.gloplacha.2013.09.005

Kallel, N., Duplessy, J.C., Labeyrie, L., Fontugne, M., Paterne, M., Montacer, M., 2000a. Mediterranean pluvial periods and sapropel formation over the last 200 000 years. Palaeogeogr. Palaeoclimatol. Palaeoecol. 157, 45–58. doi:10.1016/S0031-0182(99)00149-2

Kallel, N., Duplessy, J.C., Labeyrie, L., Fontugne, M., Paterne, M., Montacer, M., 2000b. Mediterranean pluvial periods and sapropel formation over the last 200 000 years. Palaeogeogr. Palaeoclimatol. Palaeoecol. 157, 45–58. doi:10.1016/S0031-0182(99)00149-2

Kholeif, S.E.A., 2010. Holocene paleoenvironmental change in inner continental shelf sediments, Southeastern Mediterranean, Egypt. J. African Earth Sci. 57, 143–153. doi:10.1016/j.jafrearsci.2009.08.001

Kholeif, S.E.H., Ibrahim, M.I., 2010. Palynofacies Analysis of Inner Continental Shelf and Middle Slope Sediments offshore Egypt, South-eastern Mediterranean. Geobios 43, 333–347. doi:10.1016/j.geobios.2009.10.006

Kroon, D., Alexander, I., Little, M., Lourens, L.J., Matthewson, A., Robertson, A.H.F., Sakamoto, T., 1998. Oxygen isotope and sapropel stratigraphy in the Eastern Mediterranean during the last 3.2 million years. Proc. Ocean Drill. Program, Sci. Results 160, 181–189. doi:10.2973/odp.proc.sr.160.071.1998

Loncke, L., Gaullier, V., Mascle, J., Vendeville, B., Camera, L., 2006. The Nile deep-sea fan: An example of interacting sedimentation, salt tectonics, and inherited subsalt paleotopographic features. Mar. Pet. Geol. 23, 297–315. doi:10.1016/j.marpetgeo.2006.01.001

Loutre, M.F., Berger, A., 2005. Insolation, CO2, et précipitations en période interglaciaire. Comptes Rendus - Geosci. 337, 69–78. doi:10.1016/j.crte.2004.07.009

Malanotte-Rizzoli, P., Manca, B.B., D'Alcala, M.R., Theocharis, A., Brenner, S., Budillon, G., Ozsoy, E., 1999. The Eastern Mediterranean in the 80s and in the 90s: The big transition in the intermediate and deep circulations, in: Dynamics of Atmospheres and Oceans. pp. 365–395.

doi:10.1016/S0377-0265(99)00011-1

Manohar, M., 1981. Coastal processes at the Nile Delta Coast. Shore and Beach 49, 8–15.

Pinardi, N., Mosetti, E., 2000. Variability of the large-scale general circulation of the Mediterranean Sea from observations and modelling: a review. Palaeogeogr, Palaeoclim. Palaeoecol. 158, 153–174. doi:http://dx.doi.org/10.1016/S0031-0182(00)00048-1

Reading, H.G., Richards, M., 1994. Turbidite Systems in Deep-Water Basin Margins Classified by Grain Size and Feeder System 1. Am. Assoc. Pet. Geol. Bull. 78, 792–822.

Rindsberger, M., Magaritz, M., Carmi, I., Gilad, D., 1983. The relation between air mass trajectories and the water isotope composition of rain in the Mediterranean Sea area. Geophys. Res. Lett. 10, 43–46. doi:10.1029/GL010i001p00043

Ritchie, J.C., Eyles, C.H., Haynes, C. V., 1985. Sediment and pollen evidence for an early to mid-Holocene humid period in the eastern Sahara. Nature 314, 352–355. doi:10.1038/314352a0

Rossignol-Strick, M., 1985. Mediterranean Quaternary sapropels, an immediate response of the African monsoon to variation of insolation. Palaeogeogr. Palaeoclimatol. Palaeoecol. 49, 237–263. doi:10.1016/0031-0182(85)90056-2

Rossignol-Strick, M., Nesteroff, W., Olive, P., Vergnaud-Grazzini, C., 1982. After the deluge: Mediterranean stagnation and sapropel formation. Nature 295, 105–110. doi:10.1038/295105a0

Said, R., 1993. The river Nile : geology, hydrology, and utilization. Pergamon.

Said, R., 1981. The Geological Evolution of River Nile. Springer New York. doi:10.1007/978-1-4612-5841-4

Scrivner, A.E., Vance, D., Rohling, E.J., 2004. New neodymium isotope data quantify Nile involvement in Mediterranean anoxic episodes. Geology 32, 565–568. doi:10.1130/G20419.1

Stanley, D.J., Maldonado, A., 1977. Nile cone: Late quaternary stratigraphy and sediment dispersal. Nature 266, 129–135. doi:10.1038/266129a0

Tuenter, E., Weber, S.L., Hilgen, F.J., Lourens, L.J., 2003. The response of the African summer monsoon to remote and local forcing due to precession and obliquity. Glob. Planet. Change 36, 219–235. doi:10.1016/S0921-8181(02)00196-0

Williams, M.A.J., Adamson, D., Cock, B., McEvedy, R., 2000. Late Quaternary environments in the White Nile region, Sudan. Glob. Planet. Change 26, 305–316. doi:10.1016/S0921-8181(00)00047-3

Chapter 2

Hydrological and vegetation changes in Northeast Africa over the past 23,000 years based on compound-specific δD and $\delta^{13}C$ variations of n-alkanes in sediments from the eastern Mediterranean Sea

Abstract

Hydroclimate variation and vegetation changes of the Nile River watershed area in northeast Africa since the Last Glacial Maximum (LGM) were reconstructed based on *n*-alkane molecular distributions and their carbon isotope ratios ($\delta^{13}C_{n\text{-alkanes}}$) and their hydrogen isotope ratios ($\delta D_{n\text{-alkanes}}$) in sediments from Ocean Drilling Program (ODP) Site 967 in the Eastern Mediterranean Sea (EMS). $\delta D_{n\text{-alkanes}}$, a proxy for precipitation, ranging from -199‰ to -127‰, co-varied with insolation change response to orbital forcing. Depleted $\delta D_{n\text{-alkanes}}$ were found from deglaciation to middle Holocene, suggesting increased precipitation during the African Humid Period (AHP) from 15 ka to 5 ka caused by northward migration of the Intertropical Convergence Zone (ITCZ). On the contrary, lower precipitation was inferred by enriched $\delta D_{n\text{-alkanes}}$ during LGM and late Holocene. $\delta^{13}C_{n\text{-alkanes}}$ at Site 967 did not show a trend in harmony with $\delta D_{n\text{-alkanes}}$ but exhibiting millennial-scale variations ranging from –25.9‰ to –33.2‰. These $\delta^{13}C_{n\text{-alkanes}}$ values are consistently C4 grass dominated environment in the watershed area of River Nile since LGM even during AHP.

2.1. Introduction

Present hyperarid Sahara Desert is the largest dust source of the Earth surface (Ginoux et al., 2012) transported over the Atlantic Ocean by easterly trade wind and over the Mediterranean Sea by cyclones mainly during Spring and Summer (e.g., Moulin et al., 1997, and references therein). The Sahara Desert is subjected to significant paleohydrological variations between 15-5 ka BP (Barker et al., 2004; Junginger and Trauth, 2013). This period is known as the African Humid Period (AHP) characterized by almost complete vegetation cover with annual grasses and shrubs in the present Sahara Desert so-called Green Sahara (e.g., COHMAP MEMBERS, 1988; deMenocal et al., 2000; DeMenocal and Tierney, 2012). AHP peaked between 9 ka and 6 ka when sapropel S1 deposited in the Mediterranean Sea (Ritchie et al., 1985). Summer insolation paced by precessional cycles plays a principal role in greening and desertification of Saharan Desert through precipitation in North Africa (deMenocal et al., 2000).

Stable hydrogen isotope (δD) of sedimentary n-alkanes biomarkers are employed to reconstruct past hydroclimate variations (Eglinton and Eglinton, 2008; Sachse et al., 2012) which, the δD of lipids track the δD of environmental waters (Sauer et al., 2001) and hence, it reflects the local precipitation

(Sachse et al., 2012 and references therein). Accordingly, the δD of lipids are potentially quantitative proxy for δD precipitation. $\delta D_{n\text{-alkanes}}$ values are significantly correlated with the δD signature of source water (leaf and xylem water) originated from precipitation (Sachse et al., 2012 and references therein). In the tropics, the "amount effect" is main controlling factor for δD in rain water and n-alkanes of terrestrial plants, δD values decreased with precipitation intensities (Dansgaard, 1964; Feakins and Sessions, 2010; Kahmen et al., 2013).

Compound-specific carbon isotope of n-alkanes reflect carbon fixation pathway during photosynthesis (Huang et al., 2001; Street-Perrott et al., 1997). During photosynthesis, plants discriminate against the carbon-13 isotope (^{13}C) and preferentially fix the carbon-12 isotope (^{12}C) of carbon dioxide (CO_2) to an extent that is correlated with the stomatal conductance of plant cells (Delucia et al., 1988). This discrimination against ^{13}C is more pronounced in C3 plants (Farquhar et al., 1989). Basically, 90% of plant species, including all trees, most shrubs, and cool-season grasses and sedges, use a photosynthetic pathway to produce a three-carbon molecule, 3-phosphoglyceric acid, in a process called carboxylation that is catalyzed by the enzyme ribulose 1,5-bisphosphate carboxylase-oxygenase (Rubisco). In the carboxylation reaction, CO_2 is fixed by combining it with ribulose-1,5-bisphosphate (RuBP) (Jensen and Bhar, 1977; Sage, 2001, 2004). $\delta^{13}C$ records in C3 plants range from −30‰ to −42‰ (Rommerskirchen et al., 2006; Vogts et al., 2009). C4 plants (including hot-region grasses) use the Hatch-Slack cycle, in which CO_2 is initially fixed in a compound that contains four carbon molecules (Hatch and Slack, 1966). In C4 plants photosynthetic processes occur in two types of cells: mesophyll cells and bundle-sheath cells (Brown, 1975; Kadereit et al., 2003; Muhaidat et al., 2007). In bundle-sheath cells, CO_2 is concentrated before being fixed by Rubisco. Consequently, the organic carbon of C4 plants is less depleted in ^{13}C, and their $\delta^{13}C$ values range between −18‰ and −26‰ (Rommerskirchen et al., 2006; Vogts et al., 2009). The contribution of CAM plants to the n-alkanes in sediments is negligible because of the low contribution of CAM plants to biomass production (Lüttge, 2004).

Present distribution of vegetation in North Africa (Figure 2.1) is determined by climate, mainly precipitation and temperature (White, 1983). Evergreen rainforest occurs in the most humid regions of West Africa around the equator, where woody plants account for most of the vegetation structure and phytomass (White, 1983), with >80% of the cover being woody (Good and Caylor, 2011). Woodlands characterized by open stands of trees (deciduous and semi-deciduous forests) are confined to tropical and subtropical regions on the periphery of the evergreen rainforest and extend from the Atlantic Ocean coastline toward the African Great Lakes. The dominance of woody cover (40–80%, Good and Caylor, 2011), with heliophilous grasses as a secondary constituent, distinguish the woodlands from other types of vegetation (White, 1983). A grassland ecosystem with <10% woody cover (Good and Caylor,

2011) occurs on the periphery of the Sahara Desert (White, 1983), and wooded-grasslands are confined to the woodland and grassland ecosystems with 10–40% woody cover (Good and Caylor, 2011). In the Sahara Desert ecosystem, which occupies most of North Africa, plants suffer from water scarcity owing to very small precipitation and high evaporation rates (White, 1983).

Several studies have reported origins of sedimentary n-alkanes in terms of plant species and types (e.g., Cranwell, 1973; Ficken et al., 2000; Michener and Lajtha, 2007; Nott et al., 2000; Zech et al., 2009). Submerged aquatic plants primarily produce n-alkanes shorter than n-C_{23}; n-C_{23} to n-C_{25} are indicative of floating aquatic plants (Ficken et al., 2000; Nott et al., 2000; Zech et al., 2009); n-C_{27} to n-C_{29} are generally derived from trees and shrubs; and n-C_{31} to n-C_{33} are major constituents of grasses (Cranwell, 1973; Michener and Lajtha, 2007; Zech et al., 2009). Previous studies have reconstructed paleovegetation and paleohydrological variations of Africa by using $\delta^{13}C_{n\text{-alkanes}}$ and $\delta D_{n\text{-alkanes}}$ obtained from the Atlantic Ocean (Dupont et al., 2013; Kuechler et al., 2013; Maslin et al., 2012; Niedermeyer et al., 2010; Vogts et al., 2012; Zhao et al., 2003), and the Gulf of Aden (Feakins et al., 2007). However, hydroclimate studies based on $\delta^{13}C_{n\text{-alkanes}}$ and $\delta D_{n\text{-alkanes}}$ in EMS, the catchment areas of Nile River, are still limited. Menzel et al. (2004) reconstructed vegetation cover in North Africa during Sapropel S5. At ODP Site 967, Rose et al. (2016) reconstructed changes in northeast African vegetation between 3.05 and 1.75 Ma during Plio-Pleistocene sapropel cycles. Castañeda et al. (2016) reported significant hydroclimate variability in EMS for past 28 kyrs multi-proxy records including $\delta^{13}C_{n\text{-alkanes}}$ and $\delta D_{n\text{-alkanes}}$. Because the sediment sample core GeoB7702-3 was obtained from the continental slope off Israel, Mediterranean vegetation and precipitation also might have influence on the sedimentary $\delta^{13}C_{n\text{-alkanes}}$ and $\delta D_{n\text{-alkanes}}$. Therefore, it is worth investigating hydroclimate change in Nile Basin in offshore region. Site ODP 967 is located on a seamount south of Cyprus where less influenced by direct terrigenous input from the Mediterranean Basin. Paleoceanographic studies at Site ODP 967 have been performed to reconstruct sea-surface temperature (Emeis et al., 1998; Kroon et al., 1998), aeolian dust input (Larrasoana et al., 2003) and redox condition (Azrieli-Tal et al., 2014) since LGM. However, hydroclimate change has not yet been revealed. Here we present n-alkane molecular distributions and their compound-specific isotope records in sediments from Site ODP 967 to reconstruct hydroclimate and vegetation variabilities in North Africa, watershed area of River Nile.

2.2. Material and Methods

2.2.1. Samples

Marine sediment cores used in our study were obtained at Site 967 from EMS during ODP Leg 160 (Emeis et al., 1996). Site 967 is located on the northern slope of the Eratosthenes Seamount south of Cyprus (34° 04´N, 32° 43´E, water depth: 2555 m, Fig. 2.2). Sediment samples taken from the top

2 m of Hole 967B (Core 1H-1 and 1H-2) were used to measure n-alkane concentrations and its carbon and hydrogen isotopes. The sediments from Core 1H-1 and 1H-2 were hemipelagic bioturbated nannofossil oozes and nannofossil clays with a 21-cm-thick sapropel S1 layer (Emeis et al., 1996). The measured intervals were converted to a revised meters composite depth scale (Sakamoto et al., 1998). **2.2.2. Age Model**

Age model for the uppermost part of sediment cores at Site 967 was established by Larrasoana et al. (2003) based on linear interpolation of Ba/Al ratios data versus sapropel layer S1, together with planktic foraminiferal oxygen isotope stratigraphy (Emeis et al., 2000; Kroon et al., 1998). In addition, top and bottom ages of sapropel layer S1 were well constrained by radiocarbon dating of planktic foraminifera from a number of sediment cores in EMS (10.8 ± 0.4 to 6.1 ± 0.5 cal. kyr BP; De Lange et al., 2008). The top 2 m of Hole 967B are corresponding to the past 30 kyrs.

2.2.3. n-Alkane Analyses

Ninety-eight consecutive samples (10 cc) were taken from top 2 m cores of Hole 967B at depth intervals of 2.0 cm (Table 2.1). The samples were freeze-dried with an EYELA FDU-1200 freeze dryer combined with a ULVAC GLD-051 oil-sealed rotary vacuum pump. The fore-line trap of the ULVAC OFI-200 suction filter was equipped to prevent the counter flow of diffusion oil into the freeze dryer. The freeze-dried samples were weighed and homogenized with a porcelain mortar and ultrasonically extracted with 15 ml of dichloromethane/methanol (2/1 by volume) three times for 20 min each time. The combined extracts were rotary evaporated and dried with a gentle stream of N_2. The total extract was re-dissolved in a small amount of hexane and separated by silica gel column chromatography. Glass columns (50 mm × 7 mm i.d.) were filled with silica gel that had been previously heated at 450°C for 3 hours followed by deactivation with 5 wt% H_2O. The extract was eluted with n-hexane to separate alkane fraction from polar fraction. n-Alkanes were identified and quantified by gas chromatography/mass spectrometry (GC/MS) using a Hewlett Packard model HP6890 GC/MSD5972A system. A DB-5MS capillary column (30 m × 0.25 mm i.d. film thickness 0.25 μm) was held at 50°C for 2 minutes, programmed to 120°C at 30°C/ minutes, then to 310°C at 5°C/minutes, and finally held at 310°C for 17.67 minutes. Helium was used as the carrier gas.

Stable carbon isotope ($\delta^{13}C$) measurements of n-alkanes were conducted following to Seki et al. (2010) on 48 samples taken from the top 2 m of Hole 967B (Table 2.3). The $\delta^{13}C$ analyses were carried out by gas chromatography/combustion/isotope ratio mass spectrometry (GC/C/IRMS) using a HP 6890 GC equipped with a DB-5 fused silica capillary column (30 m × 0.32 mm i.d., film thickness 0.25 μm) and an on-column injector, a combustion interface (Finnigan GC combustion III), and a

Finnigan MAT Delta Plus mass spectrometer. The combustion was performed in a microvolume furnace with CuO and Pt at 840°C (Hayes et al., 1990). The GC-IRMS equipment was calibrated daily by a mixture of C_{15} to C_{36} n-alkanes standards with known isotopic values (Vienna Pee Dee Belemnite, VPDB).

Compound-specific hydrogen isotope (δD) of n-alkanes were determined following to Seki et al. (2010) using a GC/thermal conversion/ IRMS system consisting of a HP 6890 GC connected to a Finnigan MAT Delta Plus XL mass spectrometer. Capillary GC column conditions are (30 m × 0.32 mm i.d., film thickness 0.25 μm). Pyrolysis (thermal conversion) of n-alkanes to H2 was achieved at 1450°C in a microvolume ceramic tube. C_{21} n-fatty acid methyl ester, as an internal isotopic standard with isotopic values $\delta^{13}C$ = -26.2‰ and δD = -227‰ for carbon and hydrogen compound specific isotopes were injected between measurements to check instrumental condition. A laboratory standard containing C_{16}–C_{30} n-alkanes was analyzed daily with analytical error 5‰. δD values are given in per mil (‰) notation relative to Standard Mean Ocean Water (SMOW).

A binary mixing equation was used to calculate relative contribution of C3 and C4 plants from $\delta^{13}C_{n\text{-alkanes}}$ in sediments from Hole 967B:

$$\%C4 = (Xs - Xc3) / (Xc4 - Xc3) \times 100$$

Where Xs is $\delta^{13}C_{n\text{-alkanes}}$ of sediment samples in Hole 967B. Xc3 and Xc4 are end member data for $\delta^{13}C_{n\text{-alkanes}}$ of C3 and C4 plants, respectively: Xc3 for $\delta^{13}C_{n\text{-}C31}$ is -35.7±2.8‰ and Xc4 for $\delta^{13}C_{n\text{-}C31}$ is -22.1±2.1‰ (Rommerskirchen et al., 2006; Vogts et al., 2009).

2.3. Results

2.3.1. Molecular Distribution of n-Alkanes

In Site 967 sediments, high-molecular-weight n-alkanes were characterized by a predominance of C_{27}, C_{29}, and C_{31} homologues, and weight of the n-alkanes ranged from 2.5 to 728.7 ng/g dry-sediment (Fig. 2.3; Table 2.2). In general, n-alkane concentrations at Site 967 were relatively low (<10 ng/g) at samples below 160 cm core depth and high (>10 ng/g) at samples above 160 cm core depth (Fig. 3). Significantly high n-alkane concentrations (>100 ng/g) were observed in sapropel S1 layer.

2.3.2. Compound-specific carbon and hydrogen isotope compositions of n-alkanes

$\delta^{13}C$ values of C_{23}–C_{31} n-alkanes in the top 2 m of Hole 967B were shown in Figure 2.4. For the past 23 kyrs, $\delta^{13}C$ values of n-C_{23}, n-C_{25}, n-C_{27}, n-C_{29} and n-C_{31} showed millennial-scale fluctuation within a range between –31.2‰ and –26.1‰, –31.2‰ and –27‰, –32.9‰ and –29.6‰, –33.2‰ and –28.5‰ and –32.1‰ and –25.9‰, respectively. Among them, $\delta^{13}C_{n\text{-}C27}$ values generally more

depleted than the other n-alkanes homologues (Fig. 2.4). No clear long-term trend in $\delta^{13}C_{n\text{-}alkanes}$ was observed from LGM to Holocene. In addition, $\delta^{13}C_{n\text{-}alkanes}$ did not show notable change during sapropel S1 layer where significantly high n-alkane concentrations were found.

δD values of C_{27}-C_{31} n-alkanes in the top 2 m of Hole 967B were shown in Figure 2.4. The $\delta D_{n\text{-}alkanes}$ showed similar pattern co-varied with summer insolation change at 20°N (Fig. 2.4). $\delta D_{n\text{-}alkanes}$ ranged from -199‰ to -127‰ for the past 23 kyrs with negative shift during AHP including sapropel S1 layer.

The $\delta^{13}C_{n\text{-}C31}$ data showed a large range in values (-32.1 to -25.9 ‰). These signatures are mainly controlled by the relative contribution of C3 and C4 plant waxes. Time-series changes in relative contribution of C4 plants are shown in Fig. 2.5. The relative contributions of %C4 plant ranged from 26 to 72%. The expansion of C4 plants showed millennial scale variations and no harmony with processional orbital forcing.

2.4. Discussion

2.4.1. n-Alkane Transport and Source

The Sahara Desert is a present dust source of EMS. Sedimentary hematite content derived from magnetic properties and Ti/Al ratios in EMS are proxies for aeolian dust supply from the Sahara Desert (Azrieli-Tal et al., 2014; Larrasoana et al., 2003). Larrasoana et al., (2003) have suggested that titanium is transported as aeolian dust to marine sediment, whereas aluminum is derived from both aeolian (kaolinite) and fluvial sources (smectite). Hence, the Ti/Al ratio in sediments at Site 967 is interpreted as an indicator of relative contribution of aeolian (Saharan dust) and fluvial (Nile discharge) sources. Both temporal changes in Ti/Al ratios and hematite content at Site 967 co-varied with Northern Hemisphere insolation at 20°N, suggesting distinct dust minima coincided with Northern Hemisphere insolation maxima during AHP (Larrasoana et al., 2003). African monsoon strength driven by summer insolation change are closely linked to the changes in humidity in North Africa (COHMAP MEMBERS, 1988; deMenocal et al., 2000). Summer insolation change is modulated by precession cycle (Fontugne and Calvert, 1992; Rohling, 1994; Rossignol-Strick, 1985). During pluvial/wet periods, summer African monsoon penetrates more northward beyond the central Saharan watershed. This leads to a greening of the Sahara and reduces input of Saharan aeolian dust into EMS. On the contrary during arid/dry periods, summer African monsoon shifts southward. This converts the Saharan region to a barren ecosystem and increases input of aeolian dust into EMS (Brovkin et al., 1998; Claussen et al., 1998).

Mechanisms that transport terrestrial biomarkers (e.g., C23–C33 n-alkanes) into marine sediments are primarily fluvial inputs in coastal regions (Hinrichs and Rullkotter, 1997) and aeolian

fallout in the open ocean (Pagani et al., 2000). The Nile deep-sea fan system plays a major role in sediment accumulation in EMS (Reading and Richards, 1974). Contribution of Nile particulate matter to the surface sediment south of Cyprus in EMS is inferred to be 40–50% based on $^{87}Sr/^{86}Sr$ isotopic ratios (Krom et al., 1999). At Site 967, the maxima in n-alkanes concentrations coupled with aeolian dust minima during sapropel S1 deposition in AHP (Larrasoana et al., 2003). Subsequently, at Site 967, mechanism of n-alkane transport is assumed to be fluvial during pluvial period whereas aeolian during dry period. Negative shift of $\delta D_{n\text{-}alkanes}$ suggests enhanced freshwater discharge by high rainfall in North Africa and Mediterranean region during AHP (Fig 2.4). The Mediterranean region also experienced increasing precipitation during sapropel deposition (Bar-Matthews et al., 2003, 2000, Kallel et al., 2000, 1997; Magny et al., 2002; Rossignol-Strick, 1999). Wu et al. (2016) measured Sr-Nd isotopes of detritus in sediment core CP10BC obtained off western Libya in EMS and concluded that origin of the detritus in sapropel S1 during AHP was mainly from fossil river/wadi systems along the Libyan-Tunisian margin. In contrast, during LGM and late Holocene, minima in n-alkanes concentrations at Site 967 coincided with aeolian dust maxima. This suggests an enhanced contribution by aeolian transport of n-alkanes and weaken riverine input during LGM and late Holocene. This scenario is consistent with low precipitation based on positive $\delta D_{n\text{-}alkanes}$ and abundant hematite content (Larrasoana et al., 2003) at Site 967 during LGM and late Holocene.

Origins of sedimentary n-alkanes are related to plant species and plant habitats: C_{23}, submerged aquatic plants; C_{23} to C_{25}, floating aquatic plants; C_{27} to C_{29}, trees and shrubs; and C_{31} to C_{33}, grasses (Cranwell, 1973; Ficken et al., 2000; Michener and Lajtha, 2007; Nott et al., 2000; Zech et al., 2009). Sinninghe Damsté et al. (2011) have reported that rainforest (mostly C3) n-alkanes are dominated by C_{29}. C3 savanna trees and shrubs and annual C4 grasses have a maximum at C_{31}, whereas annual C4 grasses also tend to produce higher amounts of C_{33}. In Site 967 sediments, carbon chain lengths of n-alkanes ranged from C_{23} to C_{33} (Fig. 2.3). Among the n-alkane homologues, C_{27}, C_{29} and C_{31} were relatively abundant at Site 967. Lignin analyses at Site 967 revealed that plant wax vegetation source was grass-dominated vegetation in both wet (sapropel) and dry (nannofossil ooze) periods and mainly originated from North Africa (Rose et al., 2016).

2.4.2. Relationship between Vegetation and Precipitation

Change in $\delta^{13}C_{n\text{-}alkanes}$ at Site 967 showed a different trend from the $\delta D_{n\text{-}alkanes}$. The $\delta^{13}C_{n\text{-}alkanes}$ fluctuated at millennial scale whereas $\delta D_{n\text{-}alkanes}$ exhibited clear long-term trend at orbital scale. Relative contribution of C4 plants based on the $\delta^{13}C_{n\text{-}alkanes}$ at Site 967 were 26% - 72%, suggesting considerable C4 plants cover throughout the past 23 kyrs including AHP. $\delta D_{n\text{-}alkanes}$ at Site 967 co-varied with summer insolation change at 20°N, exhibiting negative shift during AHP. Such trend is

common in North and Central Africa: EMS off Israel (Castañeda et al., 2016); Congo Basin (Schefuß et al., 2005); Gulf of Aden (Tierney and de Menocal, 2013); Lake Tanganyika (Tierney et al., 2008); and Lake Victoria (Berke et al., 2012). All of these $\delta D_{n\text{-alkanes}}$ data suggest high precipitation and strong moisture advection in the regions of watershed area of Nile River during AHP. Vegetation influences on available amount of precipitation by modulating surface evaporation so called vegetation-precipitation feedback (e.g., Ruddiman, 2001). For instance, surface evaporation increases when vegetation replaces grasses with trees (Liu et al., 2010). During AHP, less negative $\delta^{13}C_{n\text{-alkanes}}$ and highly depleted $\delta D_{n\text{-alkanes}}$ at Site 967 suggest an expansion of vegetation cover in watershed areas of Nile River with predominant C4 annual grasses. Savanna-like ecosystem with annual grasses and shrubs is a feature of "Green Sahara" during AHP (Hoelzmann et al., 1998; van Helmond et al., 2015). This implies weak vegetation-precipitation feedback in watershed areas of Nile River even during AHP.

2.4.3. Paleovegetation and Hydroclimate Changes during the Last 23 kyr

2.4.3.1. LGM (23 - 19 ka)

Enriched $\delta D_{n\text{-alkanes}}$ at Site 967 and many places in and around North Africa (Castañeda et al., 2016) indicated aridity and low precipitation in the watershed areas of Nile River during LGM. Under arid environment with weak precipitation, atmospheric moisture source is depending on local evaporation (Trenberth, 1999). Ancient sand dune distributions suggest that the Sahara Desert extended hundreds of kilometers further south than at present, the result being an equatorward contraction of vegetation zones (Hooghiemstra et al., 1992) because of southward migration of ITCZ by weakened summer monsoon (Brovkin et al., 1998). Increased aeolian dust transport from the Sahara Desert into the eastern Mediterranean Sea is also suggested by the abundant hematite content at Site 967 (Larrasoaña et al., 2003). A major retreat of rainforest during the LGM occurred; during that time, the rainforest was replaced by savanna and grassland vegetation (Runge, 1996). Annual precipitation in the eastern Congo Basin during the LGM is estimated to be 1000 mm, significantly lower than the current annual precipitation of 2000–2400 mm (Runge, 1996). Lakes Victoria and Albert, sources of the Nile River, recorded low lake levels due to extreme aridification during the LGM (Talbot and Laerdal, 2000; Williams et al., 2006). Pollen records at Core 9509 from EMS imply low arboreal pollen and abundance of C4 grasses, mainly Chenopodiaceae, Amaranthaceae (Artemisia monosperma), and Ephedra distachya, which represent steppe, saline desert, littoral sand belt, and marshy ecosystems (Langgut et al., 2011). These results suggest that the desert and semi-arid savanna ecosystems expanded during the LGM (Rommerskirchen et al., 2006).

On the contrary, glacial $\delta^{13}C_{n\text{-alkanes}}$ at Site 967 showed relatively negative values compared to the other period and estimated C4 plants contribution were ranging from 44% to 53% (Fig. 2.5). These data suggest a significant contribution of C3 plants for n-alkanes in sediments at Site 967 during LGM. A possible explanation is that considerable portion of n-alkanes were transported from the up-stream region of the Nile River.

Last glacial termination is characterized by millennial-scale abrupt climate events such as Heinrich event I, Bølling-Allerød warming, and Younger Dryas event. Castañeda et al. (2016) summarized $\delta D_{n\text{-alkanes}}$ records in and around North Africa since LGM and indicated aridity during Heirinch Stadial I (HS1) and Younger Dryas (YD) based on pronounced positive shifts of $\delta D_{n\text{-alkanes}}$. Our Site 967 data also indicates the pronounced two $\delta D_{n\text{-alkanes}}$ peaks (Fig. 2.4 and 2.5), likely to be corresponding to HS1 and YD regardless of lack of age control point.

2.4.3.2. AHP (15 - 5 ka)

As the monsoon intensified during the early Holocene insolation maximum, precipitation in North Africa increased with northward migration of ITCZ after HS1. This period is known as AHP (deMenocal et al., 2000) and was characterized by almost complete vegetation cover with annual grasses and shrubs in the present Saharan Desert (e.g., COHMAP Members, 1988; deMenocal et al., 2000; deMenocal and Tierney, 2012). The transition from dry to humid conditions archived in lake level in Lake Tana (Lamb et al., 2007) and Lake Victoria (Talbot and Laerdal, 2000). Drastic negative shift of $\delta D_{n\text{-alkanes}}$ (>40‰) were observed at Site 967 after YD, marking AHP peak when Sahara Desert was greening under humid condition (i.e., increasing of rainfall amount and migration of ITCZ more northward). Such large negative shift of $\delta D_{n\text{-alkanes}}$ denotes strong precipitation and moisture advection from far distance.

AHP peak from 11 ka to 7 ka identified by the most depleted $\delta D_{n\text{-alkanes}}$ is coincident with sapropel S1 layer formation. Sapropels (organic carbon–rich sediments) deposited periodically within Plio-Pleistocene sediments of the Mediterranean Sea are paced by the precessional cycle of Earth (e.g., Cramp and O'Sullivan, 1999). Freshwater discharge from North Africa into the Mediterranean Sea, fueled by an intensified monsoon, plays a crucial role in sapropel formation (Rohling et al., 2015). Sapropel S1 is the most recent sapropel layer deposited during the early-to-middle Holocene. The age of the top and bottom of the sapropel S1 layer is well determined (10.8 ± 0.4 to 6.1 ± 0.5 ka; De Lange et al., 2008). At Site 967, n-alkane concentrations were notably high during the sapropel S1 interval, and there were two concentration peaks (Fig. 2.3). Onset of the sapropel S1 layer formation started at 135 cm at Site 967, followed by the first n-alkane concentration peak at 130 cm. Significantly high

sedimentary concentrations of n-alkanes suggest optimal preservation of biomarkers (Menzel et al., 2003).

During AHP peak, $\delta^{13}C_{n\text{-}alkanes}$ at Site 967 showed relatively positive values and estimated C4 plants contribution were ranging from 55 to 72% (Fig. 2.5), suggesting flourishing of C4 plants. Pollen assemblage at Core 9509 indicated that total trees increased since 15 ka, reaching a maximum of 20% from several percent (Langgut et al., 2011). Regardless of the increase in tree pollens, majority of pollen assemblages at Core 9509 was grasses such as Cyperaceae. Pollen records at core PS009PC also suggest abundant annual C4 grasses during AHP (van Helmond et al., 2015). The predominant C4 plants during AHP peak indicates an expansion of savanna grassland ecosystems in North Africa and suppresses a mobilization of Saharan dust. Low Ti/Al ratio and hematite contents (Larrasoaña et al., 2003) as well as elevated Ba/Al ratio (Azrieli-Tal et al., 2014) at Site 967 support a deflation of aeolian dust during AHP peak due to migration of ITCZ more northward.

During the termination of AHP since 7 ka, $\delta D_{n\text{-}alkanes}$ signature gradually enriched, suggesting onset of aridification in North Africa as a result of southward migration of ITCZ and decreasing of rainfall amount. Pollen records (van Helmond et al., 2015) and increases in Ti/Al ratios and hematite contents (Larrasoaña et al., 2003) also indicate less wet environments. Compared to AHP peak, contribution of C4 plants decreased, suggesting shrink of green Sahara with flourished C4 grasses. This leads to a formation of today's arid Sahara Desert (Gasse, 2000).

2.4.3.3. Middle to Late Holocene (Last 5 kyrs)

Gradually enriched $\delta D_{n\text{-}alkanes}$ at Site 967 suggest progressive aridification in catchment areas of Nile River since 5 ka. Decline of lake level and long-term drying were reported in Lake Tana (Marshall et al., 2009), African Sahel (Said, 1993), and East Africa rift valley lakes (Grasse and Van Campo, 1994). Majority of tropical and subtropical African regions were shifted to a drier condition owing to the change of precipitation regimes and increase of evaporation (Marchant et al., 2004). In Kenya, pollen assemblages in sediments from Lake Bogoria, Mount Kenya, and Mount Elgon since ~5 ka have been more drought-adapted species than high-altitude forest species (Hamilton, 1982; Street-Perrott and Robert, 1983; Vincens, 1986). Slightly increased Artemisia (Langgut et al., 2011) and increased Ti/Al ratios and hematite contents (Larrasoaña et al., 2003; Konijnendijk et al., 2014) are consistent with dryer conditions in North Africa by comparing with AHP.

$\delta^{13}C_{n\text{-}alkanes}$ at Site 967 fluctuated at millennial timescale during the last 5 kyrs. The $\delta^{13}C_{n\text{-}alkanes}$ record was inconsistent with progressive aridification suggested by enriched $\delta D_{n\text{-}alkanes}$. Estimated C4 plants contribution was ranging from 42 to 70% (Fig. 2.5), suggesting that an origin of n-alkanes in sediments at Site 967 were approximately equally contributed by C3 and C4 plants. With prevailing

desertification in North Africa, transition of vegetation from green Sahara with C4 annual grasses (i.e. savannah-like ecosystem) to present barren Sahara Desert has been occurred. Since Middle-Holocene, ITCZ shifted southward with millennial and sub-millennial-scale oscillations (Haug et al., 2001; Fleitmann et al., 2007). Marriner et al. (2012) demonstrated that development of the Nile's catchment has been controlled by a precipitation change in East Africa driven by a millennial-scale southern displacement of the ITCZ. Although our age model for sediment core at Site 967 is unable to constrain the detailed timings, source of the $\delta^{13}C_{n\text{-}alkanes}$ must have been influenced by the latitudinal shift of ITCZ. When desertification proceeds in North Africa, upstream region of the Nile watershed area such as the Ethiopian Highland becomes an important source of n-alkanes source. Consequently, $\delta^{13}C_{n\text{-}alkanes}$ change at Site 967 was not in harmony with the $\delta D_{n\text{-}alkanes}$.

2.5. Conclusions

Hydroclimatic and vegetation changes of watershed areas of the Nile River in northeast Africa during the past 23 kyr BP were reconstructed based on n-alkane molecular distributions and their hydrogen and carbon isotopes in ODP 967 sediments from the EMS. $\delta D_{n\text{-}alkanes}$, a proxy for precipitation co-varied with precessional orbital forcing, while the $\delta^{13}C_{n\text{-}alkanes}$ showed millennial-scale variation and no harmony with orbital forcing. During LGM, the watershed areas of Nile River were arid but considerable portion of n-alkanes in sediments at Site ODP 967 was derived from C3 plants. This suggests that the major source of the n-alkanes was in the up-stream region of the Nile River. During AHP peak, $\delta^{13}C_{n\text{-}alkanes}$ at Site 967 showed relatively positive values suggesting greening of Sahara Desert prevailed by C4 plants as a result of increased rainfall by northward migration of ITCZ. Since AHP termination at ~7 ka, gradually enriched $\delta D_{n\text{-}alkanes}$ signature indicated progressive aridification in North Africa. The $\delta^{13}C_{n\text{-}alkanes}$ record during the last 5 kyrs fluctuated at millennial and sub-millennial timescale, inconsistent with enriched $\delta D_{n\text{-}alkanes}$. When desertification proceeds in North Africa, upstream region of the Nile watershed area such as the Ethiopian Highland becomes an important source of n-alkanes source. Consequently, $\delta^{13}C_{n\text{-}alkanes}$ change at Site 967 was not in harmony with the $\delta D_{n\text{-}alkanes}$.

References

Azrieli-Tal, I., Matthews, A., Bar-Matthews, M., Almogi-Labin, A., Vance, D., Archer, C., Teutsch, N., 2014. Evidence from molybdenum and iron isotopes and molybdenum-uranium covariation for sulphidic bottom waters during Eastern Mediterranean sapropel S1 formation. Earth Planet. Sci. Lett. 393, 231–242. doi:10.1016/j.epsl.2014.02.054

Bar-Matthews, M., Ayalon, A., Gilmour, M., Matthews, A., Hawkesworth, C.J., 2003. Sea - land

oxygen isotopic relationships from planktic foraminifera and speleothems in the Eastern Mediterranean region and their implication for paleorainfall during interglacial intervals. Geochim. Cosmochim. Acta 67, 3181–3199. doi:10.1016/S0016-7037(02)01031-1

Bar-Matthews, M., Ayalon, A., Kaufman, A., 2000. Timing and hydrological conditions of Sapropel events in the Eastern Mediterranean, as evident from speleothems, Soreq cave, Israel, in: Chemical Geology. Elsevier, pp. 145–156. doi:10.1016/S0009-2541(99)00232-6

Barker, P.A., Talbot, M.R., Street-Perrott, F.A., Marret, F., Scourse, J., Odada, E.O., 2004. Late Quaternary climatic variability in intertropical Africa, in: Past Climate Variability through Europe and Africa. Springer Netherlands, Dordrecht, pp. 117–138. doi:10.1007/978-1-4020-2121-3_7

Brovkin, V., Martin Claussen, B., Petoukhov, V., 1998. On the stability of the atmosphere-vegetation system in the Sahara/Sahel region. J. Geophys. Res. 103624, 613–31. doi:10.1029/1998JD200006

Brown, W. V., 1975. Variations in Anatomy , Associations , and Origins of Kranz Tissue ’. Am. J. Bot. 62, 395–402. doi:10.2307/2442093

Castañeda, I.S., Schouten, S., Pätzold, P., Lucassen, F., Kasemann, S., Kuhlmann, H., Schefuß, E., 2016. Hydroclimate variability in the Nile River Basin during the past 28,000 years. Earth Planet. Sci. Lett. 438, 47–56. doi:10.1016/j.epsl.2015.12.014

Claussen, M., Brovkin, V., Ganopolski, A., Kubatzki, C., Petoukhov, V., 1998. Modelling global terrestrial vegetation-climate interaction. Philos. Trans. R. Soc. B Biol. Sci. 353, 53–63. doi:10.1098/rstb.1998.0190

COHMAP MEMBERS, 1988. Climatic Changes of the Last 18,000 Years: Observations and Model Simulations. Science (80-.). 241, 1043–1052. doi:10.1126/science.241.4869.1043

Cranwell, P.A., 1973. Chain-length distribution of n-alkanes from lake sediments in relation to post-glacial environmental change. Freshw. Biol. 3, 259–265. doi:10.1111/j.1365-2427.1973.tb00921.x

Dansgaard, W., 1964. Stable isotopes in precipitation. Tellus 16, 436–468. doi:10.3402/tellusa.v16i4.8993

De Lange, G.J., Thomson, J., Reitz, A., Slomp, C.P., Speranza Principato, M., Erba, E., Corselli, C., 2008. Synchronous basin-wide formation and redox-controlled preservation of a Mediterranean sapropel. Nat. Geosci. 1, 606–610. doi:10.1038/ngeo283

Delucia, E.H., Schlesinger, W.H., Billings, W.D., 1988. Water relations and the maintenance of Sierran conifers on hydrothermally altered rock. Ecology. doi:10.2307/1940428

deMenocal, P., Ortiz, J., Guilderson, T., Adkins, J., Sarnthein, M., Baker, L., Yarusinsky, M., 2000. Abrupt onset and termination of the African Humid Period: Rapid climate responses to gradual insolation forcing, in: Quaternary Science Reviews. pp. 347–361. doi:10.1016/S0277-

3791(99)00081-5

DeMenocal, P., Tierney, J.E., 2012. Green Sahara: African Humid Periods Paced by Earth's Orbital Changes. Nat. Educ. Knowl. 3, 12.

Dupont, L.M., Rommerskirchen, F., Mollenhauer, G., Schefuß, E., 2013. Miocene to Pliocene changes in South African hydrology and vegetation in relation to the expansion of C4 plants. Earth Planet. Sci. Lett. 375, 408–417. doi:10.1016/j.epsl.2013.06.005

Eglinton, T.I., Eglinton, G., 2008. Molecular proxies for paleoclimatology. Earth Planet. Sci. Lett. 275, 1–16. doi:10.1016/j.epsl.2008.07.012

Emeis, K.-C., Schulz, H.-M., Struck, U., Sakamoto, T., Doose, H., Erlenkeuser, H., Howell, M.W., Kroon, D., Paterne, M., 1998. Stable isotope and alkenone temperature record of sapropels from sites 964 and 967: constraining the physical environment of sapropel formation in the Eastern Mediterranean Sea, in: Proceedings of the Ocean Drilling Program, Scientific Results. pp. 309–331. doi:10.1161/01.RES.66.4.883

Emeis, K.C., Robertson, a H.F., Richter, C., Al., E., 1996. Shipboard Scientific Party Site 967. Proc. Ocean Drill. Program, Initial Reports 160, 215–287.

Emeis, K.C., Sakamoto, T., Wehausen, R., Brumsack, H.J., 2000. The sapropel record of the eastern Mediterranean Sea - Results of Ocean Drilling Program Leg 160, in: Palaeogeography, Palaeoclimatology, Palaeoecology. pp. 371–395. doi:10.1016/S0031-0182(00)00059-6

Farquhar, G.D., Ehleringer, J.R., Hubick, K.T., 1989. Carbon Isotope Discrimination and Photosynthesis. Annu. Rev. Plant Physiol. Plant Mol. Biol. 40, 503–537. doi:10.1146/annurev.pp.40.060189.002443

Feakins, S.J., Eglinton, T.I., DeMenocal, P.B., 2007. A comparison of biomarker records of northeast African vegetation from lacustrine and marine sediments (ca. 3.40 Ma). Org. Geochem. 38, 1607–1624. doi:10.1016/j.orggeochem.2007.06.008

Feakins, S.J., Sessions, A.L., 2010. Controls on the D/H ratios of plant leaf waxes in an arid ecosystem. Geochim. Cosmochim. Acta 74, 2128–2141. doi:10.1016/j.gca.2010.01.016

Ficken, K.J., Li, B., Swain, D.L., Eglinton, G., 2000. An n-alkane proxy for the sedimentary input of submerged/floating freshwater aquatic macrophytes, in: Organic Geochemistry. Pergamon, pp. 745–749. doi:10.1016/S0146-6380(00)00081-4

Fontugne, M.R., Calvert, S.E., 1992. Late Pleistocene Variability of the Carbon Isotopic Composition of Organic Matter in the Eastern Mediterranean: Monitor of Changes in Carbon Sources and Atmospheric CO2 Concentrations. Paleoceanography 7, 1–20. doi:10.1029/91PA02674

Gasse, F., 2000. Hydrological changes in the African tropics since the Last Glacial Maximum, in: Quaternary Science Reviews. pp. 189–211. doi:10.1016/S0277-3791(99)00061-X

Ginoux, P., Prospero, J.M., Gill, T.E., Hsu, N.C., Zhao, M., 2012. Global-scale attribution of anthropogenic and natural dust sources and their emission rates based on MODIS Deep Blue aerosol products. Rev. Geophys. doi:10.1029/2012RG000388

Good, S.P., Caylor, K.K., 2011. Climatological determinants of woody cover in Africa. Proc. Natl. Acad. Sci. 108, 4902–4907. doi:10.1073/pnas.1013100108

Grasse, F., Van Campo, A., 1994. Abrupt post-glacial climate events in West Asia and North Africa monsoon domins. Earth Planet. Sci. Lett. 126. 126, 435,456.

Hatch, M.D., Slack, C.R., 1966. Photosynthesis by sugar-cane leaves. A new carboxylation reaction and the pathway of sugar formation. Biochem. J. 101, 103–11.

Hayes, J.M., Freeman, K.H., Popp, B.N., Hoham, C.H., 1990. Compound-specific isotopic analyses: A novel tool for reconstruction of ancient biogeochemical processes. Org. Geochem. 16, 1115–1128. doi:10.1016/0146-6380(90)90147-R

Hinrichs, K.-U., Rullkotter, J., 1997. Terrigenous and marine lipids in Amazon Fan sediments: implications for sedimentological reconstructions. Proc. Ocean Drill. Progr. Sci. Results 155, 539–553. doi:10.2973/odp.proc.sr.155.238.1997

Hoelzmann, P., Jolly, D., Harrison, S.P., Laarif, F., Bonnefille, R., Pachur, H.J., 1998. Mid-Holocene land-surface conditions in northern Africa and the Arabian peninsula: A data set for the analysis of biogeophysical feedbacks in the climate system. Global Biogeochem. Cycles 12, 35–51. doi:10.1029/97GB02733

Hooghiemstra, H., Stalling, H., Agwu, C.O.C., Dupont, L.M., 1992. Vegetational and climatic changes at the northern fringe of the sahara 250,000-5000 years BP: evidence from 4 marine pollen records located between Portugal and the Canary Islands. Rev. Palaeobot. Palynol. 74. doi:10.1016/0034-6667(92)90137-6

Huang, Y., Street-Perrott, F.A., Metcalfe, S.E., Brenner, M., Moreland, M., Freeman, K.H., 2001. Climate change as the dominant control on glacial-interglacial variations in C3 and C4 plant abundance. Science 293, 1647–51. doi:10.1126/science.1060143

Jensen, R.G., Bhar, J.T., 1977. RIBULOSE 1,5-BISPHOSPHATE CARBOXYLASE-OXYGENASE. Ann. Rev Plant Physiol 28, 379–400. doi:10.1146/annurev.pp.28.060177.002115

Junginger, A., Trauth, M.H., 2013. Hydrological constraints of paleo-Lake Suguta in the Northern Kenya Rift during the African Humid Period (15-5kaBP). Glob. Planet. Change 111, 174–188. doi:10.1016/j.gloplacha.2013.09.005

Kadereit, G., Borsch, T., Weising, K., Freitag, H., 2003. Phylogeny of Amaranthaceae and Chenopodiaceae and the Evolution of C 4 Photosynthesis. Int. J. Plant Sci. 164, 959–986. doi:10.1086/378649

Kahmen, A., Hoffmann, B., Schefuß, E., Arndt, S.K., Cernusak, L.A., West, J.B., Sachse, D., 2013. Leaf water deuterium enrichment shapes leaf wax n-alkane δD values of angiosperm plants II: Observational evidence and global implications. Geochim. Cosmochim. Acta 111, 50–63. doi:10.1016/j.gca.2012.09.004

Kallel, N., Duplessy, J.C., Labeyrie, L., Fontugne, M., Paterne, M., Montacer, M., 2000. Mediterranean pluvial periods and sapropel formation over the last 200 000 years. Palaeogeogr. Palaeoclimatol. Palaeoecol. 157, 45–58. doi:10.1016/S0031-0182(99)00149-2

Kallel, N., Paterne, M., Labeyrie, L., Duplessy, J.C., Arnold, M., 1997. Temperature and salinity records of the Tyrrhenian Sea during the last 18,000 years. Palaeogeogr. Palaeoclimatol. Palaeoecol. 135, 97–108. doi:10.1016/S0031-0182(97)00021-7

Krom, M.D., Cliff, R.A., Eijsink, L.M., Herut, B., Chester, R., 1999. The characterisation of Saharan dusts and Nile particulate matter in surface sediments from the Levantine basin using Sr isotopes. Mar. Geol. 155, 319–330. doi:10.1016/S0025-3227(98)00130-3

Kroon, D., Alexander, I., Little, M., Lourens, L.J., Matthewson, A., Robertson, A.H.F., Sakamoto, T., 1998. Oxygen isotope and sapropel stratigraphy in the Eastern Mediterranean during the last 3.2 million years. Proc. Ocean Drill. Program, Sci. Results 160, 181–189. doi:10.2973/odp.proc.sr.160.071.1998

Kuechler, R.R., Schefuß, E., Beckmann, B., Dupont, L., Wefer, G., 2013. NW African hydrology and vegetation during the Last Glacial cycle reflected in plant-wax-specific hydrogen and carbon isotopes. Quat. Sci. Rev. 82, 56–67. doi:10.1016/j.quascirev.2013.10.013

Lamb, H.F., Bates, C.R., Coombes, P. V, Marshall, M.H., Umer, M., Davies, S.J., Dejen, E., 2007. Late Pleistocene desiccation of Lake Tana, source of the Blue Nile. Quat. Sci. Rev. 26, 287–299. doi:10.1016/j.quascirev.2006.11.020

Larrasoana, J.C., Roberts, A.P., Rohling, E.J., Winklhofer, M., Wehausen, R., 2003. Three million years of monsoon variability over the northern Sahara. Clim. Dyn. 21, 689–698. doi:10.1007/s00382-003-0355-z

Liu, Z., Notaro, M., Gallimore, R., 2010. Indirect vegetation-soil moisture feedback with application to Holocene North Africa climate1. Glob. Chang. Biol. 16, 1733–1743. doi:10.1111/j.1365-2486.2009.02087.x

Lüttge, U., 2004. Ecophysiology of Crassulacean Acid Metabolism (CAM). Ann. Bot. doi:10.1093/aob/mch087

Magny, M., Miramont, C., Sivan, O., 2002. Assessment of the impact of climate and anthropogenic factors on Holocene Mediterranean vegetation in Europe on the basis of palaeohydrological records. Palaeogeogr. Palaeoclimatol. Palaeoecol. 186, 47–59. doi:10.1016/S0031-

0182(02)00442-X

Marshall, M.H., Lamb, H.F., Davies, S.J., Leng, M.J., Kubsa, Z., Umer, M., Bryant, C., 2009. Climatic change in northern Ethiopia during the past 17,000 years: A diatom and stable isotope record from Lake Ashenge. Palaeogeogr. Palaeoclimatol. Palaeoecol. 279, 114–127. doi:10.1016/j.palaeo.2009.05.003

Maslin, M.A., Pancost, R.D., Wilson, K.E., Lewis, J., Trauth, M.H., 2012. Three and half million year history of moisture availability of South West Africa: Evidence from ODP site 1085 biomarker records. Palaeogeogr. Palaeoclimatol. Palaeoecol. 317–318, 41–47. doi:10.1016/j.palaeo.2011.12.009

Menzel, D., Schouten, S., Van Bergen, P.F., Damsté, J.S.S., 2004. Higher plant vegetation changes during Pliocene sapropel formation, in: Organic Geochemistry. Pergamon, pp. 1343–1353. doi:10.1016/j.orggeochem.2004.02.011

Menzel, D., Van Bergen, P.F., Schouten, S., Sinninghe Damsté, J.S., 2003. Reconstruction of changes in export productivity during Pliocene sapropel deposition: A biomarker approach. Palaeogeogr. Palaeoclimatol. Palaeoecol. 190, 273–287. doi:10.1016/S0031-0182(02)00610-7

Michener, R.H., Lajtha, K., 2007. Stable isotopes in ecology and environmental science, Ecological methods and concepts series. doi:10.1899/0887-3593-028.002.0516

Moulin, C., Lambert, C.E., Dulac, F., Dayan, U., 1997. Control of atmospheric export of dust from North Africa by the North Atlantic Oscillation. Nature 387, 691–694. doi:10.1038/42679;

Muhaidat, R., Sage, R.F., Dengler, N.G., 2007. Diversity of Kranz anatomy and biochemistry in C4 eudicots. Am. J. Bot. 94, 362–381. doi:10.3732/ajb.94.3.362

Niedermeyer, E.M., Schefuß, E., Sessions, A.L., Mulitza, S., Mollenhauer, G., Schulz, M., Wefer, G., 2010. Orbital- and millennial-scale changes in the hydrologic cycle and vegetation in the western African Sahel: Insights from individual plant wax δD and δ13C. Quat. Sci. Rev. 29, 2996–3005. doi:10.1016/j.quascirev.2010.06.039

Nott, C.J., Xie, S., Avsejs, L.A., Maddy, D., Chambers, F.M., Evershed, R.P., 2000. n-Alkane distributions in ombrotrophic mires as indicators of vegetation change related to climatic variation. Org. Geochem. 31, 231–235. doi:10.1016/S0146-6380(99)00153-9

Pagani, M., Freeman, K.H., Arthur, M.A., 2000. Isotope analyses of molecular and total organic carbon from Miocene sediments. Geochim. Cosmochim. Acta 64, 37–49. doi:10.1016/S0016-7037(99)00151-9

Reading, H.G., Richards, M., 1974. Turbidite Systems in Deep-Water Basin Margins Classified by Grain Size and Feeder System 1. Am. Assoc. Pet. Geol. Bull. 78, 792–822.

Risi, C., Bony, S., Vimeux, F., 2008a. Influence of convective processes on the isotopic composition

(δ18O and δD) of precipitation and water vapor in the tropics: 2. Physical interpretation of the amount effect. J. Geophys. Res. Atmos. 113, D19306. doi:10.1029/2008JD009943

Risi, C., Bony, S., Vimeux, F., Descroix, L., Ibrahim, B., Lebreton, E., Mamadou, I., Sultan, B., 2008b. What controls the isotopic composition of the African monsoon precipitation? Insights from event-based precipitation collected during the 2006 AMMA field campaign. Geophys. Res. Lett. 35, L24808. doi:10.1029/2008GL035920

Ritchie, J.C., Eyles, C.H., Haynes, C. V., 1985. Sediment and pollen evidence for an early to mid-Holocene humid period in the eastern Sahara. Nature 314, 352–355. doi:10.1038/314352a0

Rohling, E.J., 1994. Review and new aspects concerning the formation of eastern Mediterranean sapropels. Mar. Geol. 122, 1–28. doi:10.1016/0025-3227(94)90202-X

Rommerskirchen, F., Plader, A., Eglinton, G., Chikaraishi, Y., Rgen, J., Tter, R., 2006. Chemotaxonomic significance of distribution and stable carbon isotopic composition of long-chain alkanes and alkan-1-ols in C 4 grass waxes. Org. Geochem. 37, 1303–1332. doi:10.1016/j.orggeochem

Rose, C., Polissar, P.J., Tierney, J.E., Filley, T., DeMenocal, P.B., 2016. Changes in northeast African hydrology and vegetation associated with Pliocene-Pleistocene sapropel cycles. Philos. Trans. R. Soc. Lond. B. Biol. Sci. 371, 399–420. doi:10.1098/rstb.2015.0243

Rossignol-Strick, M., 1999. The Holocene climatic optimum and pollen records of sapropel 1 in the eastern Mediterranean, 9000-6000 BP. Quat. Sci. Rev. 18, 515–530. doi:10.1016/S0277-3791(98)00093-6

Rossignol-Strick, M., 1985. Mediterranean Quaternary sapropels, an immediate response of the African monsoon to variation of insolation. Palaeogeogr. Palaeoclimatol. Palaeoecol. 49, 237–263. doi:10.1016/0031-0182(85)90056-2

Runge, J., 1996. Palaeoenvironmental interpretation of geomorphological and pedological studies in the rain forest “core-areas” of eastern zaire (central africa). South African Geogr. J. 78, 91–97. doi:10.1080/03736245.1996.9713613

Sachse, D., Billault, I., Bowen, G.J., Chikaraishi, Y., Dawson, T.E., Feakins, S.J., Freeman, K.H., Magill, C.R., McInerney, F.A., van der Meer, M.T.J., Polissar, P., Robins, R.J., Sachs, J.P., Schmidt, H.-L., Sessions, A.L., White, J.W.C., West, J.B., Kahmen, A., 2012. Molecular Paleohydrology: Interpreting the Hydrogen-Isotopic Composition of Lipid Biomarkers from Photosynthesizing Organisms. Annu. Rev. Earth Planet. Sci. 40, 221–249. doi:10.1146/annurev-earth-042711-105535

Sage, R.F., 2004. The evolution of C 4 photosynthesis. New Phytol. 161, 341–370. doi:10.1046/j.1469-8137.2004.00974.x

Sage, R.F., 2001. Environmental and evolutionary preconditions for the origin and diversification of the C4 photosynthetic syndrome. Plant Biol. doi:10.1055/s-2001-15206

Said, R., 1993. The river Nile : geology, hydrology, and utilization. Pergamon.

Sakamoto, T., Janecek, T., Emeis, K.-C., 1998. 4. Continuous Sedimentary Sequences From the Eastern Mediterranean Sea: Composite Depth Sections, in: Proceedings of the Ocean Drilling Program, Scientific Results. pp. 37–59.

Sauer, P.E., Eglinton, T.I., Hayes, J.M., Schimmelmann, A., Sessions, A.L., 2001. Compound-specific D/H ratios of lipid biomarkers from sediments as a proxy for environmental and climatic conditions. Geochim. Cosmochim. Acta 65, 213–222. doi:10.1016/S0016-7037(00)00520-2

Schefuß, E., Schouten, S., Schneider, R.R., 2005. Climatic controls on central African hydrology during the past 20,000 years. Nature 437, 1003–1006. doi:10.1038/nature03945

Sinninghe Damsté, J.S., Verschuren, D., Ossebaar, J., Blokker, J., van Houten, R., van der Meer, M.T.J., Plessen, B., Schouten, S., 2011. A 25,000-year record of climate-induced changes in lowland vegetation of eastern equatorial Africa revealed by the stable carbon-isotopic composition of fossil plant leaf waxes. Earth Planet. Sci. Lett. 302, 236–246. doi:10.1016/j.epsl.2010.12.025

Street-Perrott, F.A., Huang, Y.S., Perrott, R.A., Eglinton, G., Barker, P., BenKhelifa, L., Harkness, D.D., Olago, D.O., 1997. Impact of lower atmospheric carbon dioxide on tropical mountain ecosystems. Science (80-.). 278, 1422–1426. doi:10.1126/science.278.5342.1422

Talbot, M.R., Laerdal, T., 2000. The Late Pleistocene-Holocene palaeolimnology of Lake Victoria, East Africa, based upon elemental and isotopic analyses of sedimentary organic matter. J. Paleolimnol. 23, 141–164. doi:10.1023/A:1008029400463

Trenberth, K.E., 1999. Atmospheric moisture recycling: Role of advection and local evaporation. J. Clim. 12, 1368–1381. doi:10.1175/1520-0442(1999)012<1368:AMRROA>2.0.CO;2

van Helmond, N.A.G.M., Hennekam, R., Donders, T.H., Bunnik, F.P.M., de Lange, G.J., Brinkhuis, H., Sangiorgi, F., 2015. Marine productivity leads organic matter preservation in sapropel S1: Palynological evidence from a core east of the Nile River outflow. Quat. Sci. Rev. 108, 130–138. doi:10.1016/j.quascirev.2014.11.014

Vogts, A., Moossen, H., Rommerskirchen, F., Rullkötter, J., 2009. Distribution patterns and stable carbon isotopic composition of alkanes and alkan-1-ols from plant waxes of African rain forest and savanna C3 species. Org. Geochem. 40, 1037–1054. doi:10.1016/j.orggeochem.2009.07.011

Vogts, A., Schefuß, E., Badewien, T., Rullkötter, J., 2012. n-Alkane parameters from a deep sea sediment transect off southwest Africa reflect continental vegetation and climate conditions. Org. Geochem. 47, 109–119. doi:10.1016/j.orggeochem.2012.03.011

White, F., 1983. The Vegetation of Africa [WWW Document]. Paris: UNESCO. URL

http://www.scirp.org/%28S%28351jmbntvnsjt1aadkposzje%29%29/reference/ReferencesPapers.aspx?ReferenceID=1923975 (accessed 10.5.17).

Williams, M., Talbot, M., Aharon, P., Abdl Salaam, Y., Williams, F., Inge Brendeland, K., 2006. Abrupt return of the summer monsoon 15,000 years ago: new supporting evidence from the lower White Nile valley and Lake Albert. Quat. Sci. Rev. 25, 2651–2665. doi:10.1016/j.quascirev.2005.07.019

Worden, J., Noone, D., Bowman, K., 2007. Importance of rain evaporation and continental convection in the tropical water cycle. Nature 445, 528–532. doi:10.1038/nature05508

Wu, J., Böning, P., Pahnke, K., Tachikawa, K., de Lange, G.J., 2016. Unraveling North-African riverine and eolian contributions to central Mediterranean sediments during Holocene sapropel S1 formation. Quat. Sci. Rev. 152, 31–48. doi:10.1016/j.quascirev.2016.09.029

Zech, M., Zech, R., Morr??s, H., Moretti, L., Glaser, B., Zech, W., 2009. Late Quaternary environmental changes in Misiones, subtropical NE Argentina, deduced from multi-proxy geochemical analyses in a palaeosol-sediment sequence. Quat. Int. 196, 121–136. doi:10.1016/j.quaint.2008.06.006

Zhao, M., Dupont, L., Eglinton, G., Teece, M., 2003. n-Alkane and pollen reconstruction of terrestrial climate and vegetation for N.W. Africa over the last 160 kyr. Org. Geochem. 34, 131–143. doi:10.1016/S0146-6380(02)00142-0

Table 2.1. Core ID, onboard core composite depth (mbsf, Shipboard Science Party, 1996), revised meter composite depth (rmcd, Sakamoto et al., 1998), age model (cal. kyr BP), Ba/Al ratio (Azrieli-Tal et al., 2014) and Ti/Al ratio (Azrieli-Tal et al., 2014) at ODP 967.

Core	Type	Section	W/A	Depth	Onboard core composite depth (mbsf)		Revised meter composite depth (rmcd)	Age (cal kyr BP)	Ba/Al*10^4	Ti/Al
					Top	Bottom				
1	H	1	A	0-2	0	2	3	0.2		
1	H	1	A	2-4	2	4	5	0.3		
1	H	1	A	4-6	4	6	7	0.4		
1	H	1	A	6-8	6	8	9	0.5		
1	H	1	A	8-10	8	10	11	0.7		
1	H	1	A	10-12	10	12	13	0.8		
1	H	1	A	12-14	12	14	15	0.9		
1	H	1	A	14-16	14	16	17	1		
1	H	1	A	16-18	16	18	19	1.2		
1	H	1	A	18-20	18	20	21	1.3		
1	H	1	A	20-22	20	22	23	1.4		
1	H	1	A	22-24	22	24	25	1.5		
1	H	1	A	24-26	24	26	27	1.6		
1	H	1	A	26-28	26	28	29	1.8		
1	H	1	A	28-30	28	30	31	1.9		
1	H	1	A	30-32	30	32	33	2		
1	H	1	A	32-34	32	34	35	2.1		
1	H	1	A	34-36	34	36	37	2.3		
1	H	1	A	36-38	36	38	39	2.4		
1	H	1	A	38-40	38	40	41	2.5		
1	H	1	A	40-42	40	42	43	2.6		
1	H	1	A	42-44	42	44	45	2.7		
1	H	1	A	44-46	44	46	47	2.9		
1	H	1	A	46-48	46	48	49	3		
1	H	1	A	48-50	48	50	51	3.1		
1	H	1	A	50-52	50	52	53	3.2		
1	H	1	A	52-54	52	54	55	3.4		
1	H	1	A	54-56	54	56	57	3.5		
1	H	1	A	56-58	56	58	59	3.6		
1	H	1	A	58-60	58	60	61	3.7		
1	H	1	A	60-62	60	62	63	3.8		
1	H	1	A	62-64	62	64	65	4		
1	H	1	A	64-66	64	66	67	4.1		
1	H	1	A	66-68	66	68	69	4.2		
1	H	1	A	68-70	68	70	71	4.3		
1	H	1	A	70-72	70	72	73	4.5		
1	H	1	A	72-74	72	74	75	4.6		
1	H	1	A	74-76	74	76	77	4.7		
1	H	1	A	76-78	76	78	79	4.8		
1	H	1	A	78-80	78	80	81	4.9		
1	H	1	A	80-82	80	82	83	5.1		
1	H	1	A	82-84	82	84	85	5.2	20	0.085
1	H	1	A	84-86	84	86	87	5.3		
1	H	1	A	86-88	86	88	89	5.4		
1	H	1	A	88-90	88	90	91	5.6		
1	H	1	A	90-92	92	94	95	5.7		
1	H	1	A	92-94	92	94	95	5.8		
1	H	1	A	94-96	94	96	97	5.9		
1	H	1	A	96-98	96	98	99	6		
1	H	1	A	98-100	98	100	101	6.2	24	0.106
1	H	1	A	100-102	100	102	103	6.5	24	0.074

Table 2.1. cont.

Core	Type	Section	W/A	Depth	Onboard core composite depth (mbsf)		Revised meter composite depth (rmcd)	Age (cal kyr BP)	Ba/Al*10^4	Ti/Al
					Top	Bottom				
1	H	1	A	102-104	102	104	105	6.8	24	0.073
1	H	1	A	104-106	104	106	107	7	51	0.07
1	H	1	A	106-108	106	108	109	7.3	109	0.071
1	H	1	A	108-110	108	110	111	7.6	172	0.07
1	H	1	A	110-112	110	112	113	7.8	74	0.087
1	H	1	A	112-114	112	114	115	8.1	39	0.102
1	H	1	A	114-116	114	116	117	8.4	144	0.79
1	H	1	A	116-118	116	118	119	8.7	210	0.069
1	H	1	A	118-120	118	120	121	8.9	204	0.072
1	H	1	A	120-122	120	122	123	9.2	127	0.065
1	H	1	A	122-124	122	124	125	9.5	171	0.065
1	H	1	A	124-126	124	126	127	9.7	161	0.068
1	H	1	A	126-128	126	128	129	10	92	0.073
1	H	1	A	128-130	128	130	131	10.3	50	0.075
1	H	1	A	130-132	130	132	133	10.5		
1	H	1	A	132-134	132	134	135	10.8		
1	H	1	A	134-136	134	136	137	11		
1	H	1	A	136-138	136	138	139	11.3		
1	H	1	A	138-140	138	140	141	11.5		
1	H	1	A	140-142	140	142	143	11.8		
1	H	1	A	142-144	142	144	145	12	29	0.077
1	H	1	A	144-146	144	146	147	12.2		
1	H	1	A	146-148	146	148	149	12.5	32	0.075
1	H	1	A	148-150	148	150	151	12.7		
1	H	2	A	0-2	150	152	153	13		
1	H	2	A	2-4	152	154	155	13.2		
1	H	2	A	4-6	154	156	157	13.5		
1	H	2	A	6-8	156	158	159	13.7		
1	H	2	A	8-10	158	160	161	13.9		
1	H	2	A	10-12	160	162	163	14.2		
1	H	2	A	12-14	162	164	165	14.4		
1	H	2	A	14-16	164	166	167	14.7		
1	H	2	A	16-18	166	168	169	14.9		
1	H	2	A	18-20	168	170	171	15.1		
1	H	2	A	20-22	170	172	173	15.4		
1	H	2	A	22-24	172	174	175	15.6		
1	H	2	A	24-26	174	176	177	15.9		
1	H	2	A	26-28	176	178	179	16.4		
1	H	2	A	28-30	178	180	181	17.1		
1	H	2	A	30-32	180	182	183	17.8		
1	H	2	A	32-34	182	184	185	18.6		
1	H	2	A	34-36	184	186	187	19.3		
1	H	2	A	36-38	186	188	189	20		
1	H	2	A	38-40	188	190	191	20.7		
1	H	2	A	40-42	190	192	193	21.5		
1	H	2	A	42-44	192	194	195	22.2		
1	H	2	A	44-46	194	196	197	22.9		
1	H	2	A	46-48	196	198	199	23.7		
1	H	2	A	48-50	198	200	201	24.4		

Table 2. 2. n-Alkane concentrations (ng g^{-1}) at ODP 967. Revised meter composite depth (rmcd) is by Sakamoto et al. (1998).

Revised meter composite depth (rmcd)	C24	C26	C28	C30	C32	C23	C25	C27	C29	C31	C33
3	0	5	2.8	0	0	4.8	15.8	32.7	53.7	16.6	0
5	6.4	7.5	14	3.3	0	10.6	26.7	58.6	92.9	34.8	0
7	0	5.2	2.8	0	0	4.8	14.2	33.8	44.1	8.5	0
9	0	3.4	6	4.6	4.2	0	7.8	18.1	35.2	19	0
11	0	0.9	3.4	1.3	0	0	2.4	11.4	17.3	5.4	0
13	0	0.5	3.1	1.1	0	0	0	5	9.1	0	0
15	1.7	3.2	2.5	0	0	6.8	13.1	37	55.2	4.3	0
17	4.8	3.1	2.4	0	0	14.6	11.6	24.1	30.8	4.5	0
19	3.1	3.3	2.5	0	0	6.4	10.2	16.4	23.2	3.6	0
21	3.4	3.2	2.4	0	0	4.4	8.2	10.2	12.2	3.3	0
23	2.1	2.3	2.1	0	0	4.7	8.9	14.6	17.2	0	0
25	3.4	3.8	1.8	0	0	5.5	11.3	21.8	20.1	6.8	0
27	0.5	0.5	0	0	0	1.3	3.2	6.3	3.6	1.6	0
29	1.9	2.1	0.6	0	0	3.6	6.8	9.8	7.8	0	0
31	2.5	2.6	1.1	0	0	7.7	11.1	16.3	9.5	0	0
33	0	0.8	0.1	0	0	0	1.9	4.2	2.5	0	0
35	2	2.7	3.1	0	0	8.3	12	28.9	40.7	12.3	0
37	1.6	3.2	4.6	0.7	0	3.5	13.4	40.9	84.1	35.1	0
39	2.4	2.9	3.4	0	0	5.7	11.5	31.8	60.4	25.1	0
41	7.2	8.8	10.8	4.8	0	15.8	27.9	77.6	148.4	74.2	0
43	0	0.8	0.6	0	0	2.2	4.3	14.8	29.2	7.3	0
45	0	0.3	0.7	0	0	0	7	19.7	28.4	4.3	0
47	4	4.7	3.9	0	0	6.2	20.9	37.6	53.6	8.1	0
49	0.7	1.3	1.5	0	0	4.4	5.8	16.9	32.2	5.7	0
51	0.4	1.2	2.1	0	0	1	1.9	6.9	9.6	2.8	0
53	3.5	2.7	1.9	0	0	10.7	10.3	23.7	25.5	0	0
55	1.8	2.3	1.7	0	0	5.2	9	24.8	25.5	3.6	0
57	1	2.3	2	0	0	2.2	8.9	30.9	35.4	7.8	0
59	0	0.5	0.8	0	0	0	0	4.6	6.3	0	0
61	9.1	8.9	7.3	2.5	0	8.2	24.2	60	68.6	36.3	0
63	4.9	6.8	6.4	1.9	0	10.2	25.7	63.4	69.6	22.1	0
65	3.7	5.7	5.9	2.2	0	8.1	21.9	54	66.9	27.9	0
67	4.2	4.7	4.9	1.3	0	8.1	16.8	36.9	65.9	26.7	0
69	6.3	5.4	4.1	0	0	14.8	18.6	36.1	55.8	20.1	0
71	7.2	5.3	4.8	1	0	6.8	17.5	38.2	72.8	29.5	0
73	4.1	6.2	6.4	2	0	8.4	19.5	43.8	80.4	36.4	0
75	4	5.3	5	1.1	0	9.4	18.9	41.7	68.3	21.9	0
77	2.1	2.6	2.5	0	0	4	10.4	25.6	42.7	10.7	0
79	11.3	11.8	9.6	2.2	0	15.7	34.6	65.6	109	45.5	0
81	8.4	6.4	4.6	0	0	11.2	23.8	39.4	69	27.9	0
83	2.8	2.9	2.7	0	0	5.6	13.2	28.8	45	11.2	0
85	0.5	0.9	0.3	0	0	0	5.2	12.5	12.9	2.3	0
87	2.3	2.6	2.6	0	0	5	9.2	21.9	29.1	9.4	0
89	0	0.5	0.2	0	0	0	3.1	9.3	12.7	1.4	0
91	2.2	3.1	2.7	0	0	4	12	25.3	30.6	8.4	0
95											
95	7.4	11.7	13.5	6.4	0	13.1	36.8	85	127.7	69.4	6.7
97	5.1	9.5	13.4	6.4	0	8.9	30.5	87.5	187.5	96.3	5
99	2.4	3.3	4.2	1.1	0	4.5	14.7	39.6	87.9	32.7	0
101	11.2	42.3	24.1	11.7	0	16.1	51.4	120.5	204.8	121.2	8.9
103	9	15.3	14.7	7.5	0	10.5	41.4	90.5	160.6	93.3	3.4
105	7.7	25.7	11.2	4.7	0	8.9	31.1	70.4	125.7	71.2	0
107	6.9	8.7	6.2	1.4	0	6.3	24	51	80.4	32.1	0
109	0	26	33	16.2	2.6	24.6	69.3	156.3	277.6	195.6	15
111	0	69	95.6	65.8	15.5	67.8	173.2	377.2	642.8	515.1	83.6

Table 2. 2. cont.

Revised meter composite depth (rmcd)	C24	C26	C28	C30	C32	C23	C25	C27	C29	C31	C33
113	0	34.1	50.7	31.8	7.1	36	95.8	240.5	480.5	318.6	42.6
115	0	12.2	13.3	7.6	2.2	90.5	214.7	463.8	728.7	587.5	95.1
117	0	43.1	45.9	19	3.8	45.5	100.4	231	326.7	209.1	18.6
119	0	17.7	18.6	6.4	0	24.8	56.9	111.7	179.8	94.6	2.6
121	0	3.3	3.8	1.5	0	4.8	11.7	31.7	55.5	33.7	0
123	0	62.4	70.4	37.8	6.3	59	122.6	263.6	406.6	276.1	27.9
125	0	42.5	53.7	25	4.5	46.6	96.4	219.6	357	248.9	23.9
127	0	49.1	51.7	23.9	0	56.5	104.8	259.3	337.8	211.1	20.6
129	0	51.6	58.7	29.4	6	55.6	110.2	292.1	424	296.8	40
131	0	3.6	3.4	1	0	4.9	12.8	29	48	18.8	0
133	0	7.6	8.5	3.1	0	5.3	22.1	48.7	88.9	40.8	0
135	0	1.6	1.2	0	0	2.2	6.4	17	29.3	8	0
137	0	2	1.6	0	0	3.1	7.6	16.3	22.1	4.7	0
139	0	6.2	6.1	2.4	0	6.6	17.3	42.9	69	22.3	0
141	0	1.1	1.1	0	0	0	3.9	13.1	25.5	4.5	0
143	0	0.9	2.6	0	0	0.4	3.6	12.3	20.4	3.8	0
145	0.5	0.9	0.8	0	0	0	3.8	11.5	19.9	4.2	0
147	4.3	3.6	4.3	1.5	0	4.2	13	32.8	67.1	25.4	0
149	2.4	4.3	4.3	1.4	0	4.1	12.3	27.6	54.9	17.5	0
151	1.7	4.3	3.9	0	0	2.6	5.6	21.9	48.3	11.8	0
153	0.3	1	1.5	0	0	1.2	3.7	16	39.3	10.2	0
155	5.8	9.1	9.9	2.9	0	9.4	26.9	68.9	117.5	40.9	0
157	0.3	1.3	1.2	0	0	1.3	7.3	19	24.1	9.3	0
159	0.8	2	2.5	0	0	1	8.2	26.8	52	22.7	0
161	2.4	3.4	4	1.6	0	4.3	11.5	36.4	82.3	29.3	0
163	0	1.1	2.5	0	0	2.2	3.3	17.8	49.6	9.9	0
165	5.8	6.7	2.5	2.5	0	7.4	21.3	48.2	76.4	30	2.3
167	1.8	2.3	2.8	1.4	0	2.6	7.2	20.6	44.8	13.8	0
169	1.6	3.3	3.8	1.4	0	3.9	10.1	25.4	42	13.7	0
171	0.2	0.3	0.3	0	0	0.7	1.9	4.1	7.3	1	0
173	1.2	2	1.8	0.6	0	2.1	5.3	11.4	19.1	6.5	0.5
175											
177	0	0.2	0.2	0	0	0.2	1.5	4	10.1	2.2	0
179	3	5.1	5.1	9	0	5.3	12.9	29.4	65.3	32.45	2.4
181	0	0.6	0.4	0	0	0.6	2.6	7.7	17.4	0	0
183	2.4	3.7	2.8	0	0	4.3	8.3	15.7	30.8	12.3	0
185	2.8	3.1	3.1	0.9	0	4.8	9.7	23.8	57.5	15.6	0
187	0.4	0.4	0.4	0	0	1.6	2	6.1	18.5	3.3	0
189	0.1	0.4	0.6	0	0	0.3	3.1	8.1	21.3	4.4	0
191	0	0.5	1.4	0	0	0.4	3.7	9.8	23.6	6.6	0.5
193	0	0	2.2	0	0	0	4.4	11.5	25.8	8.7	0
195	4.3	7.9	6.8	0	0	6.6	21.9	44.1	73.5	21.5	0
197	3.4	4.6	3.4	0	0	5.1	15.8	31.6	67.7	25.7	0
199	2.5	4.1	5.5	3.1	0	3.7	10	25.6	54.1	36.2	6.3
201	4.7	8.8	10.4	6.6	0	7.4	21.9	50.8	107.2	71	12.1

Table 2. 3. Carbon and hydrogen isotope ratio of n-alkanes at ODP 967. Revised meter composite depth (rmcd) is by Sakamoto et al. (1998).

Revised meter composite depth (rmcd)	Carbon isotope ratio (‰ VPDB)						Hydrogen isotope ratio (‰ VSMOW)		
	C23	C25	C27	C29	C31	C33	C27	C29	C31
3	-26.9	-27.9	-30.4	-29.9	-28.1				
5	-27.7	-28.9	-30.7	-31.0	-28.2		-127	-135	-138
7	-26.9	-27.5	-30.2	-29.4	-27.9	-26.4			
9									
11	-26.4	-27.7	-29.8	-29.0	-27.6				
13									
15									
17	-26.9	-28.9	-30.4	-29.4	-28.2				
19									
21									
23									
25	-27.8	-28.0	-30.2	-29.2	-29.5				
27	-29.2	-27.0	-29.1	-28.0					
29									
31									
33									
35	-28.5	-29.4	-31.8	-31.5	-30.1				
37							-146	-142	-150
39	-28.7	-29.2	-32.0	-31.5	-29.7				
41							-147	-156	-153
43	-28.4	-29.3	-31.8	-31.2	-29.2				
45									
47	-29.2	-28.9	-31.5	-30.7	-28.6				
49							-139	-133	-136
51	-28.5	-29.0	-30.5	-29.0	-26.7				
53									
55	-26.3	-28.1	-30.3	-29.0	-27.0				
57									
59									
61							-152	-149	-154
63	-26.9	-28.0	-30.3	-29.4	-26.2				
65							-153	-155	-164
67	-27.5	-28.8	-31.6	-31.2	-29.2			-141	-159
69									
71	-29.7	-29.6	-32.2	-31.4	-29.7				
73							-149	-149	-150
75	-27.1	-29.2	-31.1	-30.4	-29.0				
77									
79	-30.7	-29.4	-31.9	-30.9	-29.9				
81									
83	-27.1	-28.5	-30.3	-30.2	-27.7				
85									
87	-28.6	-28.0	-30.7	-32.0	-27.6				
89									
91	-27.6	-31.1	-30.4	-29.9	-28.0				
95									
95	-27.3	-28.9	-30.9	-30.2	-27.5		-165	-162	-168
97									
99	-31.2	-30.1	-31.8	-32.1	-30.4				
101							-156	-161	
103	-27.9	-28.4	-31.2	-30.0	-28.9		-159	-164	-179
105									
107	-26.5	-28.2	-30.9	-29.6	-31.0		-163	-164	-186

Table 2. 3. cont.

Revised meter composite depth (rmcd)	Carbon isotope ratio (‰ VPDB)						Hydrogen isotope ratio (‰ VSMOW)		
	C23	C25	C27	C29	C31	C33	C27	C29	C31
109							-168	-167	-177
111	-28.6	-28.5	-31.1	-30.2	-28.0		-164	-165	-170
113							-169	-171	-180
115	-29.0	-30.7	-29.7	-31.3			-162	-163	-172
117							-174	-172	-181
119	-26.8	-27.0	-29.9	-28.8	-26.9	-27.4	-184	-178	-199
121									
123	-26.0	-27.5	-29.9	-28.5	-26.3	-26.2	-177	-174	-190
125									
127	-26.5	-27.8	-29.6	-28.7	-25.9	-26.3	-169	-163	-190
129									
131	-27.8	-29.1	-30.9	-30.1	-27.6	-28.1		-164	-175
133									
135	-26.9	-28.6	-31.3	-30.4	-28.4			-164	-173
137									
139	-28.6	-29.6	-31.6	-31.4	-31.5				
141									
143	-27.2	-29.2	-31.8	-31.1	-30.2				
145									
147	-28.9	-29.8	-32.2	-31.4	-30.6		-162	-170	-171
149									
151	-29.8	-29.8	-31.8	-31.7	-31.0				
153							-140	-142	-146
155		-28.2	-30.7	-30.2			-135	-135	-135
157									
159	-26.9	-28.0	-31.2	-30.0	-28.1	-27.2	-140	-138	-143
161									
163	-28.3	-29.6	-32.0	-31.2	-29.8		-153	-154	-153
165									
167		-28.5	-31.0	-31.2	-29.2		-146	-147	-152
169									
171	-30.2	-29.5	-31.2	-30.5	-29.0				
173									
175									
177	-29.4	-30.6	-32.4	-31.7	-30.2				
179	-30.2	-30.8	-32.6	-33.2	-32.1	-30.3		-140	-139
181	-30.3	-31.2	-32.9	-32.3	-30.9				
183									
185			-30.9	-29.7				-138	-143
187									
189			-32.0	-31.6	-29.7		-151	-154	-156
191									
193		-28.3	-31.7	-30.9	-28.5				
195							-147	-148	-151
197		-29.0	-32.2	-30.8	-29.4			-160	-165
199									
201							-131	-148	-144

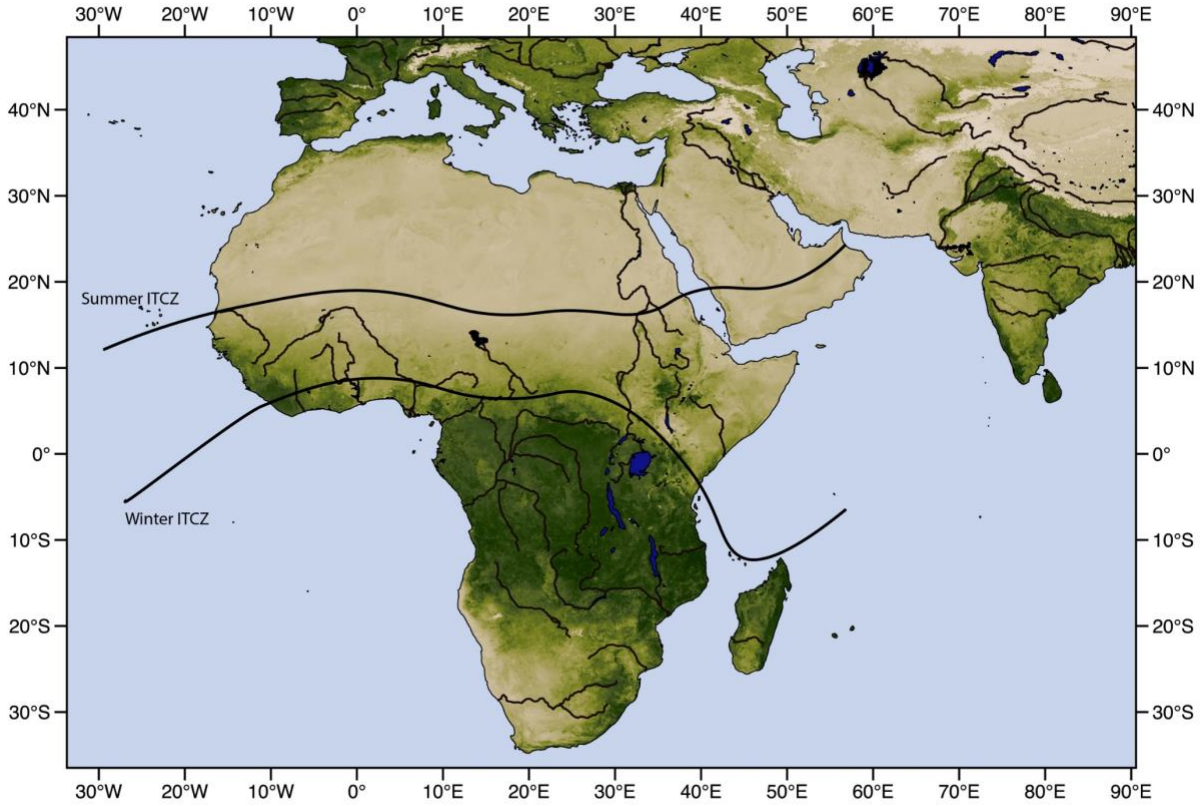

Figure 2. 1: Modern vegetation transitions and precipitation of present Africa with present hydrological system. Black lines indicate the Intertropical Convergence Zone (ITCZ) during July-August and January (Nicholson, 1996).

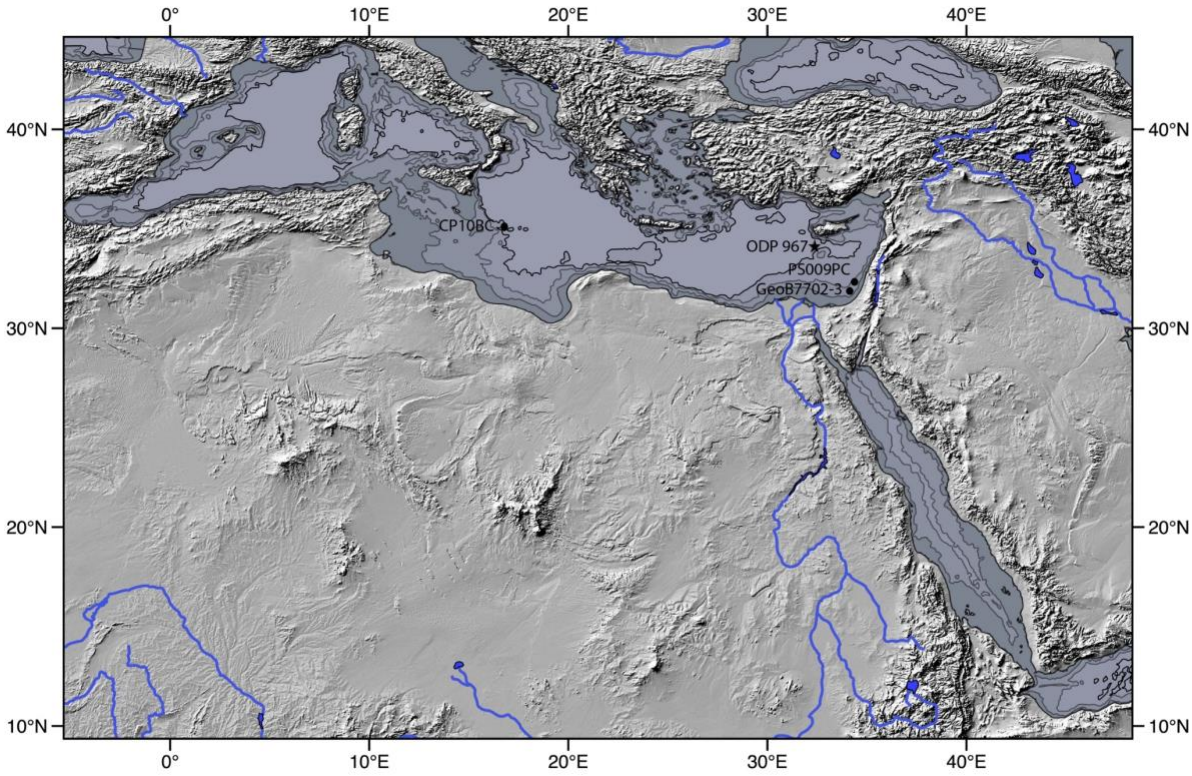

Figure 2. 2: Shaded relief map of North Africa and ODP Site 967 location with black star in the eastern Mediterranean Sea (black star) in the path of the Nile River outflow. The approximate locations of cores GeoB7702-3 (Castañeda et al., 2016), CP10BC (Wu et al. 2016) and PS009PC (van Helmond et al., 2015).

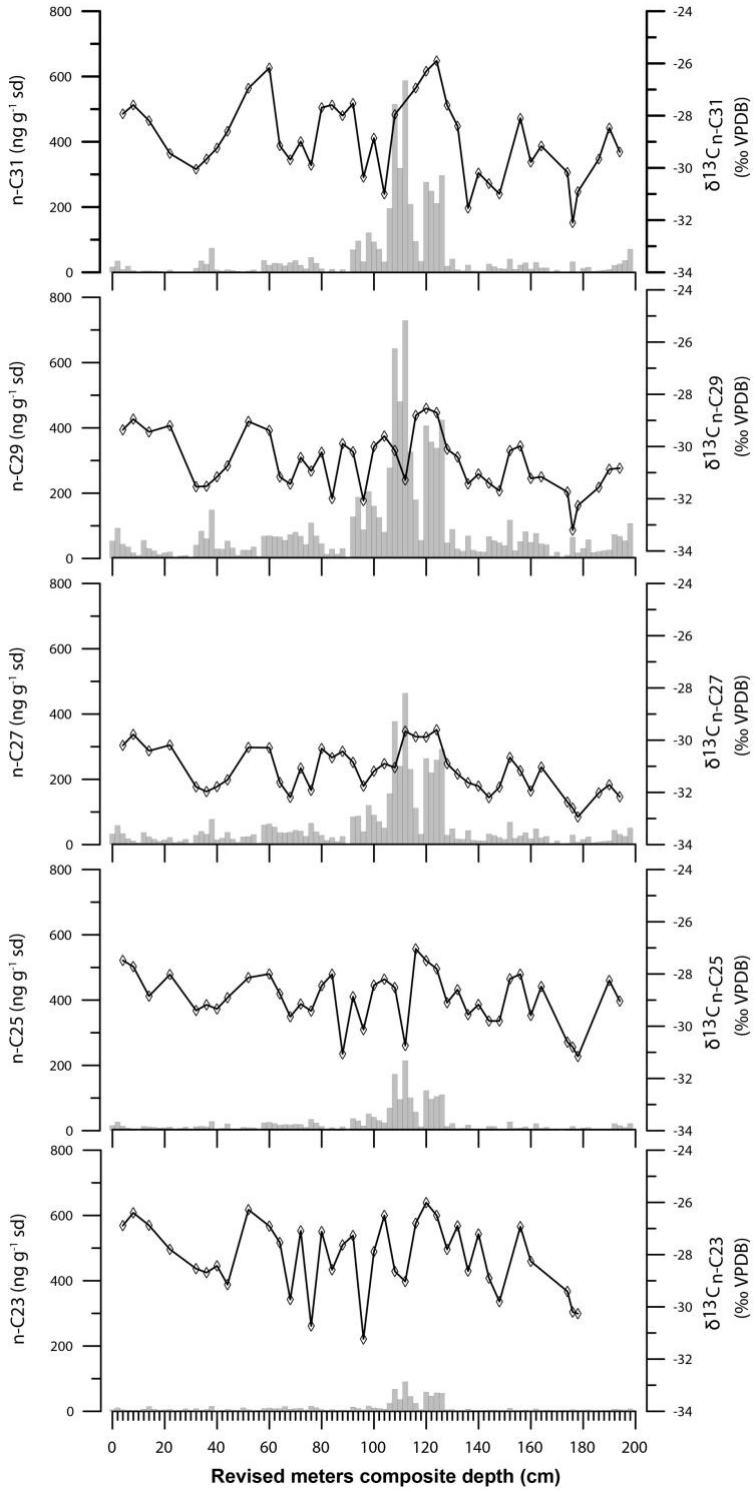

Figure 2. 3: Histograms showing the concentrations of n-alkanes (ng g^{-1} of sediment; left axis). The line graphs show stable carbon isotope ratios of n-alkanes (in ‰ VPDP, right axis) versus the revised meters composite depth for ODP site 967 in the Eastern Mediterranean Sea.

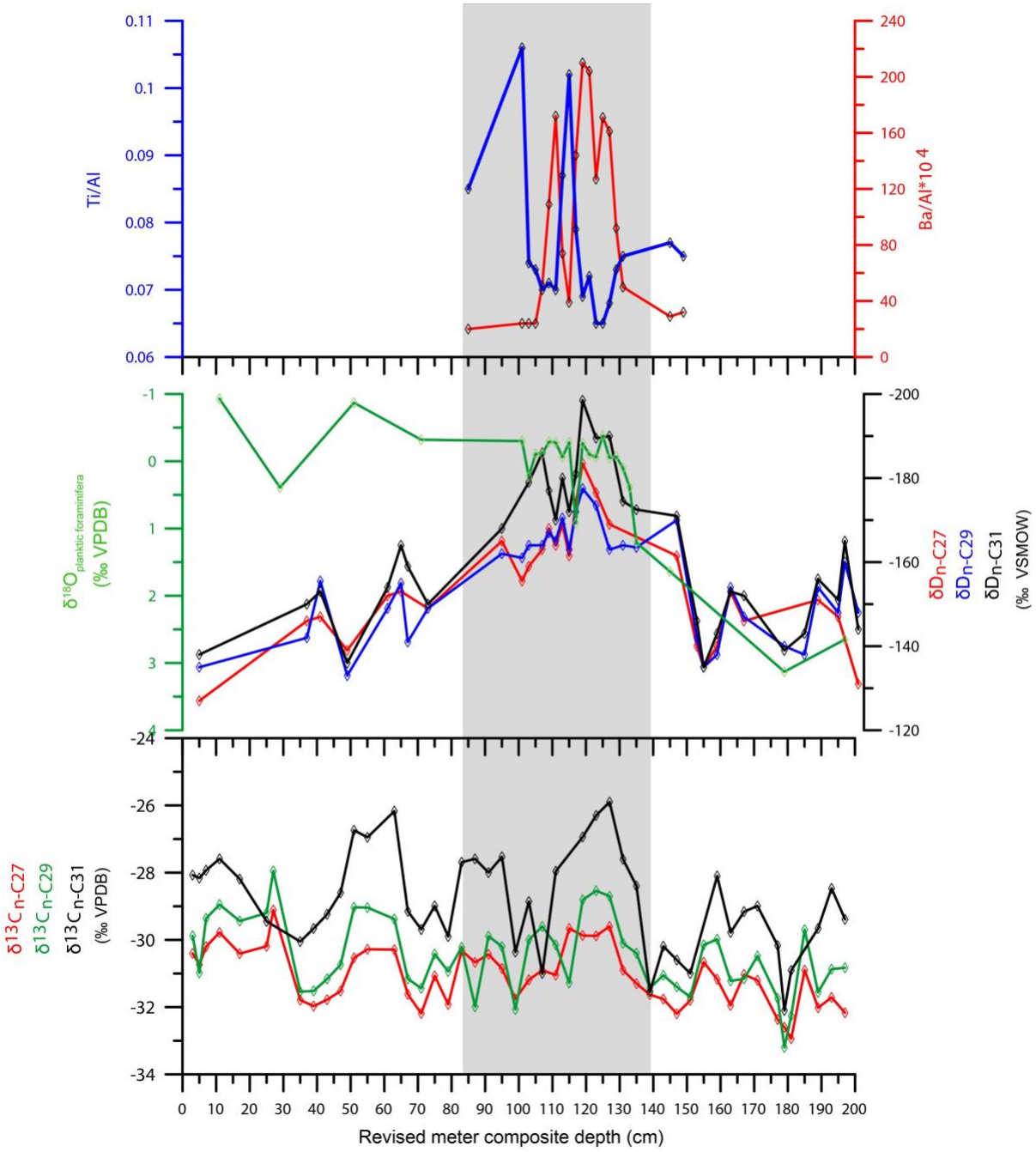

Figure 2. 4: Downcore profiles versus depth of compound specific isotopes of: A) Ti/Al ratio and B) Ba/Al ratio (Azrieli-Tal et al., 2014), C) $\delta^{18}O$ (‰ VPDB) (Emeis et al., 1998), D) Hydrogen (δD) (‰, VSMOW) and E) Carbon ($\delta^{13}C$) (‰, VPDB) of individual n-alkanes n-C_{27}, n-C_{29}, n-C_{31}.

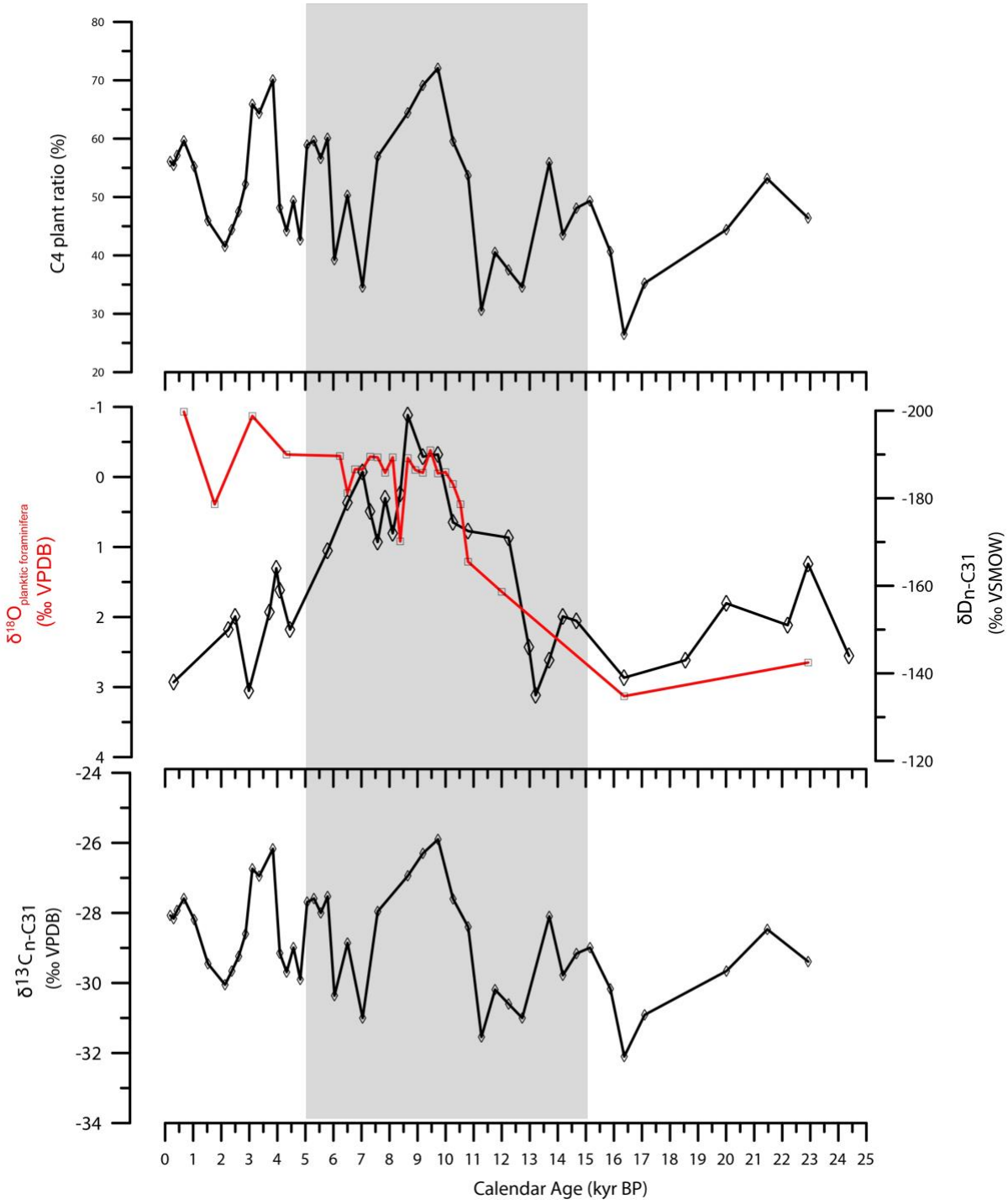

Figure 2. 5: Downcore profiles versus calendar age (kyr) of compound specific isotopes of: A) Percent pf C4 annual grasses, B) $\delta^{18}O$ (‰ VPDB) (Emeiset al., 1998), C) Hydrogen (δD)(‰ VSMOW) and D) Carbon ($\delta^{13}C$)(‰ VPDB) of individual n-alkanes n-C_{31}.

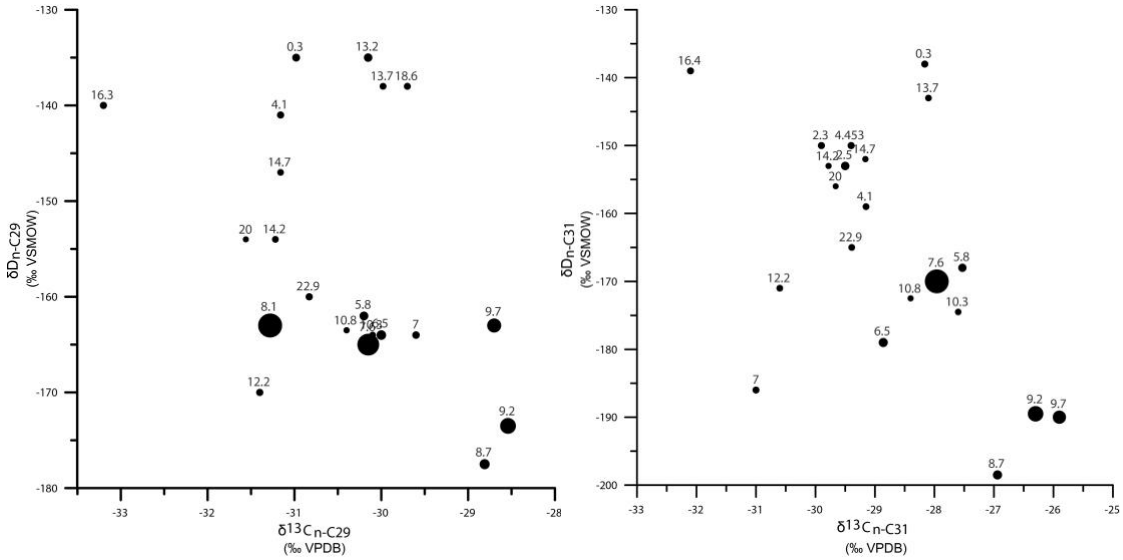

Figure 2. 6: Relationship between $\delta^{13}C$ (‰ VPDB) and δD (‰ VSMOW) of individual n-alkanes n-C_{29} and n-C_{31} since the past 23 ka. The volume of circles related to the concentration n-alkanes n-C_{29} and n-C_{31}.

Chapter 3

North African paleo-hydrological variations influence on paleoecology and microhabitat of foraminifera in eastern Mediterranean sediments during sapropel depositions

Abstract

Planktic and benthic foraminiferal assemblages in sediment core from the Nile deep sea fan in the Eastern Mediterranean Sea (EMS) were analyzed in order to understand how foraminifera respond to environmental changes during sapropel deposition. For the past 100 kyrs, three sapropel layers S1, S3, and S4 were observed at Core M70b-St#822. Total organic carbon contents showed pronounced peaks at the three sapropel layers. Negatives shifts of both $\delta^{18}O$ and $\delta^{13}C$ of *Globigerinoides ruber*, a planktic foraminiferal species living in surface water, were observed at sapropel layers S3 and S4. This indicates enhanced freshwater discharge from Nile River due to increased precipitation in North Africa caused by northward migration of the intertropical convergence zone (ITCZ). During sapropel S3 and S4, planktic foraminiferal species diversity were significantly low, possibly due to intensified halocline. Intensified halocline leads to stagnant ocean ventilation and decreases bottom water oxygen content. Benthic foraminiferal assemblages were sensitively responded to the events. During sapropel layers S4, benthic foraminifera was nearly barren, indicating anoxic bottom water. During sapropel layers S3, benthic foraminiferal species diversity was low but several infaunal species were observed. This suggests a dysoxic bottom water during sapropel S3. On the other hand, during sapropel S1, no major changes in benthic foraminiferal assemblage was found. This suggests that bottom water oxygen level did not critically decrease.

3.1. Introduction

The Eastern Mediterranean Sea (EMS) sediment is characterized by numerous brownish to black colored intercalated beds. These beds are relatively enriched in organic carbon and often well laminated, and are named sapropels (Rohling and Hilgen, 1991). Changes in the latitudinal position, timing and intensity of the African monsoon rains have had profound effects on the sedimentological characteristics of EMS. Sapropels deposited in dysoxic to anoxic bottom waters (Daux et al., 2006; Meyers, 2006) when summer monsoon was intensified (Rossignol-Strick, 1983). This allows good preservation of organic matter in the sediments and less or no bioturbation (Jorissen, 1999; Kuhnt et al., 2007; Nolet and Corliss, 1990). Increased freshwater flux from North Africa into EMS during sapropel formations have been recorded as negative planktic foraminiferal $\delta^{18}O$ values (Cita *et al.*, 1977; Cramp et al., 1988; Mangini and Schlosser, 1986; Rohling and Hilgen, 1991; Rossignol-Strick *et al.*, 1982; Rossignol-Strick, 1985; Vergnaud-Grazzini *et al*., 1977; Williams *et al*., 1978). Increased

riverain input provides not only freshwater but also nutrients and continental organic matter into EMS (Rohling and Hilgen, 1991).

The Nile deep-sea fan is one of the largest modern deep-sea turbidite and plays an important role in sedimentary accumulation in EMS. This post-Miocene deposit has approximately 10 km thickness above mobile Messinian evaporites formed by the Messinian salinity crisis from 5.96 to 5.33 Ma (Gaullier et al., 2000; Loncke et al., 2006). Therefore, the initial distribution and thickness of Messinian evaporites have strongly influenced on the present sea-floor shape and processes of sediment dispersal (Loncke et al., 2006). Mediterranean climate is characterized by hot, dry summers and cool, wet winters. Deserts of North Africa lies within a zone of the subtropical high-pressure belt (Boucher, 1975). In summer, most of the Mediterranean region particularly the southeastern part experiences drought by northward migration of the subtropical high-pressure belt (Rohling and Hilgen, 1991). Although there is no precipitation on the African Mediterranean coast in summer, there is heavy rainfall on catchment areas of the Nile River with northward migration of ITCZ. As a result, the Nile River discharges large amount of freshwater as well as numerous terrigenous inputs into EMS during summer. This process had happened naturally before building the Aswan High Dam in 1964. Since the Aswan High Dam completion, decrease in discharge of fresh water and sediment have been occurred and erosion of the Nile River delta progressed.

Aim of this study is to understand how planktic and benthic foraminifera respond to environmental changes in EMS, particularly sapropel events during the past 100 kyrs. Planktic and foraminiferal assemblages as well as their carbon and oxygen stable isotopes in sediments from the Nile deep sea fan are investigate.

3.2. Material and Methods

M70b-St#822 gravity core (32°20.92'N; 31°48.02'E; 1089 m water depth; 4.5 m long) was used in this study obtained from the Nile deep sea fun in EMS during M70b cruise of R/V Meteor in October 2006 (Fig. 3-1). Major lithology of M70b-St#822 core is homogenous clay with calcareous ooze.

3.2.1. Age Model

Age model of M70b-St#822 gravity core was established based on the astronomical tuning by comparison of sapropel midpoints with inferred 65° N summer insolation maxima with a fixed 3-kyr time lag (Lourens, 2004). The lag estimation was corrected to 2.7 ± 1.1 kyrs (Konijnendijk *et al.*, 2014). For M70b-St#82 core samples, thickness of sapropel layers was determined by total organic carbon contents (wt%). In addition, top and bottom ages of sapropel layer S1 are well constrained

based on radiocarbon dating of planktic foraminifera from the numbers of sediment cores in EMS (10.8 ± 0.4 to 6.1 ± 0.5 cal. kyr BP; De Lange *et al.*, 2008). The established age model shows top 4.5 m of M70b-St#822 is corresponding to for the past 100 kyrs. Due to a few age control points, discussions on detailed timings beyond millennial time-scales are limited.

3.2.2. Sediment Samples Analyses

Selected 46 samples of core M70b-St#822 were used for analyses on total organic carbon contents (Table 3.1). Total organic carbon contents were measured determined by acid/dichromate titration method (Gaudette et al., 1974). Approximately 0.3 g of sediment samples were dried at room temperature and placed into 500 ml Erlenmeyer flask. Exactly 10 ml of 1N $K_2Cr_2O_7$ solution was added by burette to the sediment and well mixed. 20 ml of concentrated H_2SO_4 were added by burette and were mixed by gentle rotation of the flask for about 1 minute. The mixture was allowed to stand for 30 min. A standardization blank without sediments was run with each new batch of samples. After 30 min, the solution was diluted to 200 ml volume with distilled water, and 10 ml of 85% H_3PO_4, 0.2 g of NaF and 15 drops of diphenylamine indicator were added to the sample in flask. The solution was back titrated with 0.5N ferrous ammonium sulfate solutions. The color was progressed from an opaque green-brown, to green upon the addition of approximately 10 ml of ferrous solution (Fe $(NH_4)_2SO_4$, $6H_2O$). The color continued to shift upon titration to a bluish-black-grey. At this point the addition of 10-20 drops of ferrous solution shifted the color to a brilliant green giving a one-drop end point. The results of the analysis were calculated by the following equation:

% Organic Carbon = 10 (1-T/S) [1.0N (0.003) (100/W)]

Where T= sample titration, ml ferrous solution, S= standardization blank titration, ml ferrous solution. (The T/S factor will cancel out the effect of the ferrous solution normality) 0.003 = meq. Wt of carbon, 1.0 N= normality of K2Cr2O7, 10= volume of K2Cr2O7 in ml, and W= weight of sediment sample in grams the organic carbon is converted to organic matter by multiplying the organic carbon values by the factor of 1.8 (Gaudette et al, 1974).

For foraminiferal analyses, selected 26 sediment samples were used. Sediment samples of core M70b-St#822 were dried and 10 g of the samples were weighed. The weighed samples were washed with tap water over a 63-µm sieve and dried at 60˚C (Schilman et al., 2001). The residual samples >63 µm were split by using a Micro-Splitter. Total assemblages were determined in fractions of split samples including at least 300 specimens (Javaux and Scott, 2003). Foraminiferal species identification was following to Loeblich and Tappan (1964) (Fig. 3.7 and 3.8; Table 3.2). Stable carbon and oxygen isotopes of planktic foraminifera was performed. 40 specimens of *Globigerinoides ruber*, a surface-dwelling species (0–50 m), were picked up from the size fraction >250 µm (Fontugne and

Calvert, 1992). Stable isotope measurements were performed by using IRMS Micromass Optima coupled to a Multiprep mass spectrometer at Environnements et Paléo-environnements Océaniques et Continentaux in Bordeaux, France. Isotope ratios are given in δ notations versus PDB after calibration against international NBS 18 and 19 (Coplen, 1988; Hut, 1987).

3.3. Results

3.3.1. TOC analysis

TOC contents were generally low less than 1 wt% at core M70b-St#822 (Fig. 3-2). Relatively high TOC contents were found at 20- 30 cm, 290-340 cm, 400 cm, and 430-440 cm. These timing were simultaneous with sapropel depositions.

3.3.2. Foraminiferal assemblage and stable isotopes

A total of 21 species of planktic and benthic species were identified in M70b-St#822 core sediment (Fig. 3.7 and 3.8; Table 3.2). Relative and absolute abundances of planktic and benthic foraminifera were summarized in Tables 3.3. and 3.4, respectively. Absolute abundances of planktic foraminifera showed three peaks in core M70b-St#822 at 150 cm, 280-300 cm (sapropel S3) and 420 cm (sapropel S4) (Fig. 3.4; Table 3.3). Absolute abundances of benthic foraminifera were relatively abundant in sapropel S1 and S3 but almost barren in sapropel S4 (Fig. 3.6; Table 3.4). The abundant planktic foraminiferal species were *Globigerinoides ruber* and *Globigerina bulloides*. Pronounced peaks of %*G. ruber* and % *G. bulloides* were found during sapropel S4 and S3, respectively (Fig. 3.3; Table 3.3). *Orbulina universa* was absent except for sapropel layers S3 and S4. Shannon diversity (H) of planktic foraminifera ranged from 1.2 to 1.6 except for sapropel layers where significantly low peaks were found (Fig. 3.2). Shannon diversity (H) of benthic foraminifera showed similar pattern with that of planktic foraminifera and the values were ~3 except for the sapropel layers (Fig. 3.2). Among sapropel layers, lowest Shannon diversity was observed in sapropel S4.

Down core profiles of stable oxygen and carbon isotopes of planktic foraminiferal species *G. ruber* at core M70b-St#822 were shown in Figure 3.2. Negative excursions of both $\delta^{18}O$ and $\delta^{13}C$ were found in sapropel S3 and S4 layers.

3.4. Discussion

3.4.1. Sedimentary characteristics of sapropels

Hydrological change in North Africa and EMS is closely linked to the changes in African monsoon intensity which is mainly controlled by solar radiation received at low latitudes modulated by the precession cycle (Fontugne and Calvert, 1992; Rohling, 1994; Rossignol-Strick, 1985). During

periods with precession minima, northward migrated ITCZ causes the greening of Sahara (Brovkin *et al.,* 1998; Gasse, 2000) and the reduction of Saharan aeolian dust into EMS (Larrasoana et al., 2003). Enhanced freshwater discharge plays a critical role in formation of sapropel layers by establishing halocline and providing terrigenous nutrients (Rohling et al., 2015). While during periods with precession maxima, ITCZ migrates to southward and converts the Saharan region to barren desert and causes the increase in aeolian dust into EMS (Claussen *et al.*, 1998; Brovkin *et al.,* 1998).

Freshwater, particularly derived from heavy rain has light $\delta^{18}O$ comparing to the seawater. Hence, mixing of freshwater floods to seawater causes low $\delta^{18}O$ anomalies in planktic foraminifera (see Rohling et al., 2015, review and references therein). Kallel et al., (1997, 2000) showed low $\delta^{18}O$ anomalies due to increased precipitation over the EMS and its borderlands. Negative $\delta^{18}O$ excursions of planktic foraminifera at core M70b-St#822 in Fig. 5 indicates enhanced freshwater discharge via Nile River caused by increased precipitation in watershed area of Nile River during the sapropel S3 and S4 depositions. This leads to salinity reduction and halocline development, enhancing stratification in EMS (Rossignol-Strick *et al.*, 1982; Rossignol-Strick, 1985; Van Harten, 1987; Nolet and Corliss, 1990; Negri *et al*., 2003). Our data corresponds to low $\delta^{18}O$ values of *G. ruber* (Kroon et al., 2004) and significantly low Ti/Al ratios and hematite contents (Larrasoana et al., 2003) at Site 967 that support the scenario of enhanced Nile River input and elevated soil moisture in North Africa during the sapropel layers formation.

Planktic foraminiferal carbon isotopes tell a carbon cycle in upper water column. Commonly, planktic foraminifera living in surface water forms calcite tests enriched in ^{13}C because ^{12}C is preferentially sequestered by marine algae during photosynthesis in euphotic layer and subsequently transfers to ocean interior by sinking particles (Rohling *et al.*, 2004). However, in areas where enhanced river input occur, surface waters have low $\delta^{13}C$ values due to light carbon content of freshwater ranging from –5‰ to –10‰ of inorganic carbon and as light as –27‰ of suspended organic carbon (Fontugne and Calvert, 1992). In semi-enclosed marginal sea with significant river inputs, effect of biological pumping is masked by light carbon dilution. Significantly negative $\delta^{13}C$ excursions at core M70b-St#822 during sapropel S3 and S4 are due to both elevated primary productivity fueled by nutrient supply from riverine inputs and direct influence of riverine carbon inputs.

3.4.2. Response of foraminiferal assemblages to sapropel depositions

Diversity of planktic foraminifera at core M70b-St#822 decreased during sapropel S3 and S4 depositions. Distribution of planktic foraminifera is controlled by number of environmental factors such as surface water hydrography (Zhang, 1985), water mass properties (Vincnet and Berger, 1981) and upwelling (Curry et al., 1992). Rutherford *et al*., (1999) suggests that diversity of planktic

foraminifera is controlled by structure of upper water column rather than SST because planktic foraminiferal diversity decreases in shallow thermocline. On the other hand, Rosenzweig and Abramsky (1993) suggest diversity of planktic foraminifera is controlled by productivity because the diversity decreased during an excess of productivity.

Significant decrease of planktic foraminiferal diversity during sapropel S3 and S4 at core M70b-St#822 can be explained by both intensified halocline and an excess of productivity. Pronounced negative $\delta^{18}O$ excursions of *G. ruber* indicate great influence of freshwater discharge during sapropel S3 and S4 depositions (Fig. 3.2). TOC contents showed pronounced peaks during both S3 and S4 layers, suggesting elevated productivity (Fig. 3.2). Sapropel S1 has clearly different feature of sedimentary properties without pronounced change of $\delta^{18}O$ compared to sapropels S3 and S4. Planktic foraminiferal assemblages showed difference between sapropel S3 and S4. Most abundant planktic foraminiferal species was *G. bulloides* during sapropel S3 whereas *G. ruber* during sapropel S4. *Globigerina bulloides* inhabits both mixed layer (< 400 m water depth) and known as upwelling indicator (Bé et al., 1985; Reynolds and Thunell, 1986). In the Mediterranean Sea, this species is abundant in winter (Reynolds and Thunell, 1986). *Globigerinoides ruber* is an omnivorous feeders bearing dinoflagellate symbiont (Bé and Hamlin, 1967; Hemleben *et al*., 1989; Leeuwen, 1989) with wide ecological niche of temperatures and salinities that usually thrive in the warm, nutrient-poor waters of the summer mixed layer above the thermocline (Hemleben *et al*., 1989). Therefore, abundant *G. bulloides* during sapropel S3 support an excess of productivity scenario. On the contrary, intensified halocline scenario is more likely for sapropel S4 inferred from abundant *G. ruber*. In addition, both absolute and relative abundances of *Globorotalia truncatulinoides,* living intermediate depth 200-500 m (Hemleben *et al*., 1989), decreased during sapropel S1, S3 and S4. This is perhaps due to weaken vertical mixing by halocline because the distribution of this species is related to winter convection and vertical mixing (Pujol and Grazzini, 1995). Similar the patterns of *Globigerinita glutinata* support the weaken vertical mixing during sapropel layers because this species is a proxy for the presence deep mixed layer *Globigerinita glutinata* increases (Bé and Hamlin, 1967; Hemleben *et al*., 1989; Leeuwen, 1989).

Similar to the planktic foraminifera, species diversity of benthic foraminifera significantly decreased during sapropel S3 and S4 depositions at core M70b-St#822 (Fig. 3.4). Benthic foraminiferal diversity depends on a sea-floor ecosystem. An ecosystem in stable environment is able to support a highly diverse fauna, whereas in severe environment diversity is generally low (Gooday et al., 1998). Jorissen *et al*., (1995) have indicated that highest diversities occur in mesotrophic and well-ventilated environments. In contrast, diversities are generally low in oligotrophic as well as eutrophic and oxygen-depleted benthic ecosystems. Numbers of studies have suggested that export

flux of organic carbon plays a major role in density and diversity of benthic foraminifera (Alve and Bernhard, 1995; de Stigter *et al*., 1998; Jorissen *et al.*, 1998; Loubere, 1998; Altenbach *et al.*, 1999; Bernhard and Sen Gupta, 1999; Schmiedl *et al.*, 2000; De Rijk *et al.*, 2000; Kitazato *et al.*, 2000; Morigi *et al.*, 2001, 2005, Fontanier *et al.*, 2002, 2003). A benthic foraminiferal assemblage with high absolute abundance suggests high organic carbon flux to the sea floor. With the bottom water oxygen consumption by organic carbon degradation, infaunal benthic foraminiferal species replace the less tolerant species of low oxygen condition (Jorissen *et al.,* 1995; Jorissen, 1999). During sapropel S4, benthic foraminifera at Core M70b-St#822 was barren suggesting anoxic condition on the seafloor. Several studies recorded the absence of benthic foraminifera in Mediterranean Sea during sapropel layers formation (Abu-Zied et al., 2008; Casford et al., 2003; Jorissen, 1999; Kuhnt et al., 2007; Mercone et al., 2001; Nijenhuis et al., 1996; Nolet and Corliss, 1990; Rohling et al., 1993; Schmiedl et al., 2010, 2003; Verhallen, 1991). During sapropel S3, considerable occurrences of benthic foraminifera at Core M70b-St#822 indicate that bottom water was not anoxic. Melki et al., (2010) also documented occurrences of benthic foraminifera during the deposition of sapropel S4, S6, S8 and S10 at core MD84-641.

Onset of sapropel S3 and S1 was characterized by replacement of epifaunal species (*Bolivina advena and Bolivina acuminata*) by infaunal species (*Bulimina costata, Cassidulina crassa, Cassidulina laevigata, Eponides frigidus, Gyroidina orbicularis*) suggesting dysoxic conditions. *Bolivina acuminata* was the most abundant benthic foraminiferal species during sapropel S3. Abu-Zied *et al.* (2008) mentioned that most of species in genus *Bolivina* is considered as opportunist sensitively responding to an organic matter input. The increased occurrence of *Bolivina acuminata* during sapropel S3 is consistent with an excess of productivity scenario based on abundant *G. bulloides*. Occurrences of *Bulimina costata*, *Cassidulina crassa*, *Cassidulina laevigata*, and *Uvigerina mediterranea* are shallow infauna less tolerant to low oxygen condition associated with oligotrophic to mesotrophic, well ventilated oceanic conditions (De Rijk et al., 2000; Kuhnt et al., 2007). They showed relatively high abundances during period between sapropel S1 and S3. This interval is corresponding to the last glacial period. During the last glacial period , African summer monsoon was weak and ITCZ shifted southward. Hooghiemstra *et al.*, (1992) documented that the glacial Sahara Desert extended hundreds of kilometers further south than at present based on ancient sand dune distributions. As a result, aeolian dust input into EMS was increased (Larrasoana et al., 2003). Reduced freshwater discharge during glacial period was also evidenced by planktic foraminiferal assemblage at core M70b-St#822. Increased diversity of the planktic foraminifera suggests ventilated water mass by less freshwater discharge and SST cooling. This is supported by increase of deep dwelling species *Globorotalia truncatulinoides* and cold-water species *Globigerinita glutinata*. Benthic foraminiferal

diversity also increased during glacial period perhaps because of oxygenation in bottom water by ventilation.

3.5. Conclusion

Sapropels S1, S3 and S4 were found in sediment of M70b-St#822 gravity core. Enhanced freshwater discharge via Nile River is suggested by negative excursions of $\delta^{18}O$ and $\delta^{13}C$ of *G. ruber* during sapropels S3 and S4. Simultaneously, planktic foraminiferal diversity decreased due to developed halocline. Benthic foraminiferal assemblage indicated the difference of bottom water environments between sapropel S3 and S4. Sapropel S3 was dysoxic condition whereas sapropel S4 was anoxic conditions. Notable species turnover of benthic foraminifera from epifauna to infauna was observed at the onset of sapropel S3 cause by reduced bottom water oxygen concentration.

References

Abu-Zied, R.H., Rohling, E.J., Jorissen, F.J., Fontanier, C., Casford, J.S.L., Cooke, S., 2008. Benthic foraminiferal response to changes in bottom-water oxygenation and organic carbon flux in the eastern Mediterranean during LGM to Recent times. Mar. Micropaleontol. 67, 46–68. doi:10.1016/j.marmicro.2007.08.006

Ajayi, S.O., Vanloon, G.W., 1989. Studies on redistribution during the analytical fractionation of metals in sediments. Sci. Total Environ. 87–88, 171–187. doi:10.1016/0048-9697(89)90233-7

Altenbach, A.V., Pflaumann, U., Schiebel, R., Thies, A., Timm, S., Trauth, M., 1999. Scaling percentages and distributional patterns of benthic Foraminifera with flux rates of organic carbon. J. Foraminifer. Res. 29, 173–185.

Alve, E., Bernhard, J.M., 1995. Vertical migratory response of benthic foraminifera to controlled oxygen concentrations in an experimental mesocosm. Mar. Ecol. Prog. Ser. 116, 137–152. doi:DOI 10.3354/meps116137

Ariztegui, D., Asioli, A., Lowe, J.J., Trincardi, F., Vigliotti, L., Tamburini, F., Chondrogianni, C., Accorsi, C.A., Bandini Mazzanti, M., Mercuri, A.M., Van Der Kaars, S., McKenzie, J.A., Oldfield, F., 2000. Palaeoclimate and the formation of sapropel S1: Inferences from Late Quaternary lacustrine and marine sequences in the central Mediterranean region, in: Palaeogeography, Palaeoclimatology, Palaeoecology. pp. 215–240. doi:10.1016/S0031-0182(00)00051-1

Bé, A.W.H., Bishop, J.K.B., Sverdlove, M.S., Gardner, W.D., 1985. Standing stock, vertical distribution and flux of planktic foraminifera in the Panama Basin. Mar. Micropaleontol. 9, 307–333. doi:10.1016/0377-8398(85)90002-7

Bé, A.W.H., Hamlin, W.H., 1967. Ecology of recent planktic foraminifera: Part 3: Distribution in the

North Atlantic during the summer of 1962. Micropaleontology 13, 87–106. doi:10.2307/1484808

Berger, W.H., Soutar, A., 1970. Preservation of plankton shells in an anaerobic basin off California. Bull. Geol. Soc. Am. 81, 275–282. doi:10.1130/0016-7606(1970)81[275:POPSIA]2.0.CO;2

Bernhard, J.M., Sen Gupta, B.K., 1999. Foraminifera of oxygen-depleted environments, in: Modern Foraminifera. Springer Netherlands, Dordrecht, pp. 201–216. doi:10.1007/0-306-48104-9_12

Beuning, K.R.M., Kelts, K., Russell, J., Wolfe, B.B., 2002. Reassessment of Lake Victoria-Upper Nile River paleohydrology from oxygen isotope records of lake-sediment cellulose. Geology 30, 559–562. doi:10.1130/0091-7613(2002)030<0559:ROLVUN>2.0.CO;2

Beuning, K.R.M., Talbot, M.R., Kelts, K., 1997. A revised 30,000-year paleoclimatic and paleohydrologic history of Lake Albert, East Africa. Palaeogeogr. Palaeoclimatol. Palaeoecol. 136, 259–279. doi:10.1016/S0031-0182(97)00034-5

Brovkin, V., Martin Claussen, B., Petoukhov, V., 1998. On the stability of the atmosphere-vegetation system in the Sahara[Sahel region. J. Geophys. Res. 103624, 613–31. doi:10.1029/1998JD200006

Casford, J.S.., Rohling, E.., Abu-Zied, R.., Fontanier, C., Jorissen, F.., Leng, M.., Schmiedl, G., Thomson, J., 2003. A dynamic concept for eastern Mediterranean circulation and oxygenation during sapropel formation. Palaeogeogr. Palaeoclimatol. Palaeoecol. 190, 103–119. doi:10.1016/S0031-0182(02)00601-6

Cita, M.B., Vergnaud-Grazzini, C., Robert, C., Chamley, H., Ciaranfi, N., D'Onofrio, S., 1977. Paleoclimatic record of a long deep sea core from the eastern Mediterranean. Quat. Res. 8, 205–235. doi:10.1016/0033-5894(77)90046-1

Claussen, M., Brovkin, V., Ganopolski, A., Kubatzki, C., Petoukhov, V., 1998. Modelling global terrestrial vegetation climate interaction. Philos. Trans. R. Soc. London Ser. B-Biological Sci. 353, 53–63. doi:10.1098/rstb.1998.0190

Coplen, T.B., 1988. Normalization of oxygen and hydrogen isotope data. Chem. Geol. Isot. Geosci. Sect. 72, 293–297. doi:10.1016/0168-9622(88)90042-5

Cramp, A., Collins, M., West, R., 1988. Late pleistocene-holocene sedimentation in the NW Aegean Sea: A palaeoclimatic palaeoceanographic reconstruction. Palaeogeogr. Palaeoclimatol. Palaeoecol. 68, 61–77. doi:10.1016/0031-0182(88)90017-X

Cramp, A., O'Sullivan, G., 1999. Neogene sapropels in the Mediterranean: A review. Mar. Geol. 153, 11–28. doi:10.1016/S0025-3227(98)00092-9

Curry, W.B., Ostermann, D.R., Guptha, M.V.S., Ittekkot, V., 1992. Foraminiferal production and monsoonal upwelling in the Arabian Sea: evidence from sediment traps. Geol. Soc. London, Spec. Publ. 64, 93–106. doi:10.1144/GSL.SP.1992.064.01.06

Daux, V., Foucault, A., Melieres, F., Turpin, M., 2006. Sapropel-like Pliocene sediments of Sicily deposited under oxygenated bottom water. Bull. la Soc. Geol. Fr. 177, 79–88. doi:10.2113/gssgfbull.177.2.79

De Lange, G.J., Thomson, J., Reitz, A., Slomp, C.P., Speranza Principato, M., Erba, E., Corselli, C., 2008. Synchronous basin-wide formation and redox-controlled preservation of a Mediterranean sapropel. Nat. Geosci. 1, 606–610. doi:10.1038/ngeo283

De Rijk, S., Jorissen, F.J., Rohling, E.J., Troelstra, S.R., 2000. Organic flux control on bathymetric zonation of Mediterranean benthic foraminifera, in: Marine Micropaleontology. pp. 151–166. doi:10.1016/S0377-8398(00)00037-2

De Rijk, S., Troelstra, S.R., Rohling, E.J., 1999. BENTHIC FORAMINIFERAL DISTRIBUTION IN THE MEDITERRANEAN SEA. J. Foraminifer. Res. 29.

de Stigter, H.C., Jorissen, F.J., van der Zwaan, G.J., 1998. Bathymetric distribution and microhabitat partitioning of live (Rose Bengal stained) benthic foraminifera along a shelf to bathyal transect in the southern Adriatic Sea. J. Foraminifer. Res. 28, 40–65.

Fontanier, C., Jorissen, F.., Chaillou, G., David, C., Anschutz, P., Lafon, V., 2003. Seasonal and interannual variability of benthic foraminiferal faunas at 550m depth in the Bay of Biscay. Deep Sea Res. Part I Oceanogr. Res. Pap. 50, 457–494. doi:10.1016/S0967-0637(02)00167-X

Fontanier, C., Jorissen, F.., Licari, L., Alexandre, A., Anschutz, P., Carbonel, P., 2002. Live benthic foraminiferal faunas from the Bay of Biscay: faunal density, composition, and microhabitats. Deep Sea Res. Part I Oceanogr. Res. Pap. 49, 751–785. doi:10.1016/S0967-0637(01)00078-4

Fontugne, M.R., Calvert, S.E., 1992. Late Pleistocene Variability of the Carbon Isotopic Composition of Organic Matter in the Eastern Mediterranean: Monitor of Changes in Carbon Sources and Atmospheric CO2 Concentrations. Paleoceanography 7, 1–20. doi:10.1029/91PA02674

Gasse, F., 2000. Hydrological changes in the African tropics since the Last Glacial Maximum, in: Quaternary Science Reviews. pp. 189–211. doi:10.1016/S0277-3791(99)00061-X

Gaudette, H.E., Flight, W.R., Toner, L., Folger, D.W., 1974. An inexpensive titration method for the determination of organic carbon in recent sediments. J. Sediment. Res. 44, 249–253. doi:10.1306/74D729D7-2B21-11D7-8648000102C1865D

Gaullier, V., Mart, Y., Bellaiche, G., Mascle, J., Vendeville, B.C., Zitter, T. a. C., 2000. Salt tectonics in and around the Nile deep-sea fan: insights from the PRISMED II cruise. Geol. Soc. London, Spec. Publ. doi:10.1144/GSL.SP.1999.174.01.07

Geraga, M., Tsaila-Monopolis, S., Ioakim, C., Papatheodorou, G., Ferentinos, G., 2005. Short-term climate changes in the southern Aegean Sea over the last 48,000 years. Palaeogeogr. Palaeoclimatol. Palaeoecol. 220, 311–332. doi:10.1016/j.palaeo.2005.01.010

Gooday, A.J., Bett, B.J., Shires, R., Lambshead, P.J.D., 1998. Deep-sea benthic foraminiferal species diversity in the NE atlantic and NW Arabian sea: A synthesis. Deep. Res. Part II Top. Stud. Oceanogr. 45, 165–201. doi:10.1016/S0967-0645(97)00041-6

Hemleben, C., Spindler, M., Anderson, O.R., 1989. Modern planktic foraminifera, Geobios. Springer New York. doi:10.1016/S0016-6995(89)80108-1

Higgs, N.C., Thomson, J., Wilson, T.R.S., Croudace, I.W., 1994. Modification and complete removal of eastern Mediterranean sapropels by postdepositional oxidation. Geology. doi:10.1130/0091-7613(1994)022<0423:MACROE>2.3.CO;2

Hooghiemstra, H., Stalling, H., Agwu, C.O.C., Dupont, L.M., 1992. Vegetational and climatic changes at the northern fringe of the sahara 250,000–5000 years BP: evidence from 4 marine pollen records located between Portugal and the Canary Islands. Rev. Palaeobot. Palynol. 74, 1–53. doi:10.1016/0034-6667(92)90137-6

Hut, G., 1987. NBS 28HUT, G., Consultants' Group Meeting on Stable Isotope Reference Samples for Geochemical and Hydrological Investigations, Vienna, Austria, 16 - 18 September 1985. Report to the Director General, International Atomicc Energy Agency.

Jannink, N.T., Zachariasse, W.J., Van Der Zwaan, G.J., 1998. Living (Rose Bengal stained) benthic foraminifera from the Pakistan continental margin (northern Arabian Sea). Deep. Res. Part I Oceanogr. Res. Pap. 45, 1483–1513. doi:10.1016/S0967-0637(98)00027-2

Javaux, E.J., Scott, D.B., 2003. Illustration of modern benthic foraminifera from Bermuda and remarks on distribution in other subtropical/tropical areas. Palaeontol. Electron. 6, 1–29. doi:10.1046/j.1466-822X.2002.00285.x

Jorissen, F.J., 1999. Benthic foraminiferal successions across Late Quaternary Mediterranean sapropels. Mar. Geol. 153, 91–101. doi:10.1016/S0025-3227(98)00088-7

Jorissen, F.J., de Stigter, H.C., Widmark, J.G. V, 1995. A conceptual model explaining benthic foraminiferal microhabitats. Mar. Micropaleontol. 26, 3–15. doi:10.1016/0377-8398(95)00047-X

Jorissen, F.J., Wittling, I., Peypouquet, J.P., Rabouille, C., Relexans, J.C., 1998. Live benthic foraminiferal faunas off Cape Blanc, NW-Africa: Community structure and microhabitats. Deep. Res. Part I Oceanogr. Res. Pap. 45, 2157–2188. doi:10.1016/S0967-0637(98)00056-9

Kallel, N., Duplessy, J.C., Labeyrie, L., Fontugne, M., Paterne, M., Montacer, M., 2000. Mediterranean pluvial periods and sapropel formation over the last 200 000 years. Palaeogeogr. Palaeoclimatol. Palaeoecol. 157, 45–58. doi:10.1016/S0031-0182(99)00149-2

Kallel, N., Paterne, M., Duplessy, J.C., Vergnaud-Grazzini, C., Pujol, C., Labeyrie, L., Arnold, M., Fontugne, M., Pierre, C., 1997. Enhanced rainfall in the Mediterranean region during the last

Sapropel Event. Oceanol. Acta 20, 697–712. doi:http://dx.doi.org/10.1016/S0031-0182(97)00021-7

Kitazato, H., Shirayama, Y., Nakatsuka, T., Fujiwara, S., Shimanaga, M., Kato, Y., Okada, Y., Kanda, J., Yamaoka, A., Masuzawa, T., Suzuki, K., 2000. Seasonal phytodetritus deposition and responses of bathyal benthic foraminiferal populations in Sagami Bay, Japan: preliminary results from "Project Sagami 1996–1999." Mar. Micropaleontol. 40, 135–149. doi:10.1016/S0377-8398(00)00036-0

Konijnendijk, T.Y.M., Ziegler, M., Lourens, L.J., 2014. Chronological constraints on Pleistocene sapropel depositions from high-resolution geochemical records of ODP Sites 967 and 968. Newsletters Stratigr. 47, 263–282. doi:10.1127/0078-0421/2014/0047

Kroon, D., Alexander, I., Little, M., Lourens, L.J., Matthewson, A., Robertson, A.H.F., Sakamoto, T., 2004. Oxygen isotope and sapropel stratigraphy in the Eastern Mediterranean during the last 3.2 million years. Proc. Ocean Drill. Program, Sci. Results 160, 181–189. doi:10.2973/odp.proc.sr.160.071.1998

Kuhnt, T., Schmiedl, G., Ehrmann, W., Hamann, Y., Hemleben, C., 2007. Deep-sea ecosystem variability of the Aegean Sea during the past 22??kyr as revealed by Benthic Foraminifera. Mar. Micropaleontol. 64, 141–162. doi:10.1016/j.marmicro.2007.04.003

Larrasoana, J.C., Roberts, A.P., Rohling, E.J., Winklhofer, M., Wehausen, R., 2003. Three million years of monsoon variability over the northern Sahara. Clim. Dyn. 21, 689–698. doi:10.1007/s00382-003-0355-z

Leeuwen, R., 1989. UTRECHT. Utr. Micropaleontol. Bull. 38.

Loncke, L., Gaullier, V., Mascle, J., Vendeville, B., Camera, L., 2006. The Nile deep-sea fan: An example of interacting sedimentation, salt tectonics, and inherited subsalt paleotopographic features. Mar. Pet. Geol. 23, 297–315. doi:10.1016/j.marpetgeo.2006.01.001

Loubere, P., 1998. The impact of seasonality on the benthos as reflected in the assemblages of deep-sea foraminifera. Deep. Res. Part I Oceanogr. Res. Pap. 45, 409–432. doi:10.1016/S0967-0637(97)00092-7

Lourens, L.J., 2004. Revised tuning of Ocean Drilling Program Site 964 and KC01B (Mediterranean) and implications for the δ18O, tephra, calcareous nannofossil, and geomagnetic reversal chronologies of the past 1.1 Myr. Paleoceanography 19, n/a-n/a. doi:10.1029/2003PA000997

Maiorano, P., Aiello, G., Barra, D., Di Leo, P., Joannin, S., Lirer, F., Marino, M., Pappalardo, A., Capotondi, L., Ciaranfi, N., Stefanelli, S., 2008. Paleoenvironmental changes during sapropel 19 (i-cycle 90) deposition: Evidences from geochemical, mineralogical and micropaleontological proxies in the mid-Pleistocene Montalbano Jonico land section (southern Italy). Palaeogeogr.

Palaeoclimatol. Palaeoecol. 257, 308–334. doi:10.1016/j.palaeo.2007.10.025

Mallo, M., Ziveri, P., Mortyn, P.G., Schiebel, R., Grelaud, M., 2016. Low planktic foraminiferal diversity and abundance observed in a 2013 West-East Mediterranean Sea transect. Biogeosciences Discuss. 1–31. doi:10.5194/bg-2016-266

Mangini, A., Schlosser, P., 1986. The formation of Eastern Mediterranean sapropels. Mar. Geol. 72, 115–124. doi:10.1016/0025-3227(86)90102-7

Melki, T., Kallel, N., Fontugne, M., 2010. The nature of transitions from dry to wet condition during sapropel events in the Eastern Mediterranean Sea. Palaeogeogr. Palaeoclimatol. Palaeoecol. 291, 267–285. doi:10.1016/j.palaeo.2010.02.039

Mercone, D., Thomson, J., Abu-Zied, R.H., Croudace, I.W., Rohling, E.J., 2001. High-resolution geochemical and micropalaeontological profiling of the most recent eastern Mediterranean sapropel, in: Marine Geology. pp. 25–44. doi:10.1016/S0025-3227(01)00122-0

Mercone, D., Thomson, J., Croudace, I.W., Siani, G., Paterne, M., Troelstra, S., 2000. Duration of S1, the most recent sapropel in the eastern Mediterranean Sea, as indicated by accelerator mass spectrometry radiocarbon and geochemical evidence. Paleoceanography 15, 336–347. doi:10.1029/1999PA000397

Meyers, P.A., 2006. Paleoceanographic and paleoclimatic similarities between Mediterranean sapropels and Cretaceous black shales. Palaeogeogr. Palaeoclimatol. Palaeoecol. 235, 305–320. doi:10.1016/j.palaeo.2005.10.025

Morigi, C., Jorissen, F.J., Fraticelli, S., Horton, B.P., Principi, M., Sabbatini, A., Capotondi, L., Curzi, P. V., Negri, A., 2005. Benthic foraminiferal evidence for the formation of the Holocene mud-belt and bathymetrical evolution in the central Adriatic Sea. Mar. Micropaleontol. 57, 25–49. doi:10.1016/j.marmicro.2005.06.001

Morigi, C., Jorissen, F.J., Gervais, A., Guichard, S., Borsetti, A.M., 2001. Benthic foraminiferal faunas in surface sediments off NW Africa: Relationship with organic flux to the ocean floor. J. Foraminifer. Res. 31, 350–368. doi:Doi 10.2113/0310350

Negri, A., Morigi, C., Giunta, S., 2003. Are productivity and stratification important to sapropel deposition? Microfossil evidence from late Pliocene insolation cycle 180 at Vrica, Calabria, in: Palaeogeography, Palaeoclimatology, Palaeoecology. pp. 243–255. doi:10.1016/S0031-0182(02)00608-9

Nijenhuis, I.A., Schenau, S.J., Van der Weijden, C.H., Hilgen, F.J., Lourens, L.J., Zachariasse, W.J., 1996. On the origin of Upper Miocene sapropelites: A case study from the Faneromeni Section, Crete (Greece). Paleoceanography 11, 633–645. doi:10.1029/96PA01963

Nolet, G.J., Corliss, B.H., 1990. Benthic foraminiferal evidence for reduced deep-water circulation

during sapropel deposition in the eastern Mediterranean. Mar. Geol. 94, 109–130. doi:10.1016/0025-3227(90)90106-T

Principato, M.S., Giunta, S., Corselli, C., Negri, A., 2003. Late Pleistocene-Holocene planktic assemblages in three box-cores from the Mediterranean Ridge area (west-southwest of Crete): Palaeoecological and palaeoceanographic reconstruction of sapropel S1 interval, in: Palaeogeography, Palaeoclimatology, Palaeoecology. pp. 61–77. doi:10.1016/S0031-0182(02)00599-0

Pruysers, P.A., de Lange, G.J., Middelburg, J.J., Hydes, D.J., 1993. The diagenetic formation of metal-rich layers in sapropel-containing sediments in the eastern Mediterranean. Geochim. Cosmochim. Acta 57, 527–536. doi:10.1016/0016-7037(93)90365-4

Pujol, C., Grazzini, C.V., 1995. Distribution patterns of live planktic foraminifers as related to regional hydrography and productive systems of the Mediterranean Sea. Mar. Micropaleontol. 25, 187–217. doi:10.1016/0377-8398(95)00002-I

Reynolds, L.A., Thunell, R.C., 1986. Seasonal Production and Morphologic Variation of Neogloboquadrina pachyderma (Ehrenberg) in the Northeast Pacific. Micropaleontology 32, 1–18. doi:10.2307/1485696

Rohling, E.J., 1994. Review and new aspects concerning the formation of eastern Mediterranean sapropels. Mar. Geol. 122, 1–28. doi:10.1016/0025-3227(94)90202-X

Rohling, E.J., Hilgen, F.J., 1991. The eastern Mediterranean climate at times of sapropel formation - a review. Geol. en Mijnb. 70, 253–264.

Rohling, E.J., Jorissen, F.J., Grazzini, C.V., Zachariasse, W.J., 1993. Northern Levantine and Adriatic Quaternary planktic foraminifera; Reconstruction of paleoenvironmental gradients. Mar. Micropaleontol. 21, 191–218. doi:10.1016/0377-8398(93)90015-P

Rohling, E.J., Marino, G., Grant, K.M., 2015. Mediterranean climate and oceanography, and the periodic development of anoxic events (sapropels). Earth-Science Rev. doi:10.1016/j.earscirev.2015.01.008

Rohling, E.J., Sprovieri, M., Cane, T., Casford, J.S.L., Cooke, S., Bouloubassi, I., Emeis, K.C., Schiebel, R., Rogerson, M., Hayes, A., Jorissen, F.J., Kroon, D., 2004. Reconstructing past planktic foraminiferal habitats using stable isotope data: A case history for Mediterranean sapropel S5. Mar. Micropaleontol. 50, 89–123. doi:10.1016/S0377-8398(03)00068-9

Rosenzweig, M., Abramsky, Z., 1993. How Are Diversity and Productivity Related? Species Divers. Ecol. communities 52–65.

Rossignol-Strick, M., 1985. Mediterranean Quaternary sapropels, an immediate response of the African monsoon to variation of insolation. Palaeogeogr. Palaeoclimatol. Palaeoecol. 49, 237–

263. doi:10.1016/0031-0182(85)90056-2

Rossignol-Strick, M., 1983. African monsoons, an immediate climate response to orbital insolation. Nature 304, 46–49. doi:10.1038/304046a0

Rossignol-Strick, M., Nesteroff, W., Olive, P., Vergnaud-Grazzini, C., 1982. After the deluge: Mediterranean stagnation and sapropel formation. Nature 295, 105–110. doi:10.1038/295105a0

Rutherford, S., D'Hondt, S., Prell, W., 1999. Environmental controls on the geographic distribution of zooplankton diversity. Nature 400, 749–753. doi:10.1038/23449

Schiebel, R., Schmuker, B., Alves, M., Hemleben, C., 2002. Tracking the recent and late Pleistocene Azores front by the distribution of planktic foraminifers, in: Journal of Marine Systems. pp. 213–227. doi:10.1016/S0924-7963(02)00203-8

Schilman, B., Bar-Matthews, M., Almogi-Labin, A., Luz, B., 2001. Global climate instability reflected by Eastern Mediterranean marine records during the late Holocene. Palaeogeogr. Palaeoclimatol. Palaeoecol. 176, 157–176. doi:10.1016/S0031-0182(01)00336-4

Schmiedl, G., De Bovée, F., Buscail, R., Charrière, B., Hemleben, C., Medernach, L., Picon, P., 2000. Trophic control of benthic foraminiferal abundance and microhabitat in the bathyal Gulf of Lions, western Mediterranean Sea, in: Marine Micropaleontology. pp. 167–188. doi:10.1016/S0377-8398(00)00038-4

Schmiedl, G., Kuhnt, T., Ehrmann, W., Emeis, K.C., Hamann, Y., Kotthoff, U., Dulski, P., Pross, J., 2010. Climatic forcing of eastern Mediterranean deep-water formation and benthic ecosystems during the past 22 000 years. Quat. Sci. Rev. 29, 3006–3020. doi:10.1016/j.quascirev.2010.07.002

Schmiedl, G., Mitschele, A., Beck, S., Emeis, K.C., Hemleben, C., Schulz, H., Sperling, M., Weldeab, S., 2003. Benthic foraminiferal record of ecosystem variability in the eastern Mediterranean Sea during times of sapropel S5 and S6 deposition. Palaeogeogr. Palaeoclimatol. Palaeoecol. 190, 139–164. doi:10.1016/S0031-0182(02)00603-X

Talbot, M.R., Livingstone, D.A., 1989. Hydrogen index and carbon isotopes of lacustrine organic matter as lake level indicators. Palaeogeogr. Palaeoclimatol. Palaeoecol. 70, 121–137. doi:10.1016/0031-0182(89)90084-9

Thomson, J., Mercone, D., De Lange, G.J., Van Santvoort, P.J.M., 1999. Review of recent advances in the interpretation of eastern Mediterranean sapropel S1 from geochemical evidence. Mar. Geol. 153, 77–89. doi:10.1016/S0025-3227(98)00089-9

Van Harten, D., 1987. Ostracodes and the early Holocene anoxic event in the Eastern Mediterranean - Evidence and implications. Mar. Geol. 75, 263–269. doi:10.1016/0025-3227(87)90108-3

Vergnaud-Grazzini, C., Ryan, W.B.F., Bianca Cita, M., 1977. Stable isotopic fractionation, climate change and episodic stagnation in the eastern Mediterranean during the late Quaternary. Mar.

Micropaleontol. 2, 353–370. doi:10.1016/0377-8398(77)90017-2

Verhallen, P.J.J.M., 1991. Late Pliocene to early Pleistocene Mediterranean mud-dwelling foraminifera; influence of a changing environment on community structure and evolution. Utr. Micropaleontol. Bull. 40, 219.

Vincent, E. and Berger, W.H., 1981. Planktic foraminifera and their use in paleoceanography. The sea, 7, pp.1025-1119.

Watkins, J.M., Mix, A.C., Wilson, J., 1998. Living planktic foraminifera in the central tropical Pacific Ocean: Articulating the equatorial “cold tongue” during La Nina, 1992. Mar. Micropaleontol. 33, 157–174. doi:10.1016/S0377-8398(97)00036-4

WillIams, D.F., Thunell, R.C., Kennett, J.P., 1978. Periodic Freshwater Flooding and Stagnation of the Eastern Mediterranean Sea During the Late Quaternary. Science (80-.). 201.

Zhang, J., 1985. Living planktic foraminifera from the eastern Arabian Sea. Deep Sea Res. Part A, Oceanogr. Res. Pap. 32, 789–798. doi:10.1016/0198-0149(85)90115-3.

Table 3. 1. Core depth, calendar age, total organic carbon content, and carbon and oxygen isotope ratio of Core M70b-St#822.

Depth (cm)	Age (cal. kyr. BP)	TOC (wt%)	δ^{13}C of *G. ruber* (‰ VPDB)	δ^{18}O of *G. ruber* (‰ VPDB)	Depth (cm)	Age (cal. kyr. BP)	TOC (wt%)	δ^{13}C of *G. ruber* (‰ VPDB)	δ^{18}O of *G. ruber* (‰ VPDB)
0	0	0.52			270	79.1	0.57		
5	1.3		0.86	2.28	275	79.4		1.39	3.04
10	2.6	0.89			280	79.7	0.21		
20	5.1	1.63			295	80.6		1.13	2.28
30	6.1	1.55			300	80.9	1.46		
40	7.1	0.89			305	81.2		0.37	-0.30
45	7.7		1.04	1.52	310	81.5	0.88		
50	8.2	0.52			315	81.8		1.39	-0.47
60	9.2	0.63			320	82.1	1.5		
70	10.2	1.05			325	82.4		1.08	-0.45
80	14.1	0.31			330	82.7	1.72		
90	18.1	0.37			335	83		0.80	1.30
95	20.1		1.07	1.86	340	83.3	0.68		
100	22	0.10			345	83.6		0.72	1.55
110	26	0.52			350	83.9	0.16		
120	29.9	0.52			355	85.9		0.82	0.74
130	33.9	0.42			360	87.8	0.16		
140	37.8	0.57			365	89.8		0.89	1.17
145	39.8		1.08	2.58	370	91.8	0.62		
150	41.8	0.57			375	93.7		1.51	2.45
160	45.7	0.10			380	95.7	0.16		
170	49.7	0.17			390	99.6	0.10		
180	53.6	0.63			395	100		1.99	-0.16
190	57.6	0.73			400	100.3	2.45		
195	59.5		1.17	2.66	405	100.7		1.13	-0.69
200	61.5	0.05			410	101.1	0.73		
210	65.5	0.21			415	101.4		1.06	-0.77
215	67.4		0.96	2.86	420	101.8	0.68		
220	69.4	0.26			425	102.2		1.09	-0.69
230	73.4	0.31			430	102.5	3.28		
235	75.3		1.02	2.89	435	102.9		1.05	-1.17
240	77.3	0.10			440	103.3	2.71		
250	77.9	0.47			445	103.6		1.33	-1.40
255	78.2		1.16	2.72	450	104	0.68		
260	78.5	0.37							

Table 3.2. List of foraminiferal species in Core M70b-St#822

Planktonic foraminifera	Benthic foraminifera
Globigerina bulloides	*Bolivina acuminata*
Globigerina calida	*Bolivina advena*
Globigerinita glutinata	*Bulimina marginata*
Globigerinoides immaturus	*Cassidulina crassa*
Globigerinoides obliquus	*Cassidulina laevigata*
Globigerinoides ruber	*Cibicides tabaensis*
Globorotalia truncitulinoides	*Eponoides repandus*
Orbulina universa	*Gyroidina soldanii*
Turborotalia clarkei	*Hoeglundina elegans*
	Pyrego sp.
	Quenqueloculina sp.
	Uvigerina mediterranea

Table 3.3. Count, relative abundance (%) and absolute abundance (No. g^{-1} sediment) of planktic foraminifera at Core M70b-St#822.

Core depth (cm)	10	20	40	50	100	150	200	220	240	260	280	300	310	320	330	340	350	360	370	380	400	410	420	430	440	450
Age (cal. kyr. BP)	2.6	5.1	7.1	8.2	22.0	41.8	61.5	69.4	77.3	78.5	79.7	80.9	81.5	82.1	82.7	83.3	83.9	87.8	91.8	95.7	100.3	101.1	101.8	102.5	103.3	104.0
Number of sample splits	2	2	2	3	3	4	3	2	3	3	4	4	3	3	2	2	3	2	1	2	1	2	4	3	2	2
Fraction of splitted sample	0.25	0.25	0.25	0.25	0.13	0.06	0.13	0.25	0.13	0.13	0.06	0.06	0.13	0.13	0.25	0.25	0.13	0.25	0.50	0.25	0.50	0.25	0.06	0.13	0.25	0.25
Count																										
Globigerina bulloides	26	82	120	221	87	146	111	172	30	32	74	215	200	216	184	196	188	86	180	212	216	176	95	116	52	32
Globigerina calida	0	0	0	0	3	0	0	0	2	0	0	0	5	0	0	0	0	0	0	0	12	28	43	14	7	2
Globigerinita glutinata	46	58	40	39	57	3	29	32	39	30	25	13	17	18	16	28	28	40	62	76	4	12	4	3	0	0
Globigerinoides immaturus	0	0	0	0	0	0	0	0	0	0	0	0	0	0	0	0	0	0	0	0	62	38	32	0	0	0
Globigerinoides obliquus	0	0	0	0	6	1	2	8	13	25	8	9	10	6	32	12	4	4	14	31	20	16	5	0	0	13
Globigerinoides ruber	56	81	125	49	20	20	8	104	100	110	95	38	66	70	160	96	10	90	64	75	88	140	94	228	268	263
Globorotalia truncitulinoides	45	70	54	20	36	31	10	40	6	11	6	12	3	0	0	12	20	68	28	20	10	44	2	6	0	0
Orbulina universa	0	0	0	0	0	0	0	0	3	0	0	0	30	0	4	0	0	0	0	0	0	0	2	12	9	3
Turborotalia clarkei	79	59	28	115	85	86	96	68	125	90	45	8	58	14	28	88	64	18	30	64	4	16	0	0	0	0
Total planktic foraminfiera	252	350	367	444	294	287	256	424	318	298	253	295	389	324	424	432	314	306	378	478	416	470	277	379	336	313
%																										
Globigerina bulloides	10.3	23.4	32.7	49.8	29.6	50.9	43.4	40.6	9.4	10.7	29.2	72.9	51.4	66.7	43.4	45.4	59.9	28.1	47.6	44.4	51.9	37.4	34.3	30.6	15.5	10.2
Globigerina calida	0	0	0	0	1.0	0	0	0	0.6	0	0	0	1.3	0	0	0	0	0	0	0	2.9	6.0	15.5	3.7	2.1	0.6
Globigerinita glutinata	18.3	16.6	10.9	8.8	19.4	1.0	11.3	7.5	12.3	10.1	9.9	4.4	4.4	5.6	3.8	6.5	8.9	13.1	16.4	15.9	1.0	2.6	1.4	0.8	0	0
Globigerinoides immaturus	0	0	0	0	0	0	0	0	0	0	0	0	0	0	0	0	0	0	0	0	14.9	8.1	11.6	0	0	0
Globigerinoides obliquus	0	0	0	0	2.0	0.3	0.8	1.9	4.1	8.4	3.2	3.1	2.6	1.9	7.5	2.8	1.3	1.3	3.7	6.5	4.8	3.4	1.8	0	0	4.2
Globigerinoides ruber	22.2	23.1	34.1	11.0	6.8	7.0	3.1	24.5	31.4	36.9	37.5	12.9	17.0	21.6	37.7	22.2	3.2	29.4	16.9	15.7	21.2	29.8	33.9	60.2	79.8	84.0
Globorotalia truncitulinoides	17.9	20.0	14.7	4.5	12.2	10.8	3.9	9.4	1.9	3.7	2.4	4.1	0.8	0.0	0.0	2.8	6.4	22.2	7.4	4.2	2.4	9.4	0.7	1.6	0	0
Orbulina universa	0	0	0	0	0	0	0	0	0.9	0	0	0	7.7	0	0.9	0	0	0	0	0	0	0	0.7	3.2	2.7	1.0
Turborotalia clarkei	31.3	16.9	7.6	25.9	28.9	30.0	37.5	16.0	39.3	30.2	17.8	2.7	14.9	4.3	6.6	20.4	20.4	5.9	7.9	13.4	1.0	3.4	0	0	0	0
No. g^{-1} sediment																										
Globigerina bulloides	10	33	48	88	70	234	89	69	24	26	118	344	160	173	74	78	150	34	36	85	43	70	152	93	21	13
Globigerina calida	0	0	0	0	2	0	0	0	2	0	0	0	4	0	0	0	0	0	0	0	2	11	69	11	3	1
Globigerinita glutinata	18	23	16	16	46	5	23	13	31	24	40	21	14	14	6	11	22	16	12	30	1	5	6	2	0	0
Globigerinoides immaturus	0	0	0	0	0	0	0	0	0	0	0	0	0	0	0	0	0	0	0	0	12	15	51	0	0	0
Globigerinoides obliquus	0	0	0	0	5	2	2	3	10	20	13	14	8	5	13	5	3	2	3	12	4	6	8	0	0	5
Globigerinoides ruber	22	32	50	20	16	32	6	42	80	88	152	61	53	56	64	38	8	36	13	30	18	56	150	182	107	105
Globorotalia truncitulinoides	18	28	22	8	29	50	8	16	5	9	10	19	2	0	0	5	16	27	6	8	2	18	3	5	0	0
Orbulina universa	0	0	0	0	0	0	0	0	2	0	0	0	24	0	2	0	0	0	0	0	0	0	3	10	4	1
Turborotalia clarkei	32	24	11	46	68	138	77	27	100	72	72	13	46	11	11	35	51	7	6	26	1	6	0	0	0	0
Total PF (No. g^{-1})	101	140	147	178	235	459	205	170	254	238	405	472	311	259	170	173	251	122	76	191	83	188	443	303	134	125

Table 3.4. Count, relative abundance (%) and absolute abundance (No. g^{-1} sediment) data of benthic foraminifera at Core M70b-St#822.

Core depth (cm)	10	20	40	50	100	150	200	220	240	260	280	300	310	320	330	340	350	360	370	380	400	410	420	430	440	450
Age (cal. kyr. BP)	2.6	5.1	7.1	8.2	22.0	41.8	61.5	69.4	77.3	78.5	79.7	80.9	81.5	82.1	82.7	83.3	83.9	87.8	91.8	95.7	100.3	101.1	101.8	102.5	103.3	104.0
Number of sample splits	0	0	2	2	2	2	2	2	2	0	2	2	2	2	2	2	2	0	0	2	0	0	0	0	0	0
Fraction of splitted sample	1	1	0.25	0.25	0.25	0.25	0.25	0.25	0.25	1	0.25	0.25	0.25	0.25	0.25	0.25	0.25	1	1	0	1	1	1	1	1	1
Count																										
Bolivina acuminata	147	85	175	129	33	47	156	65	104	64	96	112	320	184	184	104	144	160	136	96	0	0	0	0	0	0
Bolivina advena	90	41	17	33	40	25	20	49	96	112	40	64	32	24	32	24	8	16	28	20	0	0	0	0	0	0
Bulimina marginata	83	47	63	64	49	32	56	31	80	0	24	32	56	24	72	56	88	0	16	36	0	0	0	0	0	0
Cassidulina crassa	40	35	27	24	49	73	28	17	48	0	0	40	0	8	16	16	56	32	40	44	0	0	0	0	0	0
Cassidulina laevigata	17	40	37	17	15	120	29	23	24	16	16	72	8	24	16	16	56	0	0	4	0	0	0	0	0	0
Cibicides tabaensis	41	62	51	113	137	73	19	57	24	32	40	40	0	8	104	88	56	16	8	24	0	0	0	0	0	0
Eponoides repandus	0	0	0	0	0	0	0	0	0	16	16	8	0	16	8	0	0	0	24	16	0	0	0	0	0	0
Gyroidina soldanii	0	9	0	0	0	0	8	7	0	0	0	8	0	16	32	24	0	40	48	20	0	0	0	0	0	0
Hoeglundina elegans	15	110	0	7	17	0	17	25	0	32	32	0	0	32	32	80	48	16	4	0	0	0	0	0	0	0
Pyrego sp.	7	7	4	9	7	0	0	9	8	0	8	8	0	0	0	0	0	8	16	12	0	0	0	0	0	0
Quenqueloculina sp.	2	1	0	6	1	0	0	7	8	16	0	0	8	0	0	0	8	0	8	4	0	0	0	0	0	0
Uvigerina mediterranea	43	33	98	65	71	64	21	87	56	96	32	32	0	0	16	0	0	24	20	16	0	0	0	0	0	0
Total benthic foraminifera	485	470	472	467	419	434	354	377	448	384	304	416	424	336	512	408	464	312	348	292	0	0	0	0	0	0
%																										
Bolivina acuminata	30.3	18.1	37.1	27.6	7.9	10.8	44.1	17.2	23.2	16.7	31.6	26.9	75.5	54.8	35.9	25.5	31.0	51.3	39.1	32.9	0	0	0	0	0	0
Bolivina advena	18.6	8.7	3.6	7.1	9.5	5.8	5.6	13.0	21.4	29.2	13.2	15.4	7.5	7.1	6.3	5.9	1.7	5.1	8.0	6.8	0	0	0	0	0	0
Bulimina marginata	17.1	10.0	13.3	13.7	11.7	7.4	15.8	8.2	17.9	0.0	7.9	7.7	13.2	7.1	14.1	13.7	19.0	0.0	4.6	12.3	0	0	0	0	0	0
Cassidulina crassa	8.2	7.4	5.7	5.1	11.7	16.8	7.9	4.5	10.7	0.0	0.0	9.6	0.0	2.4	3.1	3.9	12.1	10.3	11.5	15.1	0	0	0	0	0	0
Cassidulina laevigata	3.5	8.5	7.8	3.6	3.6	27.6	8.2	6.1	5.4	4.2	5.3	17.3	1.9	7.1	3.1	3.9	12.1	0.0	0.0	1.4	0	0	0	0	0	0
Cibicides tabaensis	8.5	13.2	10.8	24.2	32.7	16.8	5.4	15.1	5.4	8.3	13.2	9.6	0.0	2.4	20.3	21.6	12.1	5.1	2.3	8.2	0	0	0	0	0	0
Eponoides repandus	0.0	0.0	0.0	0.0	0.0	0.0	0.0	0.0	0.0	4.2	5.3	1.9	0.0	4.8	1.6	0.0	0.0	0.0	6.9	5.5	0	0	0	0	0	0
Gyroidina soldanii	0.0	1.9	0.0	0.0	0.0	0.0	2.3	1.9	0.0	0.0	0.0	1.9	0.0	4.8	6.3	5.9	0.0	12.8	13.8	6.8	0	0	0	0	0	0
Hoeglundina elegans	3.1	23.4	0.0	1.5	4.1	0.0	4.8	6.6	0.0	8.3	10.5	0.0	0.0	9.5	6.3	19.6	10.3	5.1	1.1	0.0	0	0	0	0	0	0
Pyrego sp.	1.4	1.5	0.8	1.9	1.7	0.0	0.0	2.4	1.8	0.0	2.6	1.9	0.0	0.0	0.0	0.0	0.0	2.6	4.6	4.1	0	0	0	0	0	0
Quenqueloculina sp.	0.4	0.2	0.0	1.3	0.2	0.0	0.0	1.9	1.8	4.2	0.0	0.0	1.9	0.0	0.0	0.0	1.7	0.0	2.3	1.4	0	0	0	0	0	0
Uvigerina mediterranea	8.9	7.0	20.8	13.9	16.9	14.7	5.9	23.1	12.5	25.0	10.5	7.7	0.0	0.0	3.1	0.0	0.0	7.7	5.7	5.5	0	0	0	0	0	0
No. g^{-1} sediment																										
Bolivina acuminata	15	9	70	52	13	19	62	26	42	6	38	45	128	74	74	42	58	16	14	38	0	0	0	0	0	0
Bolivina advena	9	4	7	13	16	10	8	20	38	11	16	26	13	10	13	10	3	2	3	8	0	0	0	0	0	0
Bulimina marginata	8	5	25	26	20	13	22	12	32	0	10	13	22	10	29	22	35	0	2	14	0	0	0	0	0	0
Cassidulina crassa	4	4	11	10	20	29	11	7	19	0	0	16	0	3	6	6	22	3	4	18	0	0	0	0	0	0
Cassidulina laevigata	2	4	15	7	6	48	12	9	10	2	6	29	3	10	6	6	22	0	0	2	0	0	0	0	0	0
Cibicides tabaensis	4	6	20	45	55	29	8	23	10	3	16	16	0	3	42	35	22	2	1	10	0	0	0	0	0	0
Eponoides repandus	0	0	0	0	0	0	0	0	0	2	6	3	0	6	3	0	0	0	2	6	0	0	0	0	0	0
Gyroidina soldanii	0	1	0	0	0	0	3	3	0	0	0	3	0	6	13	10	0	4	5	8	0	0	0	0	0	0
Hoeglundina elegans	2	11	0	3	7	0	7	10	0	3	13	0	0	13	13	32	19	2	0	0	0	0	0	0	0	0
Pyrego sp.	1	1	2	4	3	0	0	4	3	0	3	3	0	0	0	0	0	1	2	5	0	0	0	0	0	0
Quenqueloculina sp.	0	0	0	2	0	0	0	3	3	2	0	0	3	0	0	0	3	0	1	2	0	0	0	0	0	0
Uvigerina mediterranea	4	3	39	26	28	26	8	35	22	10	13	13	0	0	6	0	0	2	2	6	0	0	0	0	0	0
Total BF (No. g^{-1})	49	47	189	187	168	174	142	151	179	38	122	166	170	134	205	163	186	31	35	117	0	0	0	0	0	0

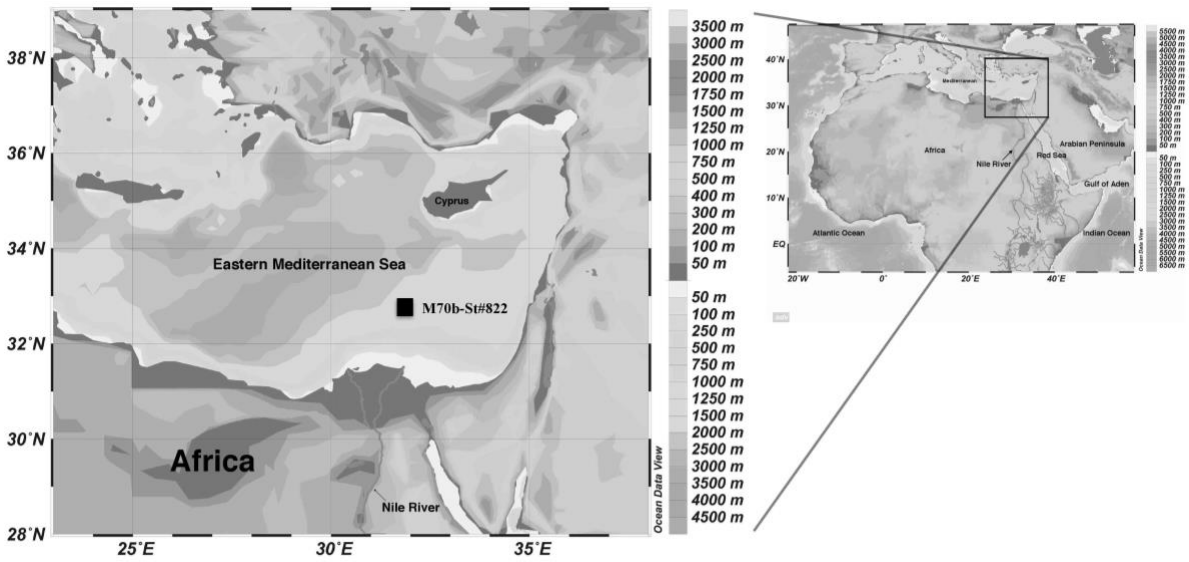

Figure 3. 1. Map of EMS and its surrounding area with bathymetric and topographic information. Black square indicates the study site of M70b-St#822. Map drawn by Ocean Data View (Schlitzer, R., Ocean Data View, http://odv.awi.de, 2015).

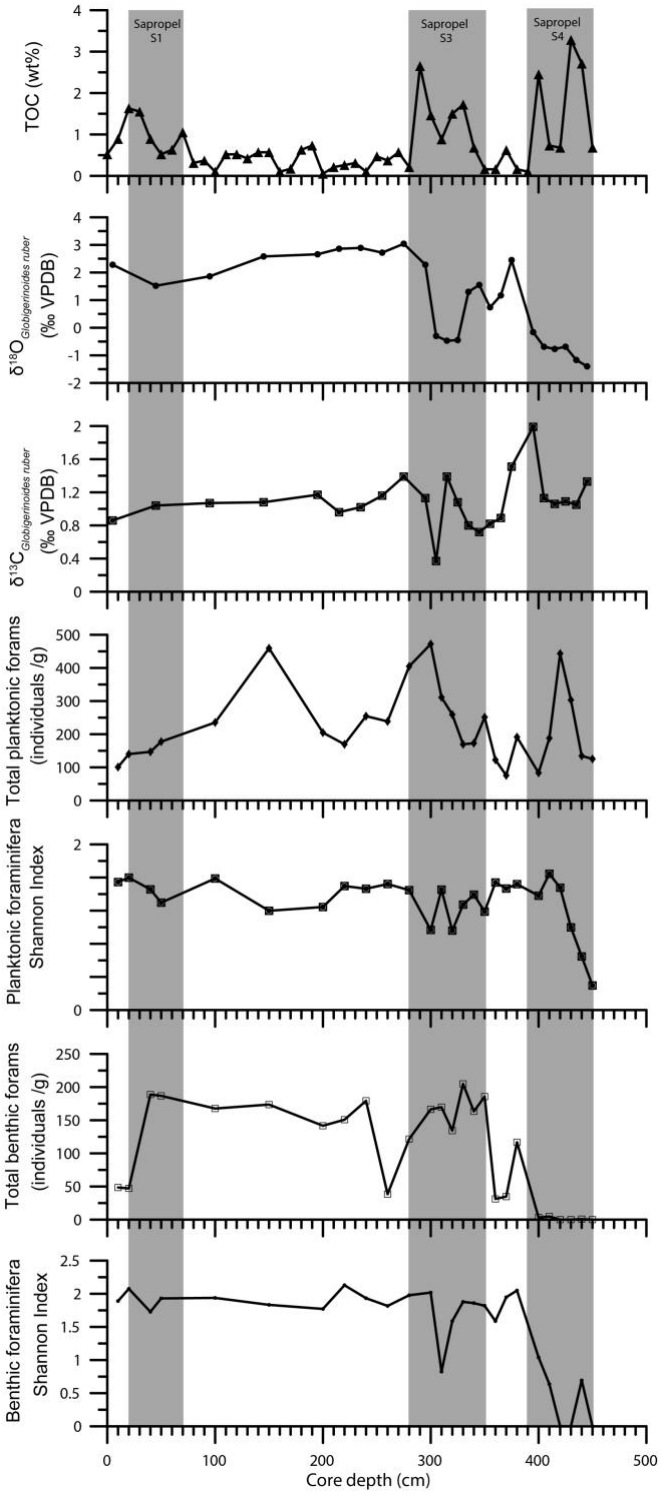

Figure 3. 2. Down core profiles of total organic carbon (TOC, wt%), planktic foraminiferal (*Globigerinoides ruber*) $\delta^{18}O$ (‰ VPDB) and $\delta^{13}C$ (‰ VPDB), total planktic and benthic foraminifera abundances (individual/g) and Shannon index of planktic and benthic foraminifera at core M70b-St#822. Sapropel layers (gray color) are indicated.

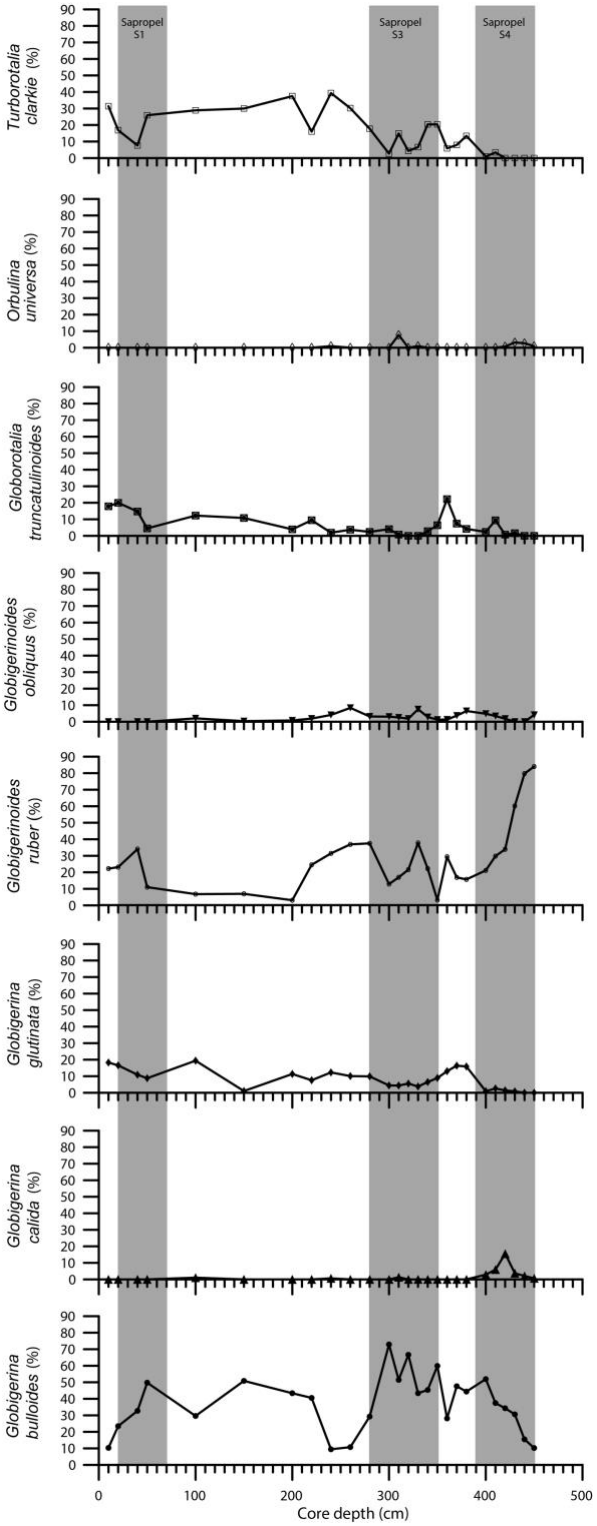

Figure 3. 3. Relative abundance of planktonic foraminiferal species at core M70b-St#822. Sapropel layers (gray color) are indicated.

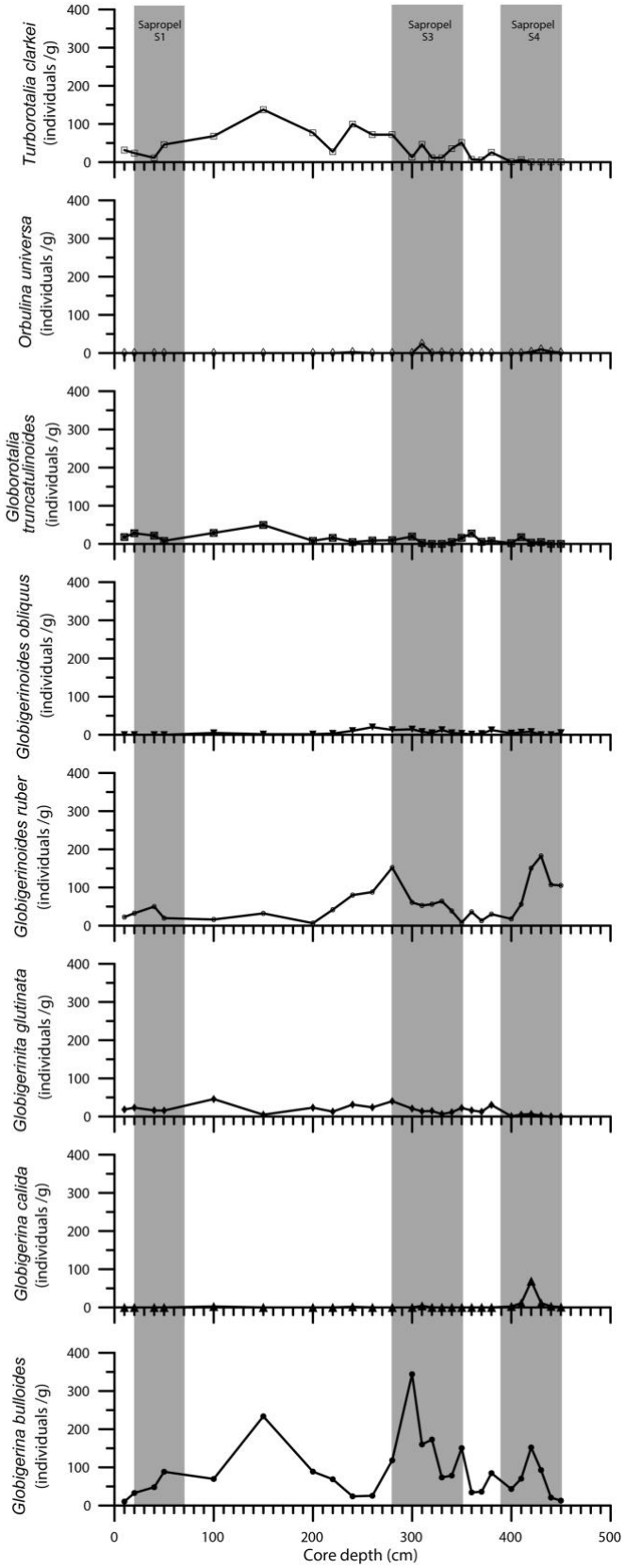

Figure 3. 4. Absolute abundance of planktonic foraminiferal species at core M70b-St#822. Sapropel layers (gray color) are indicated.

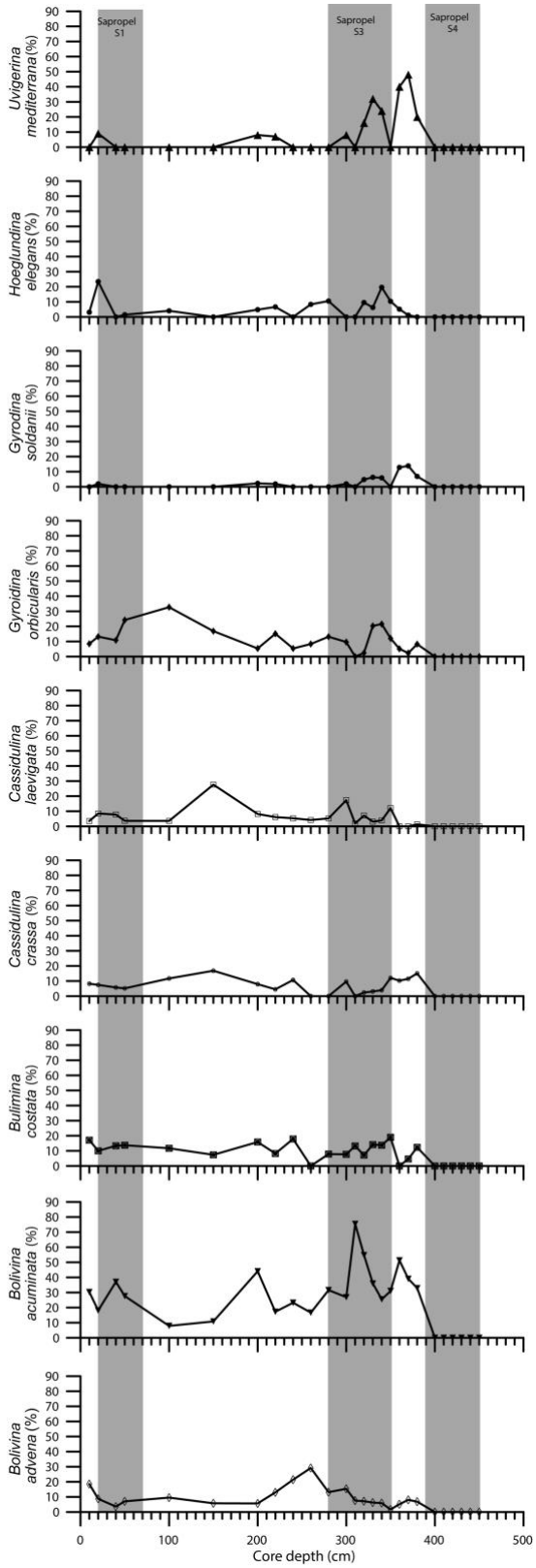

Figure 3. 5. Relative abundance of benthic foraminiferal species at core M70b-St#822. Sapropel layers (gray color) are indicated.

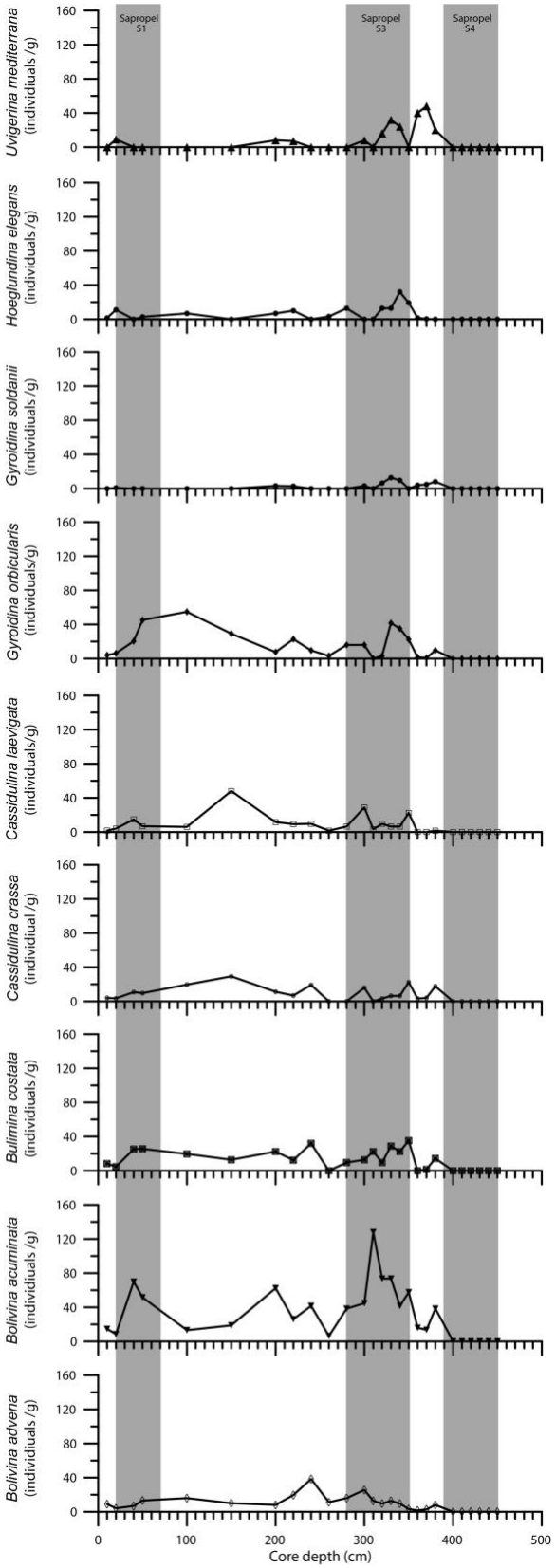

Figure 3. 6. Absolute abundance of benthic foraminiferal species at core M70b-St#822. Sapropel layers (gray color) are indicated.

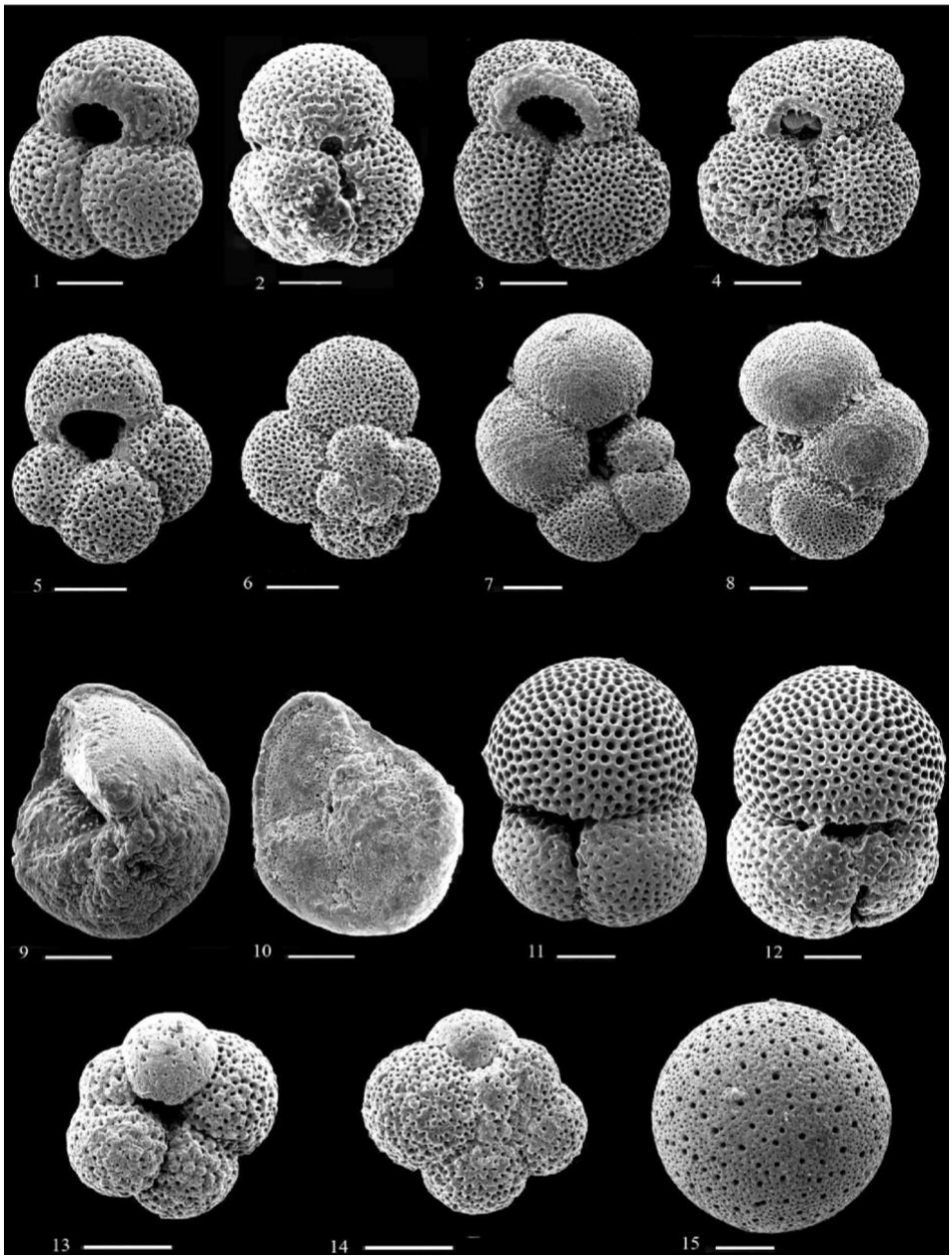

Figure 3. 7: SEM photomicrograph of some selected foraminifera. Species name is followed by depth in cm. Scale bar = 200 µm for Figs. 1-10; 13-14, and = 150 µm for Figs. 11-12, 15. 1-2 *Globigerinoides ruber* (D'Orbigny), 1839, 420 cm. 3-4 *Globigerinoides obliquus* Bolli 1957, 450 cm. 5-6 *Globigerina bulloides* D'orbigny, 1826, 450 cm. 7-8 *Globigerina calida* Parker 1962, 440 cm. 9-10 *Globorotalia truncatulinoides* (d'Orbigny), 1839, 410 cm. 11-12 *Globigerinoides immaturus* Le Roy 1939, 420 cm. 13-14 *Turborotalia clarkei* Rogl & Bolli 1973, 410 cm. 15 *Orbulina universa* D'orbigny, 1839, 430 cm.

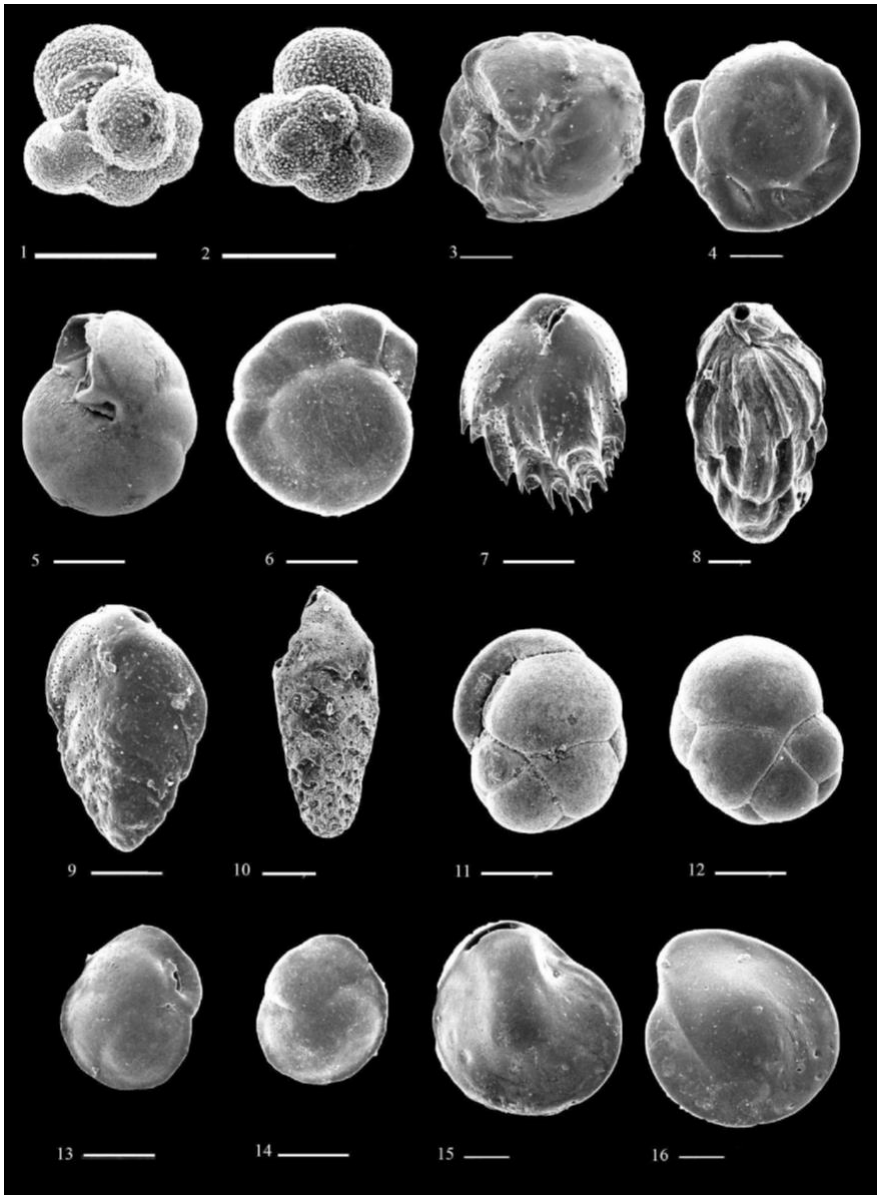

Figure 3. 8: SEM photomicrograph of some selected foraminifera. Species name is followed by depth in cm. Scale bar = 200 µm for Figs. 1-7, 9-14, and = 150 µm for Figs. 15-16, and = 100 µm for Fig. 8. 1-2 *Globigerinita glutinata* (Egger), 1895, 410 cm. 3-4 *Gyroidina soldanii* d'Orbigny, 1826, 410 cm. 5-6 *Gyroidina orbicularis* d'Orbigny, 1826, 410 cm. 7 *Bulimina costata* d'Orbigny, 1852, 340 cm. 8 *Uvigerina mediterranea* Hofker, 1932, 370 cm. 9 *Bolivina acuminata* (Natland), 1946, 380 cm. 10 *Bolivina advena* Cushman var. striatella Cushman, 1925, 380 cm. 11-12 *Cassidulina crassa* d´Orbigny, 1839, 380 cm. 13-14 *Cassidulina laevigata* d'Orbigny, 1826, 200 cm. 15-16 *Hoeglundina elegans* d'Orbigny, 1826, 380 cm.

Chapter 4. Conclusions

Within this thesis, compound-specific isotope signature (Carbon and hydrogen) of long-chain n-alkanes from marine sediment core ODP site 967B and foraminiferal assemblages from marine sediment core M70b-St#822 were scrutinized in order to understand the hydrological cycle system effect of the North African monsoon since the Last Glacial Maximum (LGM) on terrestrial ecosystems of North Africa and effect of humid periods on marine ecosystems of Eastern Mediterranean Sea. In particular the focus is placed on the drastic regime shift from arid conditions of LGM to the humid and vegetated conditions of the mid-Holocene in North Africa. $\delta D_{n\text{-}alkanes}$ and $\delta^{13}C_{n\text{-}alkanes}$ measurements agree well with previous results which, $\delta D_{n\text{-}alkanes}$ co-varied with insolation change response to orbital forcing. Depleted $\delta D_{n\text{-}alkanes}$ were found from deglaciation to middle Holocene, suggesting increased precipitation during the African Humid Period (AHP) caused by northward migration of the Intertropical Convergence Zone (ITCZ). $\delta^{13}C_{n\text{-}alkanes}$ at Site 967 did not show a trend in harmony with $\delta D_{n\text{-}alkanes}$ but exhibiting millennial-scale variations ranging from –25.9‰ to –33.2‰. These $\delta^{13}C_{n\text{-}alkanes}$ values are consistently C4 grass dominated environment in the watershed area of River Nile since LGM even during AHP. The greening of Sahara Desert was dominated by C4 plants during AHP coupled with formation of Sapropel layers in Eastern Mediterranean Sea fueled by African monsoon changes in North Africa. The discharge of freshwater into Mediterranean Sea via Nile River and Wadi connective system in Sahara Desert could alter marine ecosystems in EMS. The focus is placed on the drastic changes of foraminiferal assemblages during Sapropels (AHPs) and non-sapropelic layers (dry periods). These isotopic excursions of *Globigerinoides ruber* are interpreted as a result of enhanced freshwater discharge caused by increased precipitation and terrigenous input in watershed area of Nile River. Increased %*Globigerina bulloides*, a high productivity indicator, suggest nutrient rich condition. Benthic foraminiferal assemblages were employed to reconstruct oxygen conditions in pore water. Notable species turnover to deep infauna species, dysoxic indicator, were observed in sapropel layers. Low species diversities of both planktic and benthic foraminifera are likely due to thermocline shallowing by enhanced freshwater discharge and dysoxic bottom water caused by high productivity during sapropel layer formations.